Bingham Research Center
UtahStateUniversity

2023 ANNUAL REPORT

BINGHAM RESEARCH CENTER

Seth Lyman (editor)
Colleen Jones
John Lawson
Marc Mansfield
Liji David
Trevor O'Neil
Brant Holmes

DOCUMENT NUMBER: BRC_231015A
REVISION: ORIGINAL RELEASE
DATE: NOVEMBER 2023

Executive Summary

Mission of the Bingham Research Center

The mission of Utah State University's Bingham Research Center is to conduct high-quality academic research that can be used by industry, government, and the public to develop efficient and effective solutions to environmental problems. The Center focuses on research that benefits Utah and the Uinta Basin, but scientists at the Center carry out projects around the world and strive for all their work to be globally relevant.

Purpose of this Report

This report provides information about all activities undertaken by the Bingham Research Center over the past twelve months, and it contains some cumulative information about the Center's work. The report focuses on winter ozone research, as this is a core focus area for the Center, and it serves as an annual report to the Utah Legislature and Uintah Special Service District 1, the primary funders of the Center's winter ozone research. The report also contains information about other projects funded by other entities, as well as information about the Center's goals and performance. This and past reports are available at https://www.usu.edu/binghamresearch/papers-and-reports. The Center's Management Plan is available here: https://usu.box.com/s/877z4o8nwynu3uwcze8uxj8jaant7auw.

Background Information about Wintertime Ozone

Ozone negatively impacts respiratory health, especially for those with lung diseases. During wintertime temperature inversion episodes, ozone in the Uinta Basin sometimes increases to levels that exceed the standard of 70 ppb set by the U.S. Environmental Protection Agency (EPA). Because of this, the portions of Uintah and Duchesne Counties that are below 6,250 feet in elevation are currently designated by EPA as an ozone nonattainment area.

The Uinta Basin is one of only two places in the world that are known to routinely experience wintertime ozone in excess of EPA standards (Wyoming's Upper Green River Basin is the other). Ozone forms in the atmosphere from reactions involving oxides of nitrogen (NO_X) and organic compounds, and the majority of NO_X and organic compound emissions in the Uinta Basin are from oil and gas development. Inversion conditions trap these pollutants near ground level, increasing their concentrations and allowing them to generate ozone. The unique mix of pollutants during inversion episodes in the Uinta Basin leads to the formation of wintertime ozone, in contrast to the fine particulate matter ($PM_{2.5}$) pollution that is prevalent during winters on the Wasatch Front.

The number of ozone exceedance days and concentrations of ozone that occur each year are closely tied to meteorology. Years with persistent snow cover and high barometric pressure tend to have more days with strong winter inversions and high ozone. In the absence of snow cover and winter inversions, ozone concentrations in the Basin are similar to those in other rural, high-elevation locations around the

western United States. Changes in emissions of organic compounds and NO_X can also impact ozone levels.

Because wintertime ozone is relatively new to science, some aspects of the meteorology, chemistry, and emissions that allow ozone to form during winter are still poorly understood. Federal and state agencies are required by law to promulgate regulations that reduce ozone-forming emissions in the Uinta Basin. These regulations will mostly target the local oil and gas industry, which is the basis for the majority of the Basin's economy. Scientific research to better elucidate the causes and characteristics of winter ozone can help industry and regulators craft emissions reductions that maximize effectiveness and minimize costs to the local industry and economy. Since 2010, we (scientists at the Bingham Research Center) have conducted research to improve understanding of winter ozone in the Uinta Basin.

A cumulative summary of all significant research findings that relate to Uinta Basin air quality from 2010 through the present is available here: https://www.usu.edu/binghamresearch/cumulative-research-summary.

Highlights from This Document

The following are some highlights and key findings from this report:

- *Many exceedances of the EPA ozone standard occurred over the past winter:* Nearly 100% snow cover across the Uinta Basin, with many strong inversion episodes, created the perfect conditions for ozone formation. Read more about air quality during winter 2022-23 in Section 3. In spite of the bad winter, and even though emissions appear to be trending up as oil and gas activity has increased (Section 12), emissions are still down compared to the high point in 2010-2013 (Section 5).

- *NO_X and organic compound emission reductions would both help reduce winter ozone:* Box models show that NO_X emissions matter less early in the season and more in later winter when there is more sunlight and longer days. Read more in Section 9.

- *Choice of chemical mechanism impacts photochemical model performance:* A chemical mechanism is the list of chemical reactions used in 3D photochemical models to calculate atmospheric chemistry. Several mechanisms exist, and all of them were developed for summertime, urban ozone, not for winter ozone. Section 7 describes the latest in a series of projects to understand how choice of mechanism impacts model outcomes. It shows that both ozone and carbonyl production are impacted.

- *Research priorities, performance, and plans:* Sections 17 through 20 provide information about our performance over the past year, what we've done to engage stakeholders, our research priorities, and our plans for the coming year. We developed the priorities and plans with input from a stakeholder committee, which includes representatives from the oil and gas industry, public health agencies, local government representatives, and regulators.

Contents

List of Tables

List of Figures

1. Winter Ozone Background and Introduction

Ozone has been measured continuously in Utah's Uinta Basin since summer 2009 when air quality monitoring stations were established in Ouray and Red Wash. During winter 2009-10, and about half of the winters since then, ozone concentrations in the Uinta Basin have exceeded U.S. Environmental Protection Agency (EPA) standards. Ozone in excess of EPA standards is more typically found in urban areas during summer and has only been routinely observed during winter months in two places in the world: the Uinta Basin and Wyoming's Upper Green River Basin. In 2010, Uintah and Duchesne Counties (through the Uintah Impact Mitigation Special Service District, now merged into Uinta Special Service District 1) engaged our team at Utah State University to investigate the extent and causes of wintertime air pollution in the Uinta Basin, and we have carried out a wide variety of air quality research projects since that time. The results of these studies can be found in reports and peer-reviewed papers available at https://www.usu.edu/binghamresearch/papers-and-reports.

In general, wintertime air quality in the Uinta Basin becomes impaired when strong, multi-day temperature inversions occur. Strong, multi-day inversions only occur when (1) stagnant, high-pressure meteorological conditions exist and (2) sufficient snow cover exists to reflect incoming sunlight, which keeps the ground from absorbing sunlight and warming. Snow also increases the amount of sunlight available to provide energy for the chemical reactions that form ozone. Numerous exceedances of EPA's ozone standard have occurred during winters with adequate snow cover and sustained high-pressure conditions, and no wintertime exceedances have ever been observed without snow cover.

Ozone forms in the atmosphere from reactions involving oxides of nitrogen (NO_X) and organic compounds, and the majority of NO_X and organic compound emissions in the Uinta Basin are due to oil and gas development. Inversion conditions trap these pollutants near ground level, increasing their concentrations and their ability to generate ozone. During strong, multi-day inversion episodes, high ozone first forms in the low-elevation center of the Basin and builds day-upon-day in concentration while expanding towards the Basin's margins. The highest ozone occurs primarily in areas at the lowest elevation and secondarily in areas with the most oil and gas development. Longer episodes and episodes that occur late in the winter season (because of increased sunlight) tend to lead to higher ozone. The relative ability of reductions in NO_X or organic compound emissions to decrease wintertime ozone depends on the season. Reductions in organics are predicted to lead to ozone decreases throughout the winter, while the utility of NO_X reductions is predicted to increase as the winter season progresses towards spring.

Even with adequate emissions of NO_X and organic compounds (ozone precursors), significant ozone production only occurs when sufficient snow cover and multi-day temperature inversions exist (a temperature inversion occurs when the air temperature aloft is warmer than the temperature at the surface). Sunlight is the energy that fuels ozone production, and since snow reflects sunlight, snow cover increases the amount of energy available to produce ozone. By the same process, snow limits the amount of energy absorbed by the earth's surface, keeping the surface and the air immediately above it cooler than the air aloft, which promotes inversion formation and persistence. Inversions trap NO_X and

organic compounds near their emission sources, allowing them to build up to concentrations that allow for rapid ozone production.

The Uinta Basin experiences other forms of air quality impairment in addition to wintertime ozone, including (1) fine particulate matter ($PM_{2.5}$) concentrations that are elevated during winter inversions and summer wildfires, (2) summertime ozone, which is usually associated with intrusions of ozone-rich stratospheric air or wildfires, and (3) elevated concentrations or organic compounds that can have a direct impact on human health, including benzene. While the primary focus of air quality research at the Bingham Research Center is wintertime ozone, we also perform research to understand these other issues.

On 3 August 2018, the portions of Uintah and Duchesne Counties that are below 6,250 feet in elevation were officially designated an ozone nonattainment area by EPA. This designation formalized a process already begun by the Utah Division of Air Quality, the Ute Indian Tribe, EPA, the oil and gas industry, and other stakeholders to mitigate the winter ozone problem by reducing NO_X and organic compound emissions in the Uinta Basin. As part of the nonattainment designation, regulatory agencies were required to evaluate ozone levels over calendar years 2018, 2019, and 2020 to determine whether the Basin had come into attainment of the federal ozone standard. The Basin failed to attain the standard over those years because of high ozone in 2019, but local agencies requested and received an extension of that timeline, meaning that 2019, 2020, and 2021 would be used to determine attainment. More recently, they requested another extension that would move the window of consideration to 2020, 2021, and 2022, but this request has not been approved by EPA. Ozone was low enough in 2020, 2021, and 2022 that the Uinta Basin will officially attain the federal ozone standard if the second extension is approved. High ozone returned in 2023, however, with many days exceeding the standard in January and February. As of this writing, it is not clear whether EPA will approve the second extension, bringing the Basin into official attainment, or disapprove it, pushing the Basin to a more regulatorily strict level of nonattainment.

Throughout this regulatory process, efforts by the USU Bingham Research Center and many other entities have improved understanding of the causes and impacts of elevated ozone during Uinta Basin winters, allowing industry and regulators to make more efficient and effective decisions relating to air quality. Much about this issue remains poorly understood, however, and additional research is needed to provide information that will allow industry and regulators to continue to develop sound, cost-effective air emissions reduction strategies.

A cumulative summary of all significant research findings that relate to Uinta Basin air quality from 2010 through the present is available here: https://www.usu.edu/binghamresearch/cumulative-research-summary.

2. Terminology and Spelling

2.1. Winter

In this document, "winter 2022-23," "winter," "winter season," or similar phrases refer to the period from 1 December through 31 March.

2.2. Volatile Organic Compounds (VOC)

The term volatile organic compounds (VOC) is defined by the U.S. Environmental Protection Agency (EPA) as "any compound of carbon, excluding carbon monoxide, carbon dioxide, carbonic acid, metallic carbides or carbonates, and ammonium carbonate, which participates in atmospheric photochemical reactions. This includes any such organic compound other than the following, which have been determined to have negligible photochemical reactivity, [including] methane [and] ethane (EPA, 2022)." In keeping with this definition, regulatory inventories of VOC emissions do not include methane or ethane. However, ethane has non-negligible photochemical reactivity during winter ozone episodes in the Uinta Basin (Koss et al., 2015; Stoeckenius et al., 2014), confounding the regulatory definition of VOC. In this work, we use the following terms in the following ways:

- "organic compounds" or "organics" in reference to all organic compounds, including methane and ethane;
- "non-methane organic compounds" or "non-methane organics" to refer to all organics other than methane;
- "non-methane hydrocarbons" to refer to all hydrocarbons other than methane; and
- "volatile organic compounds" or VOC to refer to the EPA definition of VOC (i.e., no methane or ethane). We only use this term when making comparisons with the regulatory emissions inventory.

2.3. Uinta versus Uintah

Confusion and inconsistency exist about the use of "Uinta" versus "Uintah." Many assert that Uinta should be used for all natural features and that Uintah should be used for government boundaries and entities, but exceptions to this rule exist, as do confusing contradictions (e.g., Uintah River High School). For clarity in this document, we use Uinta except when referring to specific entities, organizations, and places that have Uintah in their official names. We also retain the original spellings used in the titles of papers and reports we reference. More information and opinions on this topic are available at these links:

- http://theedgemagazine.blogspot.com/2010/11/uinta-vs-uintah.html
- https://www.fs.usda.gov/detail/uwcnf/learning/history-culture?cid=fsem_035514
- https://www.deseret.com/2009/7/27/20331126/what-s-in-a-name-a-slew-of-western-history

3. Winter 2022-23 Air Quality and Meteorology

Author: Seth Lyman

This section reports on air quality conditions that occurred during winter 2022-23.

3.1. Methods

Quality assurance results for the methods described here are available in Section 17.5.2.

3.1.1. Ozone

During winter 2022-23, eleven monitoring stations that measured ozone operated in the Uinta Basin. Table 3-1 contains a list of all monitoring stations, including locations, elevations, and operators. We obtained data for stations operated by organizations other than USU from the U.S. Environmental Protection Agency (EPA)'s AQS database (https://aqs.epa.gov/api). We utilized an Ecotech Model 9810 ozone analyzer at the Horsepool site and 2B Technology Model 205 ozone monitors at other stations operated by USU. We performed calibration checks at all USU stations at least every other week using NIST-traceable ozone standards. Calibration checks passed if monitors reported in the range of ±5 ppb when exposed to 0 ppb ozone and if monitors were within ±7% deviation from expected values when exposed to higher concentrations of ozone. We only included data bracketed by successful calibration checks in the final dataset.

Table 3-1. Air quality monitoring stations that operated during winter 2022-23. All stations measured ozone and basic meteorological parameters. Stations that measured organic compounds, NO_X, and/or $PM_{2.5}$ are indicated. NO_X* signifies NO_2 measured with a photolytic NO_2 (rather than molybdenum) converter. NPS is the National Park Service. UDAQ is the Utah Division of Air Quality. BLM is the Bureau of Land Management. AQS is the EPA AQS air quality database (https://aqs.epa.gov/api).

	Operator	Latitude	Longitude	Elev. (m)	Organics	NO_X, $PM_{2.5}$	Data Source
Seven Sisters	USU	39.981	-109.345	1618	N/A	N/A	USU
Castle Peak	USU	40.051	-110.020	1605	Yes	NO_X*	USU
Dinosaur N.M.	NPS	40.437	-109.305	1463	N/A	N/A	AQS
Red Wash	Ute Tribe	40.204	-109.352	1689	N/A	NO_X	AQS
Vernal	UDAQ	40.453	-109.510	1606	N/A	NO_X, $PM_{2.5}$	AQS
Whiterocks	Ute Tribe	40.484	-109.906	1893	N/A	NO_X	AQS
Ouray	Ute Tribe	40.055	-109.688	1464	N/A	NO_X	AQS
Roosevelt	DAQ/USU	40.294	-110.009	1587	Yes	NO_X*, $PM_{2.5}$	AQS/USU
Myton	Ute Tribe	40.217	-110.182	1610	N/A	NO_X	AQS
Horsepool	USU	40.144	-109.467	1569	Yes	NO_X*, $PM_{2.5}$	USU
Rangely	NPS/BLM	40.087	-108.762	1648	N/A	NO_X, $PM_{2.5}$	AQS

3.1.2. Reactive Nitrogen

We measured NO, true NO_2 (via a photolytic converter), and NO_Y at Roosevelt with a Teledyne-API NO_X analyzer. We measured NO, true NO_2, and NO_Y with a Thermo 42i with a photolytic converter at Horsepool, and we measured NO and true NO_2 with a Thermo 42i with a photolytic converter at Castle Peak. All three photolytic converters were manufactured by Air Quality Design, Inc. NO_X is the sum of NO and NO_2. NO_Y is the sum of NO_X and other reactive nitrogen compounds in the gas and fine particulate phases. We calibrated the systems weekly with NO standards and for NO_2 and NO_Y via gas-phase titration using a dilution calibrator. Once during the season, we calibrated NO_Y instrumentation with nitric acid and isopropyl nitrate permeation tubes. All sites operated by other organizations measured NO and NO_2 via a molybdenum converter-based system, a method known to bias NO_2 and NO_X results high due to NO_Y interference (Jung et al., 2017).

3.1.3. Methane and Total Non-methane Hydrocarbons

We measured methane and total non-methane hydrocarbons at Horsepool and Roosevelt with a Chromatotec ChromaTHC and a Thermo 55i, respectively. We calibrated these systems every week with certified gas standards (containing methane and propane) and a dilution calibrator.

3.1.4. Speciated Non-methane Hydrocarbons and Alcohols

To measure speciated non-methane hydrocarbons and alcohols, we collected whole-air samples with silonite-coated 6 L stainless steel canisters at Horsepool, Roosevelt, and Castle Peak. We collected at most one can per day via an automated sampling manifold (we filled some cans from 0:30 to 3:30 local standard time and the others from 12:30 to 15:30). We used silonite-coated critical orifice-based flow

regulators to regulate flow into the canisters, and we controlled sample collection with a nickel-plated brass manifold with inert solenoid valves (Clippard part number O-ET-2M-12). Tubing and fittings were all either PFA Teflon or stainless steel. A PTFE filter upstream of the sample line filtered particles (5 µm pore size).

We analyzed the canisters for 54 hydrocarbons, methanol, ethanol, and isopropanol using a method similar to guidance provided by EPA for Photochemical Assessment Monitoring Stations (EPA, 1998). We used cold trap dehydration (Wang and Austin, 2006) with an Entech 7200 preconcentrator and a 7016D autosampler to preconcentrate samples. We analyzed samples with two Shimadzu GC-2010 gas chromatographs (GCs), a flame ionization detector (for C2 and C3 NMHC), and a mass spectrometer (for all other compounds). We used a Restek rtx1-ms column (all compounds; 60 m, 0.32 mm ID), a Restek Alumina BOND/Na_2SO_4 column (C2 and C3 NMHC; 50 m,0.32 mm ID), and another Restek rtx1-ms column (all other compounds; 30 m, 0.25 mm ID) to separate compounds in the GCs.

We used 5-point curves to calibrate the flame ionization detector and mass spectrometer at least monthly. We analyzed a duplicate sample, at least one blank, and at least one calibration check during each batch. We accepted data if calibration curves had r^2 values greater than 0.99, if all values for blanks were less than 1 ppb, if duplicate values for each compound averaged within 10% of each other, and if calibration checks for each compound were within 20% of expected values. We used blank values to correct sample results.

More information about our canister analysis protocols and results is available in Lyman et al. (2021) and Lyman et al. (2018). Table 3-2 lists the organic compounds measured.

Table 3-2. List of organic compounds measured, the compound group for each, and the analytical method used.

Compound	Group	Analytical method
Ethane	Alkane	GC/GC/MS
Ethylene	Alkene	GC/GC/MS
Propane	Alkane	GC/GC/MS
Propylene	Alkene	GC/GC/MS
Isobutane	Alkane	GC/GC/MS
n-Butane	Alkane	GC/GC/MS
Acetylene	Alkyne	GC/GC/MS
Trans-2-butene	Alkene	GC/GC/MS
1-Butene	Alkene	GC/GC/MS
Cis-2-butene	Alkene	GC/GC/MS
Isopentane	Alkene	GC/GC/MS
N-Pentane	Alkane	GC/GC/MS
Trans-2-pentene	Alkene	GC/GC/MS
1-Pentene	Alkene	GC/GC/MS
Cis-2-pentene	Alkene	GC/GC/MS
2,2-Dimethylbutane	Alkane	GC/GC/MS

Compound	Group	Analytical method
Cyclopentane	Alkane	GC/GC/MS
2,3-Dimethylbutane	Alkane	GC/GC/MS
2-Methylpentane	Alkane	GC/GC/MS
3-Methylpentane	Alkane	GC/GC/MS
Isoprene	Alkene	GC/GC/MS
1-Hexene	Alkene	GC/GC/MS
n-Hexane	Alkane	GC/GC/MS
Methylcyclopentane	Alkane	GC/GC/MS
2,4-Dimethylpentane	Alkane	GC/GC/MS
Benzene	Aromatic	GC/GC/MS
Cyclohexane	Alkane	GC/GC/MS
2-Methylhexane	Alkane	GC/GC/MS
2,3-Dimethylpentane	Alkane	GC/GC/MS
3-Methylhexane	Alkane	GC/GC/MS
2,2,4-Trimethylpentane	Alkane	GC/GC/MS
n-Heptane	Alkane	GC/GC/MS
Methylcyclohexane	Alkane	GC/GC/MS
2,3,4-Trimethylpentane	Alkane	GC/GC/MS
Toluene	Aromatic	GC/GC/MS
2-Methylheptane	Alkane	GC/GC/MS
3-Methylheptane	Alkane	GC/GC/MS
n-Octane	Alkane	GC/GC/MS
Ethylbenzene	Aromatic	GC/GC/MS
m/p-Xylene	Aromatic	GC/GC/MS
Styrene	Alkene	GC/GC/MS
o-Xylene	Aromatic	GC/GC/MS
n-Nonane	Alkane	GC/GC/MS
Isopropylbenzene	Aromatic	GC/GC/MS
n-Propylbenzene	Aromatic	GC/GC/MS
1-Ethyl-3- methylbenzene	Aromatic	GC/GC/MS
1-Ethyl-4-methylbenzene	Aromatic	GC/GC/MS
1,3,5-Trimethylbenzene	Aromatic	GC/GC/MS
1-Ethyl-2- methylbenzene	Aromatic	GC/GC/MS
1,2,4-Trimethylbenzene	Aromatic	GC/GC/MS
n-Decane	Alkane	GC/GC/MS
1,2,3-Trimethylbenzene	Aromatic	GC/GC/MS
1,3-Diethylbenzene	Aromatic	GC/GC/MS

Compound	Group	Analytical method
1,4-Diethylbenzene	Aromatic	GC/GC/MS
Methanol	Alcohol	GC/GC/MS
Ethanol	Alcohol	GC/GC/MS
Isopropanol	Alcohol	GC/GC/MS
Formaldehyde	Carbonyl	HPLC
Acetaldehyde	Carbonyl	HPLC
Acrolein	Carbonyl	HPLC
Acetone	Carbonyl	HPLC
Propionaldehyde	Carbonyl	HPLC
Crotonaldehyde	Carbonyl	HPLC
Butyraldehyde	Carbonyl	HPLC
Methacrolein	Carbonyl	HPLC
2-Butanone	Carbonyl	HPLC
Benzaldehyde	Carbonyl	HPLC
Valeraldehyde	Carbonyl	HPLC

3.1.5. Carbonyls

We collected samples on DNPH cartridges and eluted and analyzed them using modifications of the methods of Uchiyama et al. (2009), Anneken et al. (2015), Shimadzu method LAAN-J-LC-E090 (Shimadzu, 2011), and Restek Lit. Cat. # EVSS2393A-UNV (Restek, 2018). These techniques are somewhat different from U.S. EPA Method TO-11A (EPA, 1999), which has become outdated due to improved instrumentation capabilities and column separation technologies. The sample path upstream of the cartridges was composed entirely of PFA Teflon, with a PTFE filter upstream of the sample line to filter particles (5 µm pore size). Sample collection times were the same as those for the canisters described above (3 hours).

We eluted cartridges within 14 days of sampling and analyzed the eluent within 30 days. To elute DNPH cartridge samples, we flushed cartridges with 5 mL of a solution of 75% acetonitrile and 25% dimethyl sulfoxide (percent by volume). We collected the solution into 5 mL volumetric flasks and brought the flasks to a volume of 5 mL using 0.5–1 mL of the acetonitrile/dimethyl sulfoxide solution. Finally, we pipetted a 1.6 mL aliquot from the 5 mL flask into two 2 mL autosampler vials for analysis by high-performance liquid chromatography (HPLC). The second vial was kept as a spare in case of contamination or equipment failure.

We used a commercial standard mixture (M-1004; AccuStandard, New Haven, CT, USA) of derivatized carbonyls in acetonitrile for calibration. We analyzed samples with a Shimadzu (Somerset, NJ, USA) Nexera-i LC-2040C 3d Plus HPLC and a Shimadzu Shim-Pack Velox C18 column. We used a mixture of acetonitrile, tetrahydrofuran, and water as the eluent. We calibrated the instrument on each analysis day with a 5-point calibration curve and ran at least one additional calibration standard at the beginning and end of each analysis batch to check for retention time drift or other errors.

Additional information about the methods used is available in Lyman et al. (2021). Table 3-2 lists the organic compounds that we measured.

3.1.6. Particulate Matter Measurements

We measured particulate matter with aerodynamic diameter smaller than 2.5 micrometers ($PM_{2.5}$) at Horsepool with a BAM 1020 monitor. We operated the instrument according to manufacturer protocols, with leak checks, flow and mass calibrations, detector calibrations, and cleanings performed at regular intervals. We obtained particulate matter values for other sites from the EPA AQS database (https://aqs.epa.gov/api).

3.1.7. Meteorological Measurements

We deployed solar radiation sensors at Horsepool (incoming and outgoing shortwave and longwave with a Kipp and Zonen CNR-4 and UV-A and UV-B with Kipp and Zonen UV radiometers), Roosevelt (incoming and outgoing shortwave with a Kipp and Zonen CNR-4), and Castle Peak (incoming and outgoing shortwave with a Hukseflux NR01 radiometer). We check these sensors against calculations of clear-sky radiation annually.

We operated a suite of comprehensive, research-grade meteorological instruments at all sites operated by USU. We checked wind speed and direction, temperature, humidity, and barometric pressure against a NIST-traceable standard once annually. We checked snow depth sensors against a height standard annually. We also obtained meteorological data from the EPA AQS database.

3.2. Results and Discussion

3.2.1. Ozone

Significant snow cover arrived on 10 December 2022 and lasted through the end of the winter (Figure 3-1). Low sunlight and frequent storms kept ozone below the EPA standard until January, but strong inversions and plenty of sunlight led to multiple exceedances of the standard in January, February, and early March at sites across the Uinta Basin (Figure 3-2). Several studies have shown decreasing trends in ozone and its precursors since maxima in 2010-2013 (Lin et al., 2021; Mansfield and Lyman, 2021), so the high ozone at so many sites came as a surprise. Section 5 puts winter 2022-23 into the context of long-term air quality trends.

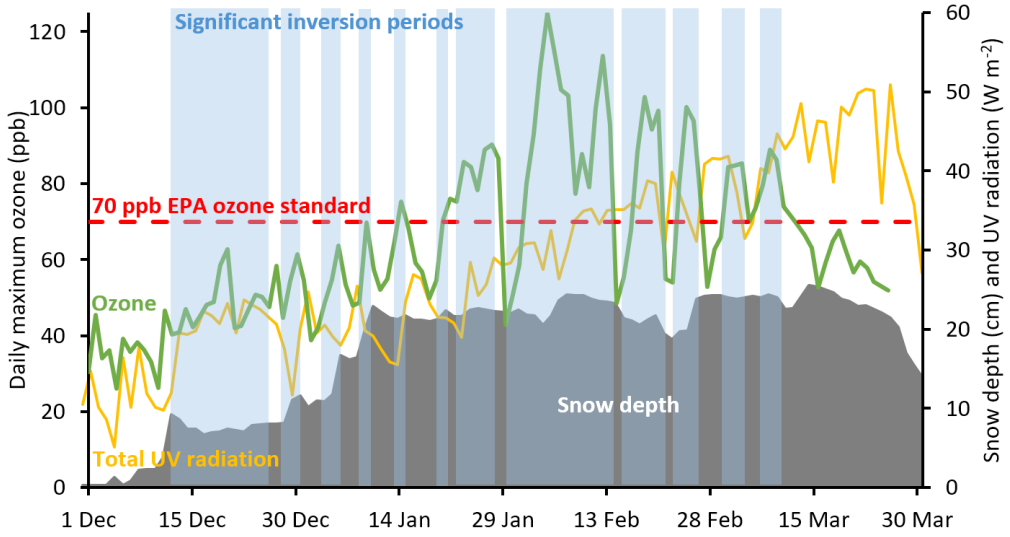

Figure 3-1. Horsepool daily maximum ozone, average snow depth, and daytime average total UV radiation (incoming + reflected) during winter 2022-23. Inversion periods are shown as light blue boxes.

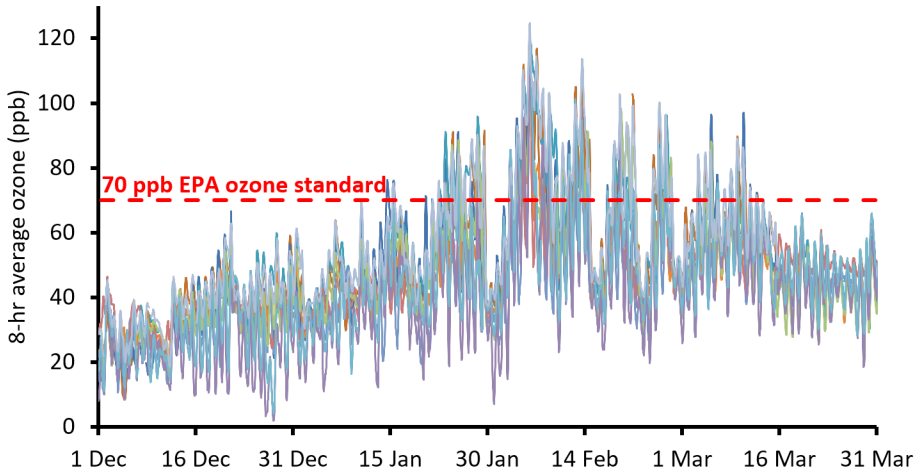

Figure 3-2. 8-hr average ozone from all sites listed in Table 2-1 during winter 2022-23.

Table 3-3 provides information about ozone observed at all monitoring stations in the Uinta Basin during winter 2022-23. Every monitoring station experienced exceedances of the EPA ozone standard during the winter. An exceedance occurs when the daily maximum 8-hr average ozone value at a station is greater than the EPA standard of 70 ppb. The average of the fourth-highest daily maximum 8-hr average ozone value over three consecutive calendar years is used to determine regulatory compliance with the standard. USU's Horsepool site had the most exceedances and the highest fourth-high daily maximum ozone. Of monitoring stations that are used for regulatory compliance, Dinosaur National Monument had the most exceedance days and the highest fourth-high daily maximum ozone.

Table 3-3. Eight-hr average ozone concentrations around the Uinta Basin, winter 2022-23.

	Mean	Maximum	Minimum	4th Highest Daily Maximum	Number of Exceedances
Seven Sisters	52.5	116.8	8.4	108.5	34
Castle Peak	51.7	117.1	12.1	97.1	37
Dinosaur N.M.	54.3	119.0	14.9	98.3	34
Red Wash	46.2	105.8	17.8	81.5	11
Vernal	41.8	101.8	10.6	82.8	12
Whiterocks	46.6	105.0	17.4	88.1	13
Ouray	49.2	102.8	13.0	91.4	27
Roosevelt	40.1	112.5	1.9	93.9	23
Myton	44.7	119.8	4.1	94.5	29
Horsepool	57.4	124.8	18.5	110.3	39
Rangely	40.8	92.0	16.1	71.6	5

Figure 3-3 shows the spatial distribution of the fourth-highest daily maximum 8-hr average ozone concentration around the Uinta Basin during winter 2022-23. All sites in the Basin exceeded the 70 ppb EPA ozone standard, but ozone tended to be lower at the Basin edges, in Whiterocks, Vernal, and Rangely. Ouray has typically had ozone in the same range as Horsepool and Seven Sisters, but this year Ouray had fewer exceedance days and lower ozone overall than those two sites. The reason for this is unclear.

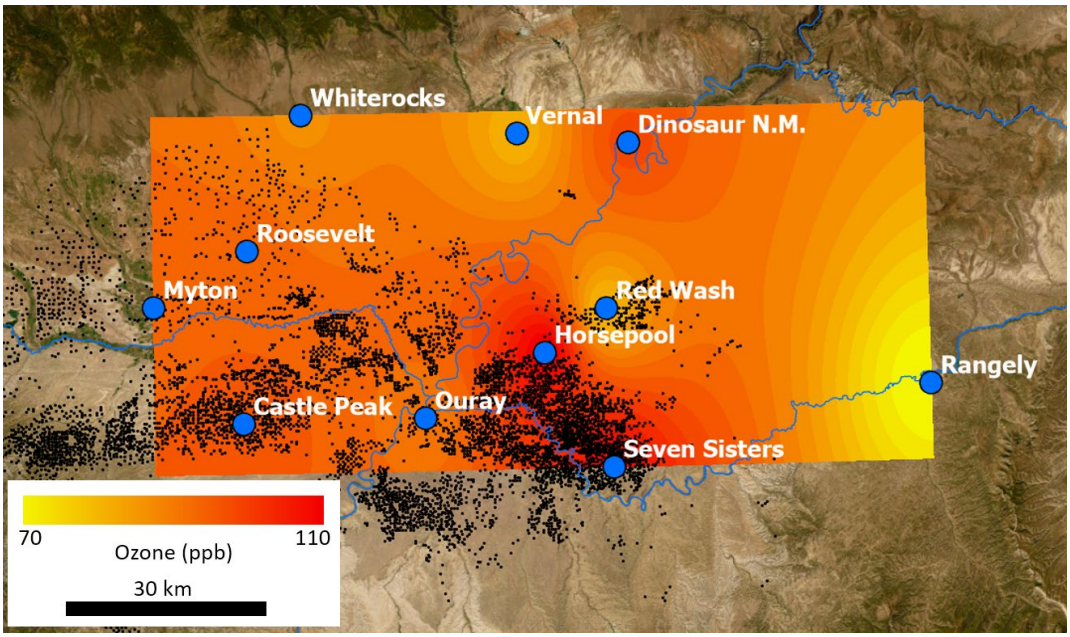

Figure 3-3. Fourth-highest daily maximum 8-hr average ozone in the Uinta Basin during winter 2022-23. The background color indicates ozone concentration and was interpolated using the inverse distance weighting method in ArcGIS Pro.

3.2.2. *Particulate Matter*

$PM_{2.5}$ concentrations stayed below the EPA standard of 35 µg m^{-3} during winter 2022-23 at Vernal, Rangely, and Horsepool but exceeded the standard multiple times at the Roosevelt monitoring station during stagnant and inverted conditions (Figure 3-4).

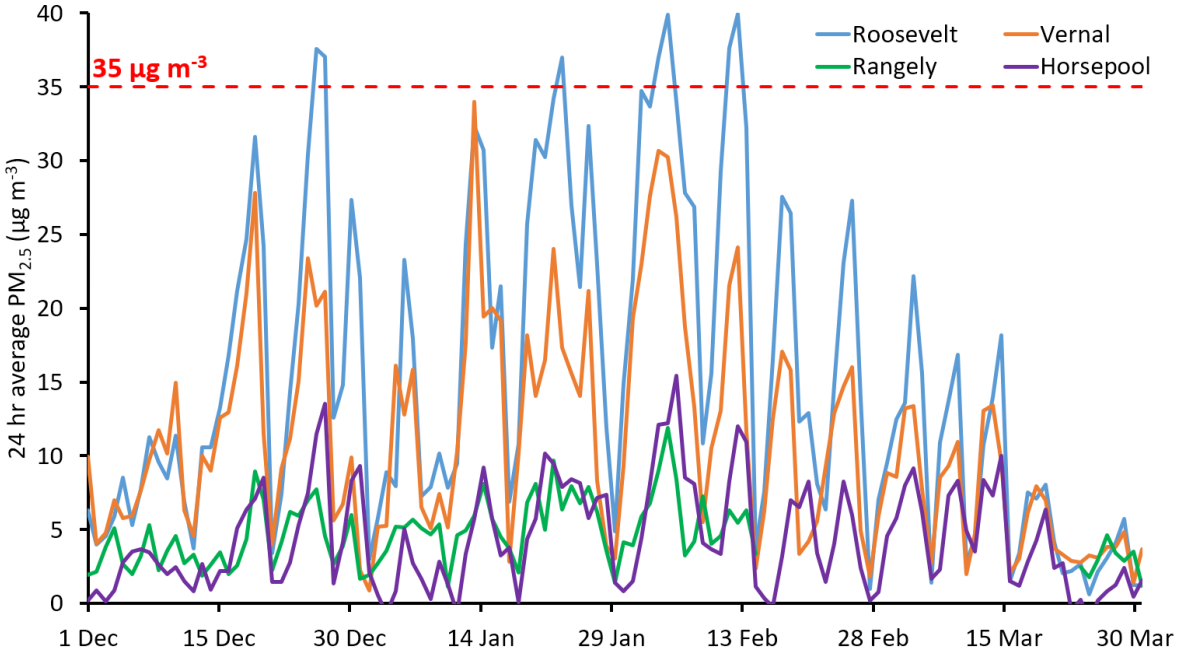

Figure 3-4. 24-hr average $PM_{2.5}$ at monitoring stations around the Uinta Basin during winter 2022-23. The red dashed line indicates the EPA $PM_{2.5}$ standard.

Figure 3-5 shows box and whisker plots of $PM_{2.5}$ at monitoring stations around the Uinta Basin.

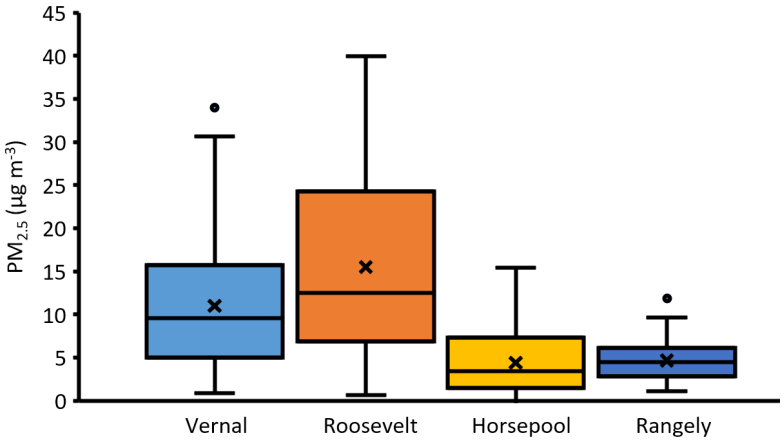

Figure 3-5. Box-and-whisker plots of 24-hr average $PM_{2.5}$ at four monitoring stations during winter 2022-23. X's indicate average values. Lines within the boxes indicate medians. Tops and bottoms of boxes indicate the third

and first quartiles. Top and bottom whiskers indicate maximum and minimum values. Circles indicate outliers.

Comparison of Roosevelt, Horsepool, and Castle Peak Data

The Horsepool and Roosevelt monitoring stations began operating in winter 2011-12 and were designed to contain nearly identical suites of instrumentation. At both stations, for example, we measure NO_X with instrumentation that doesn't bias NO_2 during winter inversion episodes, whereas all regulatory monitoring stations in the Uinta Basin use alternative, biased instrumentation. The areas surrounding the Horsepool and Roosevelt stations are different from one another. The Horsepool station is on the northern edge of an area of dense oil and gas development (mostly gas), whereas the Roosevelt station is within a small city. Oil and gas development exists within and near the city of Roosevelt (mostly oil). The two stations are at very similar elevations (Table 3-1).

In 2017, Utah DAQ donated a NO_X analyzer that we upgraded with a photolytic converter and installed at our Castle Peak monitoring station. Castle Peak is in an area of dense oil development, and its elevation is less than 100 meters higher than the Roosevelt and Horsepool stations.

Figure 3-6 shows NO_X measured at Roosevelt, Horsepool, and Castle Peak during winter 2022-23, and Figure 3-7 shows NO_Z at Roosevelt and Horsepool. NO_X is the sum of NO and NO_2, which are important precursors to ozone production. NO_Y (not shown in the figures) is the sum of NO_X and all other reactive nitrogen compounds (e.g., nitric and nitrous acids, organic nitrates, and particulate-bound nitrogen compounds). NO_Z is the sum of all reactive nitrogen compounds except NO_X (in other words, it is NO_Y minus NO_X). While NO_X is an ozone precursor, the compounds that comprise NO_Z are mostly generated along with ozone as a result of photochemical reactions and are byproducts and indicators of atmospheric photochemical conditions.

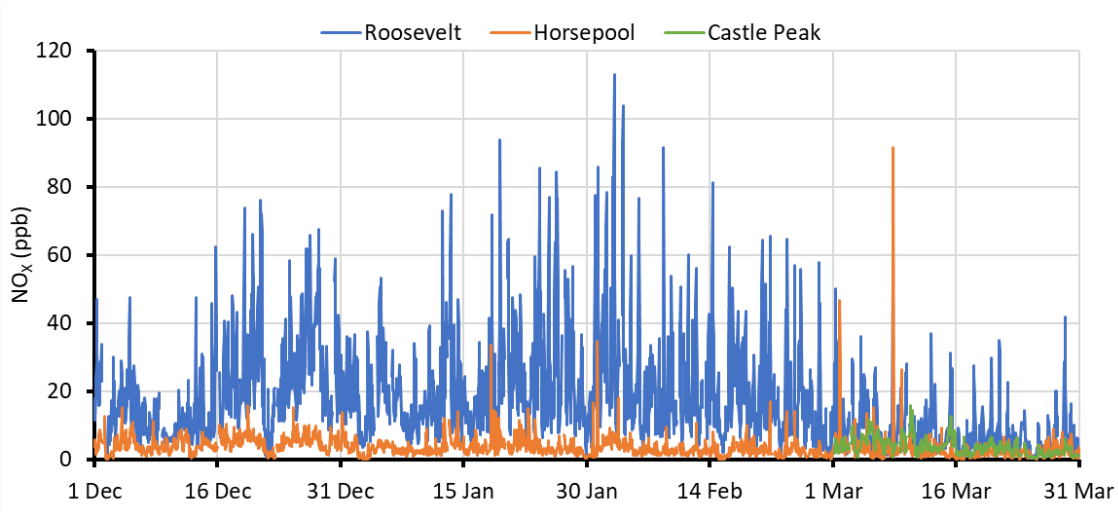

Figure 3-6. Hourly average NO_X measured at Roosevelt, Horsepool, and Castle Peak during winter 2022-23.

During winter 2022-23, as in previous winters, NO_X was higher in Roosevelt than at Horsepool and Castle Peak (Figure 3-6) and was 5.1 times higher than Horsepool on average. NO_X in Roosevelt is emitted from

urban sources like cars and home heating, as well as from oil and gas sources, while NO_X in the vicinity of Horsepool and Castle Peak originates almost entirely from oil and gas activity. Because of instrument failure, NO_X measurements were only available at Castle Peak in March, but for the available measurement period, NO_X at Castle Peak was only 7% higher than Horsepool (p-value for a t-test of difference was 0.05). NO_Z was 1.8 times higher at Roosevelt than at Horsepool (Figure 3-7).

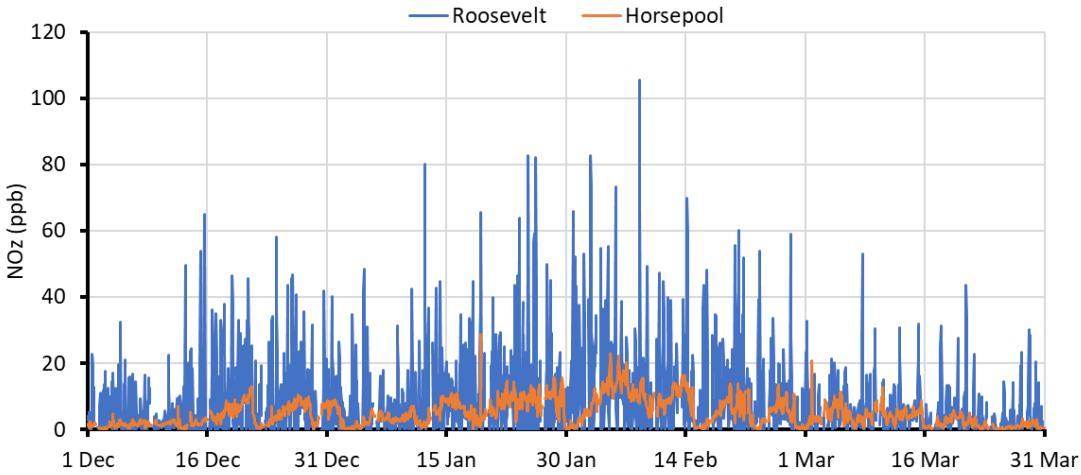

Figure 3-7. Hourly average NO_Z measured at Roosevelt and Horsepool during winter 2022-23.

NO_X at Roosevelt exhibited a pronounced peak in the morning and a lesser peak in the late afternoon and early evening, probably due to morning and afternoon peaks in local traffic (Figure 3-8). Horsepool and Castle Peak did not show a pronounced peak, probably because the majority of NO_X emissions at the sites were due to stationary, continuous sources rather than traffic-related sources.

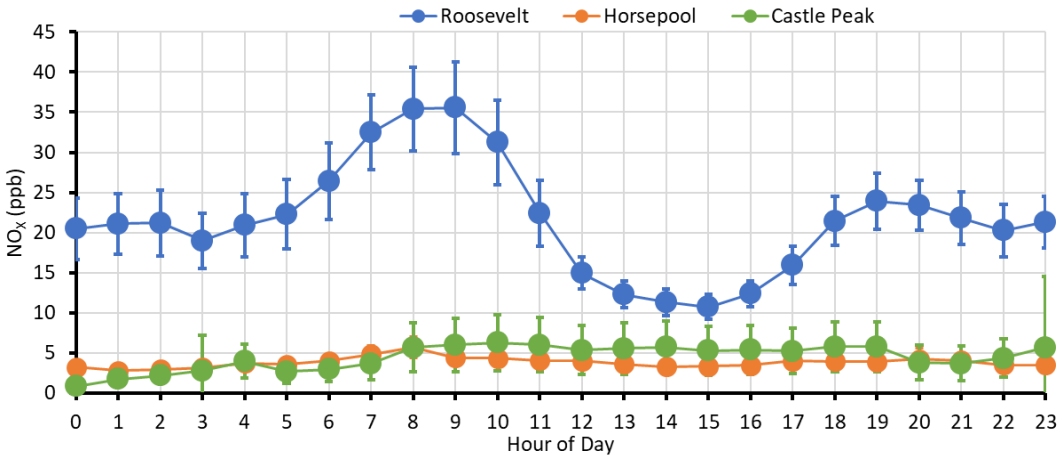

Figure 3-8. Average NO_X at Roosevelt, Horsepool, and Castle Peak during each hour of the day during inversion episodes that occurred during winter 2022-23. Whiskers represent 95% confidence intervals.

While average methane was slightly higher at Horsepool than at Roosevelt (Figure 3-9), average total non-methane hydrocarbons (measured as a single group of compounds with a methane/non-methane hydrocarbon GC) were 17% higher at Roosevelt (Figure 3-10). In the past, both were higher at Horsepool, but new oil and gas activity near Roosevelt appears to be increasing emissions in the area.

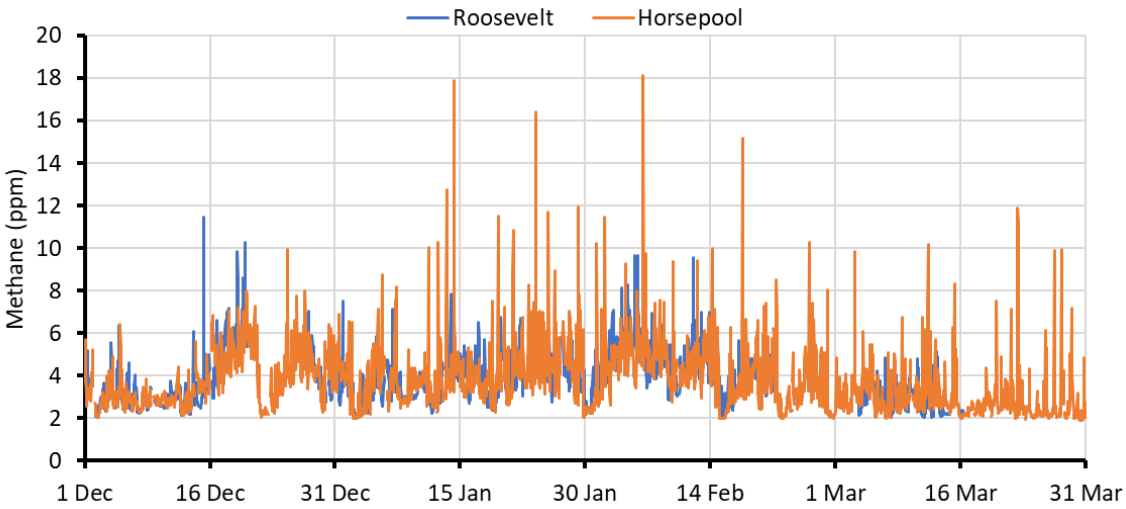

Figure 3-9. Hourly average methane measured at Roosevelt and Horsepool during winter 2022-23.

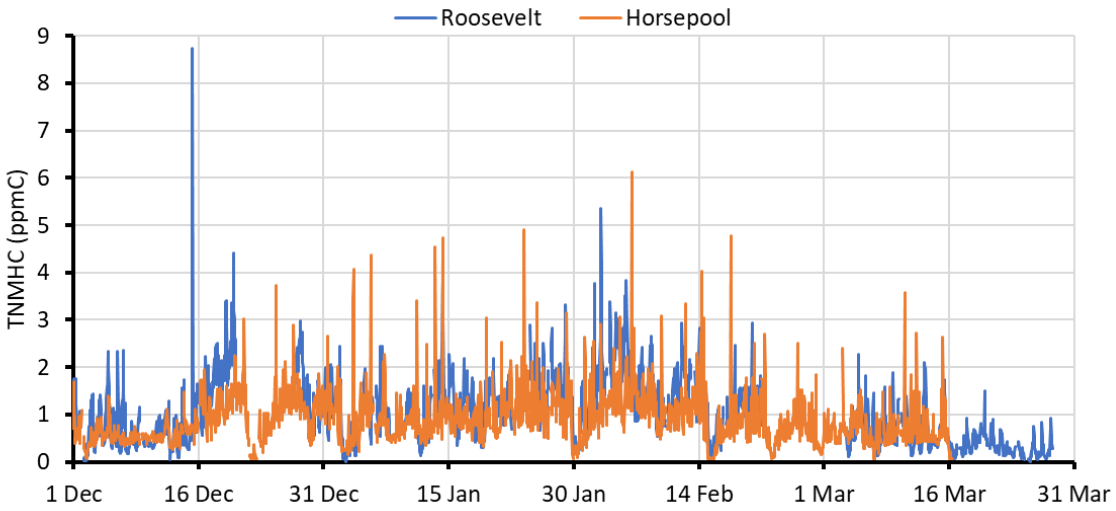

Figure 3-10. Hourly average total non-methane hydrocarbons (TNMHC) measured at Roosevelt and Horsepool during winter 2022-23. ppmC is parts-per-million of carbon atoms.

Snow depth was higher and lasted longer at the three sites than during most years, with snow cover beginning in early December and persisting until the end of March (Figure 3-11). Snow cover led to high albedo (i.e., surface reflectance) at Roosevelt and Castle Peak (Figure 3-12). The solar radiometer at Horsepool was not operational during winter 2022-23.

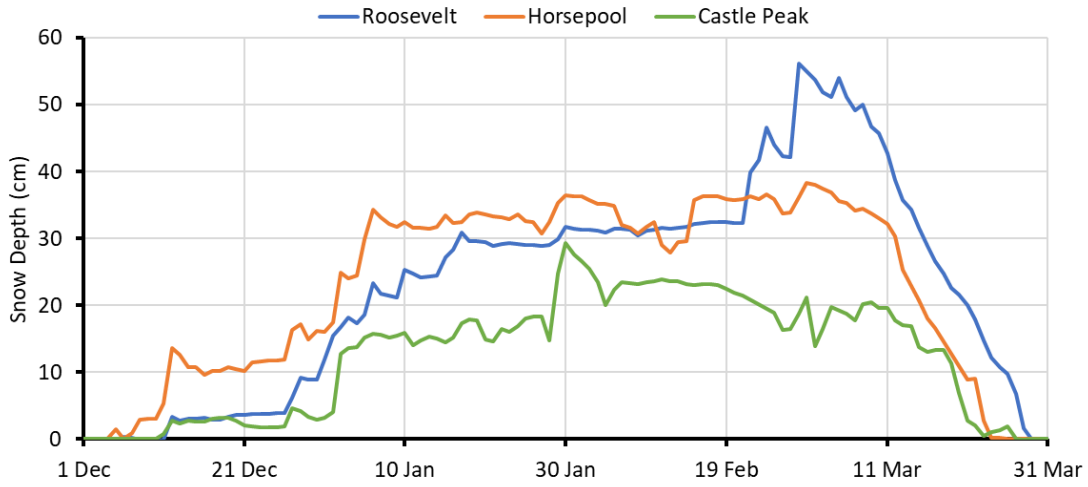

Figure 3-11. Snow depth at the Roosevelt, Horsepool, and Castle Peak stations during winter 2022-23.

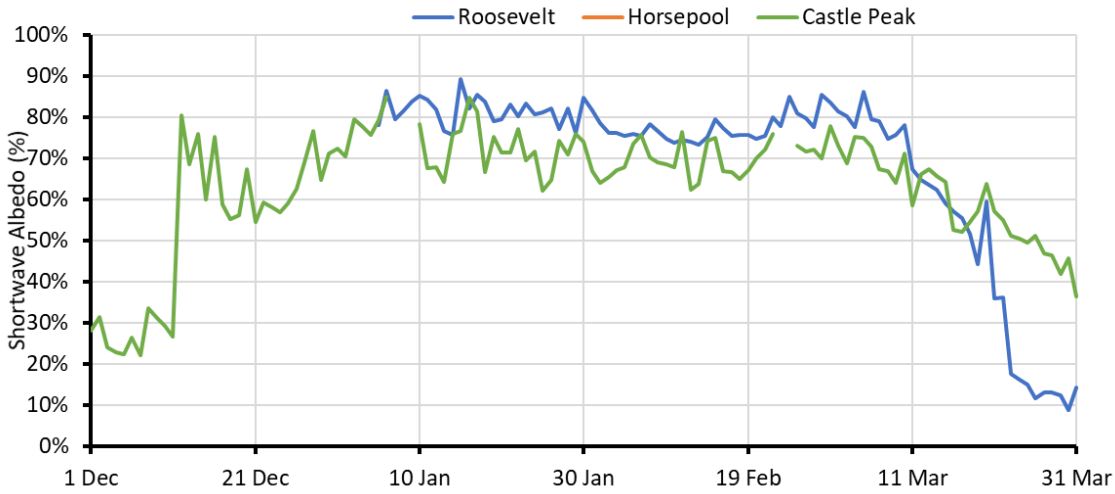

Figure 3-12. Shortwave albedo at the Roosevelt and Castle Peak stations during winter 2022-23. Shortwave radiation is visible light from the sun. Albedo is the percentage of radiation that is reflected by the earth's surface.

Roosevelt had fewer ozone exceedance days and lower fourth-high daily maximum ozone than Horsepool and Castle Peak (Table 3-3; Figure 3-13). This was the case even though NO_X and non-methane hydrocarbons were both higher at Roosevelt than at Horsepool and even though snow depth and albedo were similar at all sites. The difference between daytime and nighttime ozone was also greater in Roosevelt than at Horsepool and Castle Peak, as has been observed in previous winters. We expect that this occurred because the atmosphere at Roosevelt has more NO_X than is needed for ozone production. Too much NO_X can allow NO_X to react with and destroy ozone, suppressing ozone concentrations. At night, when no photochemistry occurs, ozone is not formed, but NO_X can still react with and destroy ozone, leading to the larger NO_X reduction at night in Roosevelt compared to the other locations.

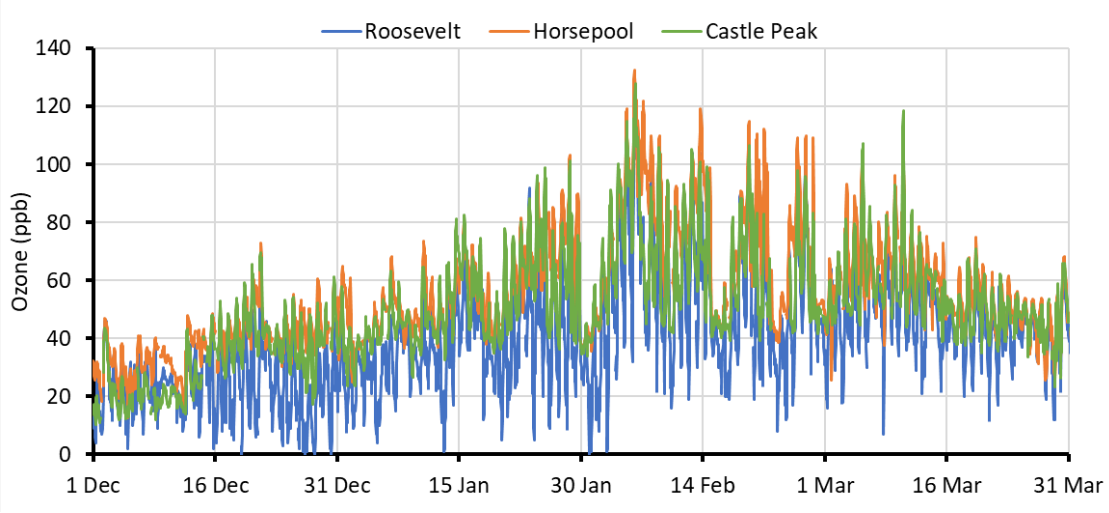

Figure 3-13. Hourly average ozone measured at Roosevelt, Horsepool, and Castle Peak during winter 2022-23.

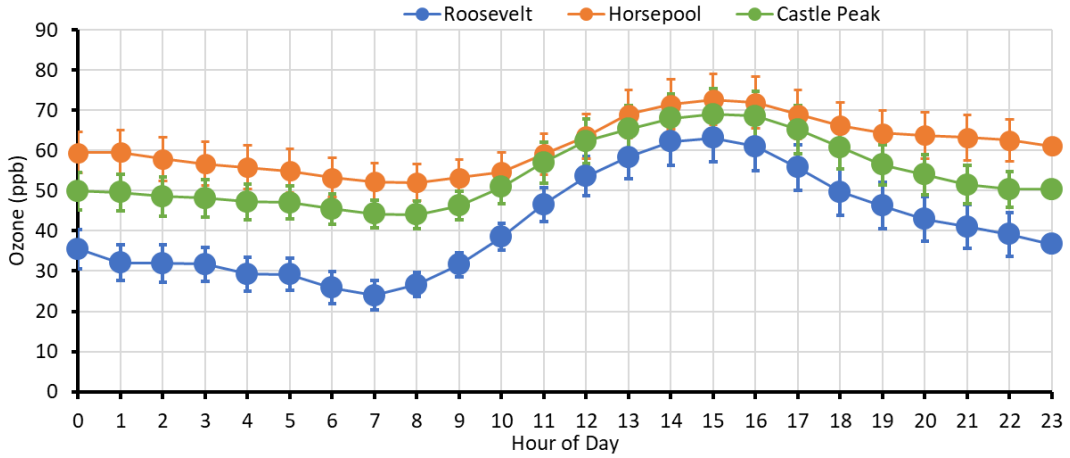

Figure 3-14. Average ozone at Roosevelt, Horsepool, and Castle Peak during each hour of the day during inversion episodes that occurred during winter 2022-23. Whiskers represent 95% confidence intervals.

3.2.4. Speciated Volatile Organic Compounds

This section focuses on measurements of individual organic compounds measured from whole air canister samples (Section 3.2.4) and DNPH cartridge samples (Section 3.2.5).

As in previous years, organic compounds in the atmosphere at field sites were dominated by alkanes, especially lighter alkanes (Figure 3-15 and Figure 3-16). Benzene, toluene, xylenes, and other aromatics were relatively low, and C8 and larger aromatics were rarely observed. The organic compound speciation at all sites was similar, indicating that the locations were all influenced by the same general source type (oil and natural gas production).

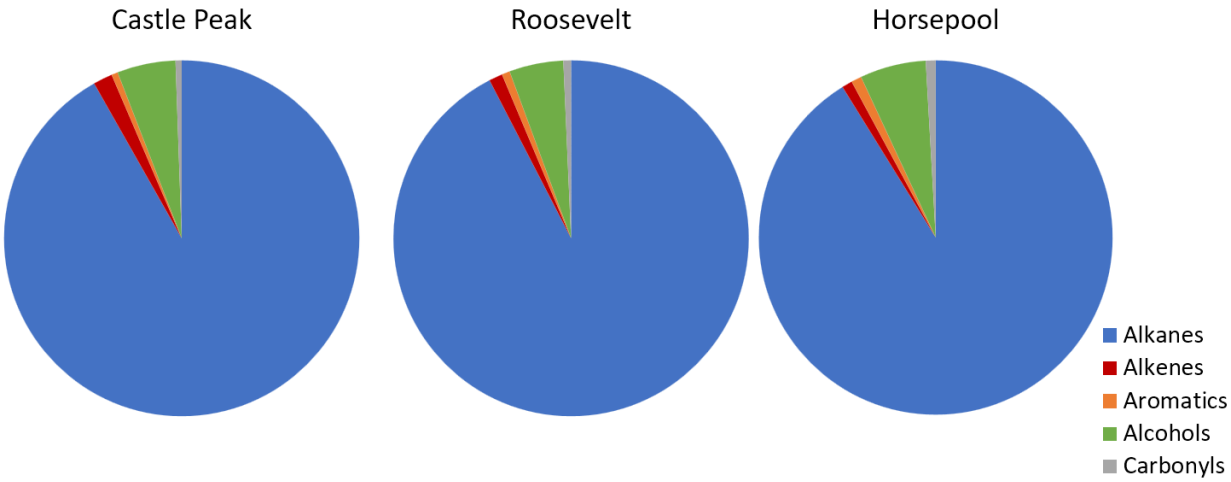

Figure 3-15. Percent by volume of measured organics at Castle Peak, Horsepool, and Roosevelt during winter 2022-23 comprised of alkanes, alkenes, aromatics, alcohols, and carbonyls.

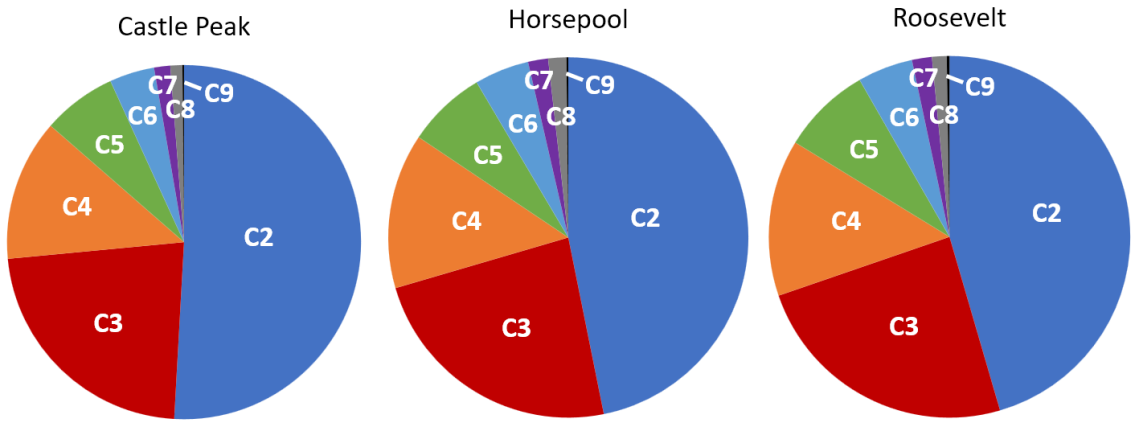

Figure 3-16. Percent by volume of measured non-methane hydrocarbons at Castle Peak, Horsepool, and Roosevelt during winter 2022-23 comprised of compounds containing 2-9 carbon atoms (i.e., C2-C9; excludes alcohols and carbonyls).

Hydrocarbon concentrations at Roosevelt, Horsepool, and Castle Peak generally tracked each other and tended to be higher during winter inversion periods (Figure 3-17). Roosevelt's total non-methane hydrocarbons, measured as the sum of individual compounds, were 33% higher than at Horsepool (a statistically significant difference, $p = 0.04$ for a t-test), whereas Castle Peak was only 8% higher than Horsepool, a difference that was not significant (Figure 3-19).

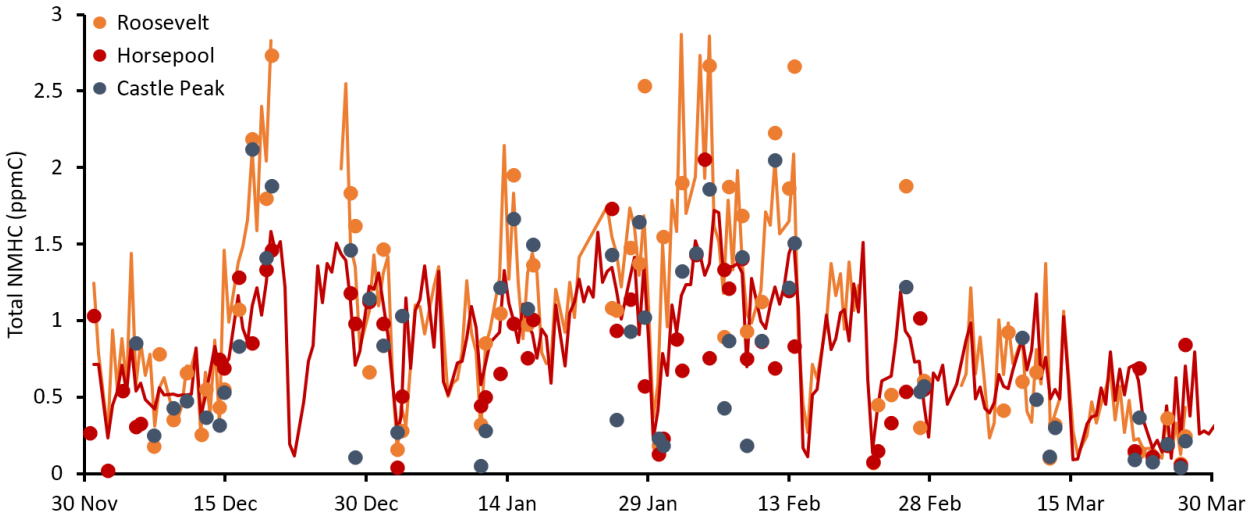

Figure 3-17. Time series of total non-methane hydrocarbons (NMHC) at Roosevelt, Horsepool, and Castle Peak during winter 2022-23. Units are parts per million of carbon atoms. Circles show the sum of speciated organic compounds derived from 3-hr canister measurements. Lines show 12-hour averages from continuously operating gas chromatographs.

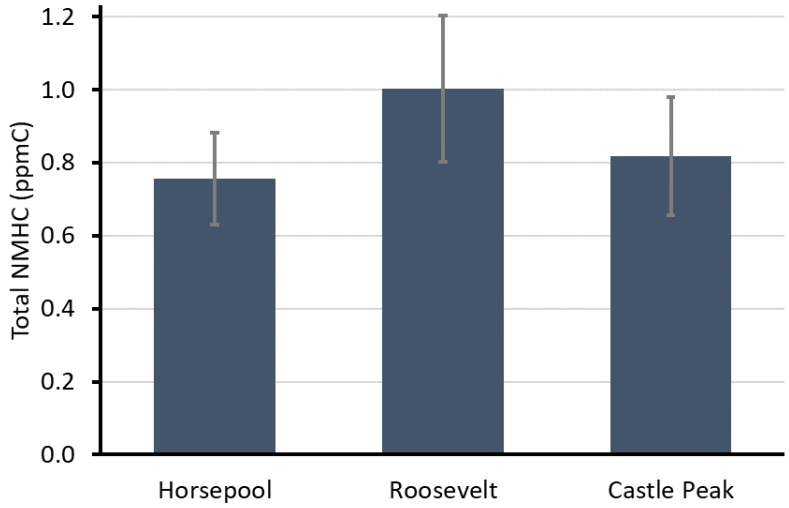

Figure 3-18. Average total NMHC at Horsepool, Roosevelt, and Castle Peak. Values are the sum of individual compounds measured from canister samples in units of parts per million of carbon atoms. Whiskers show 95% confidence intervals.

Compared to Horsepool, non-methane hydrocarbons at Roosevelt and Castle Peak tended to include more C5-C8 alkanes relative to lighter alkanes and aromatics. While the differences were small (see Figure 3-18), they were meaningful and are due to a higher prevalence of C5-C8 hydrocarbons in emissions from oil wells relative to gas wells (Wilson et al., 2020).

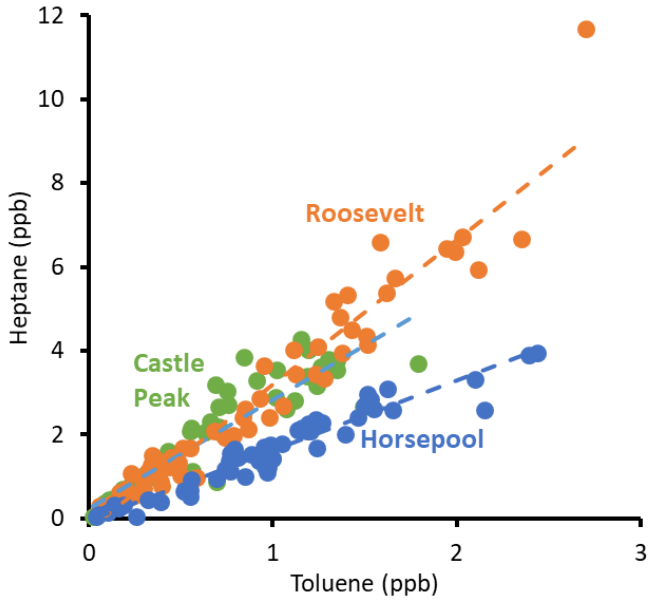

Figure 3-19. Heptane versus toluene at Horsepool, Roosevelt, and Castle Peak.

3.3. Acknowledgments

This work was funded by the Utah Legislature and Uintah Special Service District 1.

4. Summertime Air Quality

Author: Seth Lyman

Only one exceedance of the U.S. Environmental Protection Agency (EPA) ozone standard of 70 ppb occurred during the spring and summer seasons in 2023. Ozone was 71 ppb in Myton on 24 April and was close to exceeding the standard at several other sites on that day. Figure 4-1 shows a time series of all sites that operated in the Basin during this period, and Table 4-1 shows a list of fourth-high daily maximum 8-hour average ozone at those stations for the spring and summer seasons. These data are from EPA's real-time AirNowTech database, are not final, and may change.

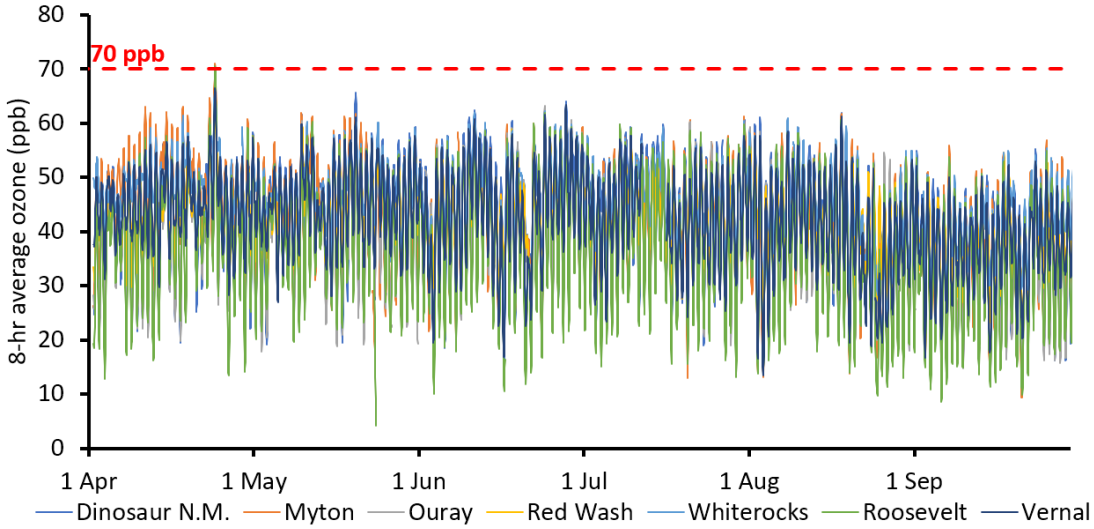

Figure 4-1. 8-hr moving average ozone at all monitoring stations that operated in the Uinta Basin during summer 2023. The red dashed line shows the EPA ozone standard of 70 ppb.

Table 4-1. Fourth-highest daily maximum 8-hour average ozone for the period of 1 April through 30 September 2023 at all monitoring stations that were operating in the Uinta Basin.

	4th-high 8-hr ozone
Dinosaur N.M.	62
Myton	63
Ouray	61
Red Wash	60
Whiterocks	62
Roosevelt	61
Vernal	61

Figure 4-2 shows a time series of basin-wide daily maximum 8-hr average ozone along with basin-wide maximum $PM_{2.5}$ for 1 April through 30 September 2023. Smoke emitted from fires is rich in $PM_{2.5}$

(visible smoke *is* mostly $PM_{2.5}$). Figure 4-2 shows that $PM_{2.5}$ increased to more than 30 µg m^{-3} on one day in May, but it did not approach the EPA standard (the standard is for a 24-hr average).

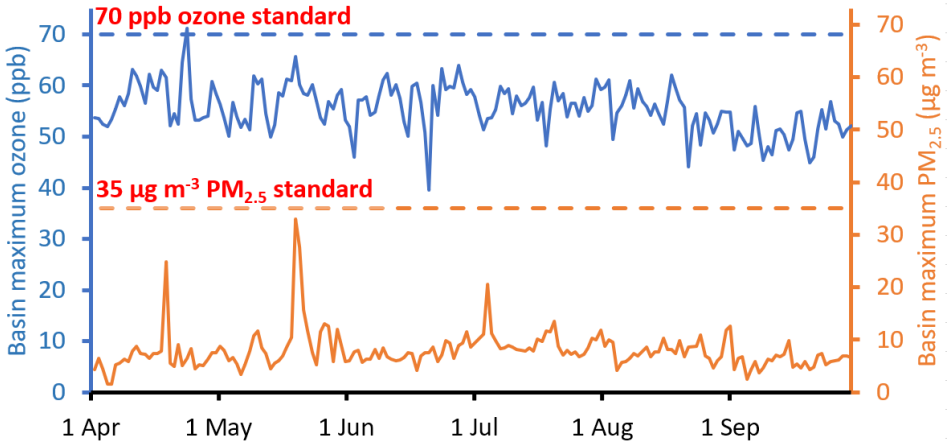

Figure 4-2. Maximum ozone measured at any site in the Uinta Basin and Basin-average $PM_{2.5}$ (average of Vernal and Roosevelt) for 1 April through 30 September 2023. All values are 8-hr moving averages. The EPA ozone standard of 70 ppb and the EPA $PM_{2.5}$ standard of 35 µg m^{-3} are also shown. The $PM_{2.5}$ standard is for a 24-hr average.

$PM_{2.5}$ was low on 24 April, the Myton ozone exceedance day, indicating that wildfires were not to blame for the exceedance. Snow had long since melted, so local ozone production was not the likely cause, either. Instead, we expect that the high ozone on 24 April was due to intrusion of ozone-rich air from the stratosphere.

4.1. Acknowledgments

This work was funded by the Utah Legislature and Uintah Special Service District 1.

5. Air Quality Trends

5.1. Introduction

The purpose of this section is to track changes in Uinta Basin air quality, including changes in pollutant levels in the atmosphere and the reasons for those changes. We seek to answer:

1. Are levels of ozone and its precursors changing over time?
2. What are the causes of any changes that occur?

In general, temporal trends in ozone and its precursors, if they exist, can be expected to be caused by changes in meteorology or changes in pollutant emissions. In this section, we use statistical methods to attempt to separate the two.

5.2. Ozone

Figure 5-1 shows a time series of ozone concentrations at several sites in the Uinta Basin from July 2009 (when continuous measurements began) through March 2023. As the figure shows, the 4th-highest 8-hr average ozone concentration was greater than the EPA standard at at least one location during eight of the fourteen winters for which measurement data are available (57%). Ozone statistics from the five sites shown in Figure 5-1 are summarized in Table 5-1.

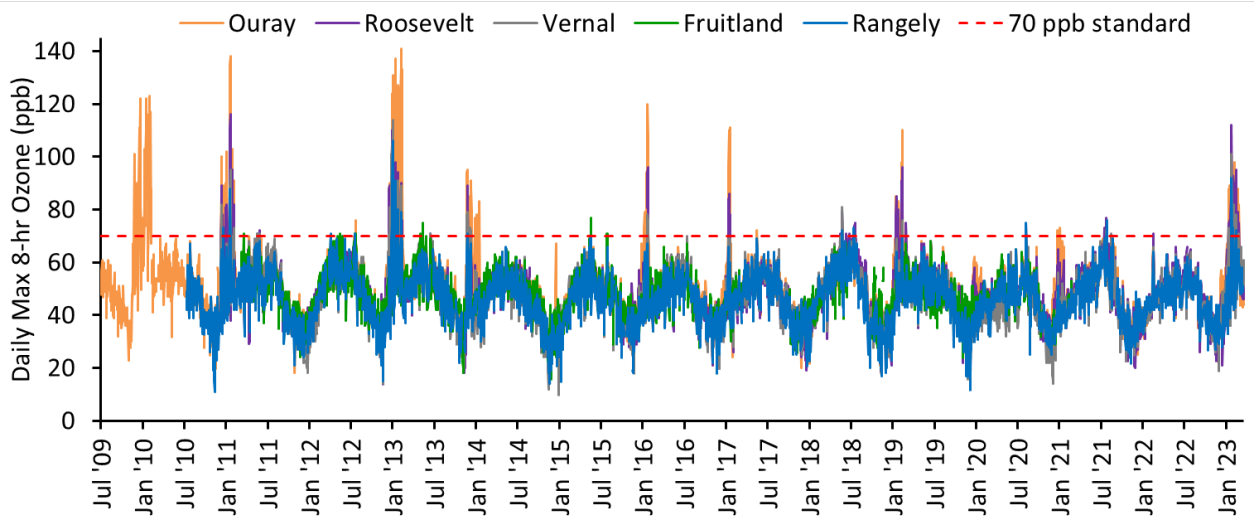

Figure 5-1. Time series of daily maximum 8-hr average ozone concentration at five sites in the Uinta Basin from July 2009 through March 2023. The red dashed line shows 70 ppb, the EPA standard for ozone.

Table 5-1. Ozone summary statistics for five sites in the Uinta Basin over 15 calendar years. All values were calculated from daily maximum 8-hr average concentrations.For 2023, only data through 31 March are shown.

Year	Site	Mean	Median	Max	Min	4th High Daily Max	Exceedance Days (>70 ppb)
2009 (July-Dec)	Ouray	46	47	101	23	67	1
	Fruitland	--	--	--	--	--	--
	Vernal	--	--	--	--	--	--
	Roosevelt	--	--	--	--	--	--
	Rangely	--	--	--	--	--	--
2010	Ouray	56	54	123	20	117	45
	Fruitland	--	--	--	--	--	--
	Vernal	--	--	--	--	--	--
	Roosevelt	--	--	--	--	--	--
	Rangely	41	42	67	11	58	--
2011	Ouray	53	52	138	18	119	28
	Fruitland	48	50	71	24	65	1
	Vernal	55	55	95	33	84	12
	Roosevelt	55	54	116	29	103	21
	Rangely	48	50	88	21	73	4
2012	Ouray	48	50	76	18	67	1
	Fruitland	49	49	71	26	70	3
	Vernal	45	46	68	14	64	0
	Roosevelt	49	51	70	14	67	0
	Rangely	46	47	71	15	69	2
2013	Ouray	57	54	141	24	132	52
	Fruitland	49	50	75	18	69	2
	Vernal	52	52	114	20	102	32
	Roosevelt	56	54	110	25	104	35
	Rangely	50	50	106	22	91	13
2014	Ouray	48	50	91	17	79	8
	Fruitland	47	49	65	16	64	0
	Vernal	43	45	64	12	62	0
	Roosevelt	46	49	63	16	62	0
	Rangely	44	46	66	14	62	0
2015	Ouray	45	47	71	21	68	2
	Fruitland	46	46	77	23	69	3
	Vernal	43	43	67	10	64	0
	Roosevelt	42	42	66	14	60	0
	Rangely	43	45	70	15	66	0
2016	Ouray	49	48	120	20	96	11
	Fruitland	47	47	67	30	62	0
	Vernal	47	46	78	20	73	5

Year	Site	Mean	Median	Max	Min	4th High Daily Max	Exceedance Days (>70 ppb)
	Roosevelt	47	47	96	20	81	5
	Rangely	45	45	67	18	61	0
2017	Ouray	50	50	111	20	103	11
	Fruitland	41	42	57	26	53	0
	Vernal	48	49	69	25	68	0
	Roosevelt	48	48	86	24	78	8
	Rangely	47	48	69	25	64	0
2018	Ouray	48	48	72	18	67	1
	Fruitland	47	46	68	22	64	0
	Vernal	48	50	81	20	69	2
	Roosevelt	49	49	79	18	71	8
	Rangely	47	48	73	17	68	2
2019	Ouray	50	51	110	21	98	16
	Fruitland	48	49	68	24	64	0
	Vernal	46	48	76	16	65	1
	Roosevelt	50	51	96	19	87	10
	Rangely	45	47	70	12	64	0
2020	Ouray	49	48	74	26	65	1
	Fruitland	47	47	72	28	64	1
	Vernal	42	41	67	14	63	0
	Roosevelt	46	47	71	24	63	1
	Rangely	45	45	75	25	65	2
2021	Ouray	50	50	73	21	72	5
	Fruitland	43	44	53	34	48	0
	Vernal	47	47	72	23	68	3
	Roosevelt	48	48	77	20	72	4
	Rangely	46	45	76	22	69	1
2022	Ouray	46	46	68	23	64	0
	Vernal	46	46	66	19	63	0
	Roosevelt	47	48	71	20	66	1
	Rangely	45	46	64	27	62	0
2023 (Jan-Mar)	Ouray	62	60	102	35	91	27
	Vernal	56	54	101	33	82	12
	Roosevelt	60	57	112	29	93	23
	Rangely	51	51	92	32	71	5

Utah DAQ also measured ozone in Vernal during 2006 and 2007, but those data are not publicly available and are not included here. No wintertime exceedances of the ozone standard were measured in Vernal during that period. Summertime exceedances are considered in Section 4 of this document.

The three-year average of annual fourth-highest daily maximum 8-hr averages for a given site (using calendar years) is referred to as a design value. The design value is the value EPA uses to determine whether an airshed is in attainment of the 70 ppb ozone standard (design values of 71 and above are out of attainment). EPA used the 2014-16 period in their 2018 decision to designate the Uinta Basin as a nonattainment area for ozone. Table 5-2 shows the ozone design value for the past several three-year periods for the same monitoring stations shown in Figure 5-1, as well as for the Whiterocks station. The design value for 2021-23 shown in Table 5-2 only includes data through 31 March. Note that these are not official design values. Regulatory agencies may exclude some data or consider other criteria in the process of determining official design values.

Table 5-2. Average of the fourth-highest daily maximum 8-hr average ozone during three consecutive calendar years for several monitoring stations in the Uinta Basin (a.k.a. ozone design values). Only 2023 data collected through March are used. Values in exceedance of the EPA standard are in bold font. Values shown may include summertime ozone events that could be excluded from regulatory consideration.

Station	Ouray	Fruitland	Vernal	Roosevelt	Rangely	Whiterocks
2013-15	**93**	67	**76**	**75**	**73**	66
2014-16	**81**	65	66	67	63	**71**
2015-17	**89**	61	68	**73**	62	**71**
2016-18	**88**	59	70	**76**	64	**72**
2017-19	**89**	60	67	**78**	63	67
2018-20	**76**	64	65	**73**	65	67
2019-21	**78**	58	65	**74**	66	66
2020-22	67		64	67	65	65
2021-23	**75**		**71**	**77**	67	**72**

Figure 5-2 and Figure 5-3 show the number of ozone exceedances and the annual fourth-highest daily maximum 8-hr average ozone, respectively, for each entire calendar year at the same monitoring stations shown in the previous tables and figures. These figures show that air quality is extremely variable from year to year and across measurement stations in the Uinta Basin. For example, Ouray experienced more than 40 exceedance days in 2010 and 2013 but had only one in 2012, 2018, and 2020, and only two in 2015. Some exceedances shown in Figure 5-2 occurred during summer, not winter, and the summertime exceedances were likely due to intrusions of ozone-rich stratospheric air or wildfires (see Section 4).

Figure 5-3 shows that the fourth-highest daily maximum 8-hr average ozone at the five sites shown is always about 60 ppb or higher. The natural summertime background ozone level in the intermountain western United States is 60 to 65 ppb (Parrish et al., 2022). During years with low wintertime ozone (2012, 2015, 2018, 2020, and 2022), the highest ozone is observed during summer and is usually in the range of 60-65 ppb. Ozone is also spatially variable. Figure 5-3 shows that Ouray and Roosevelt tend to have higher ozone than Vernal and Rangely.

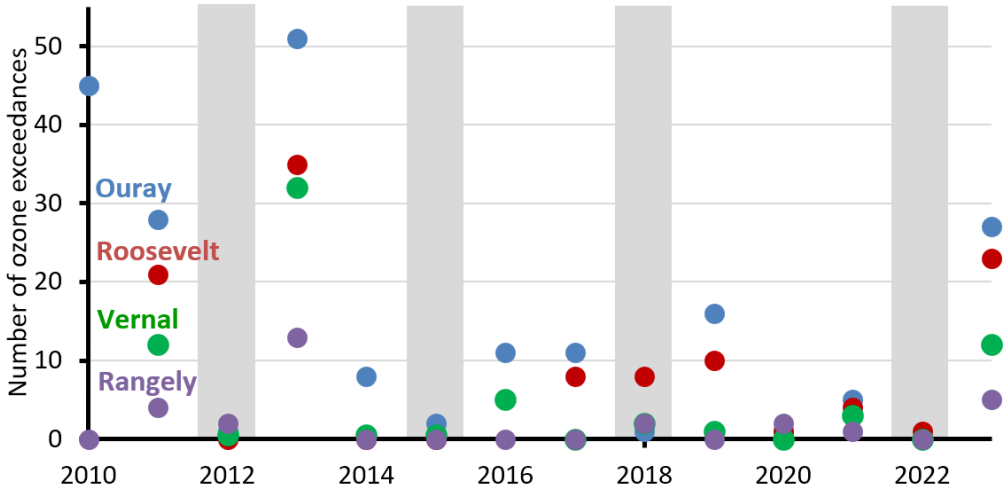

Figure 5-2. Number of annual ozone exceedances at five sites from 2010 through March 2023. The grey bars indicate years with little snow cover.

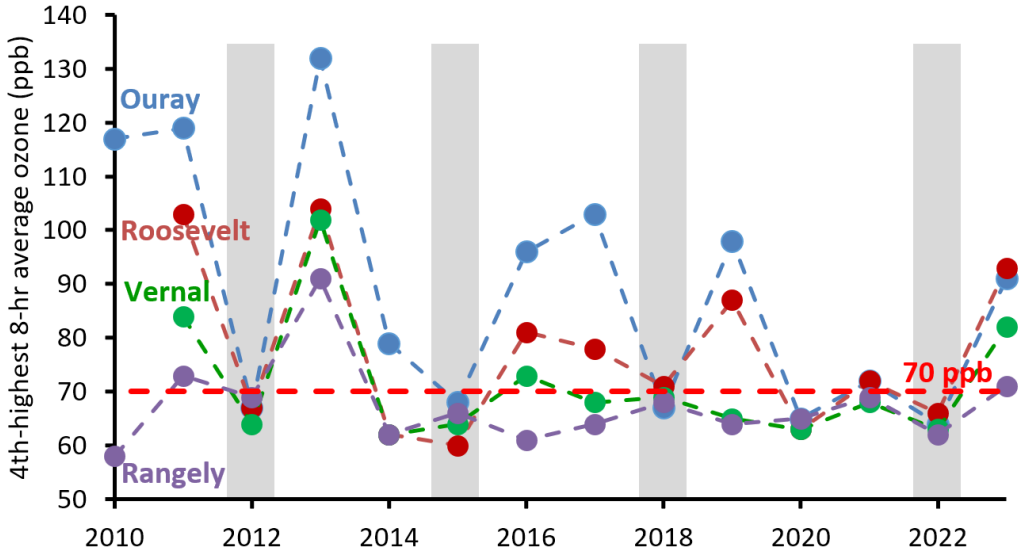

Figure 5-3. Annual fourth-highest 8-hr average daily maximum ozone at five sites from 2010 through March 2023. The red dashed line indicates 70 ppb, the current EPA standard for ozone. The grey bars indicate years with little snow cover.

5.3. Particulate Matter

Figure 5-4 shows a time series of all $PM_{2.5}$ measurements that have ever been collected in the Uinta Basin. Exceedances of the EPA $PM_{2.5}$ standard sometimes occur during winter but are more common during summer months. These summertime spikes in $PM_{2.5}$ concentrations are typically caused by wildfire smoke.

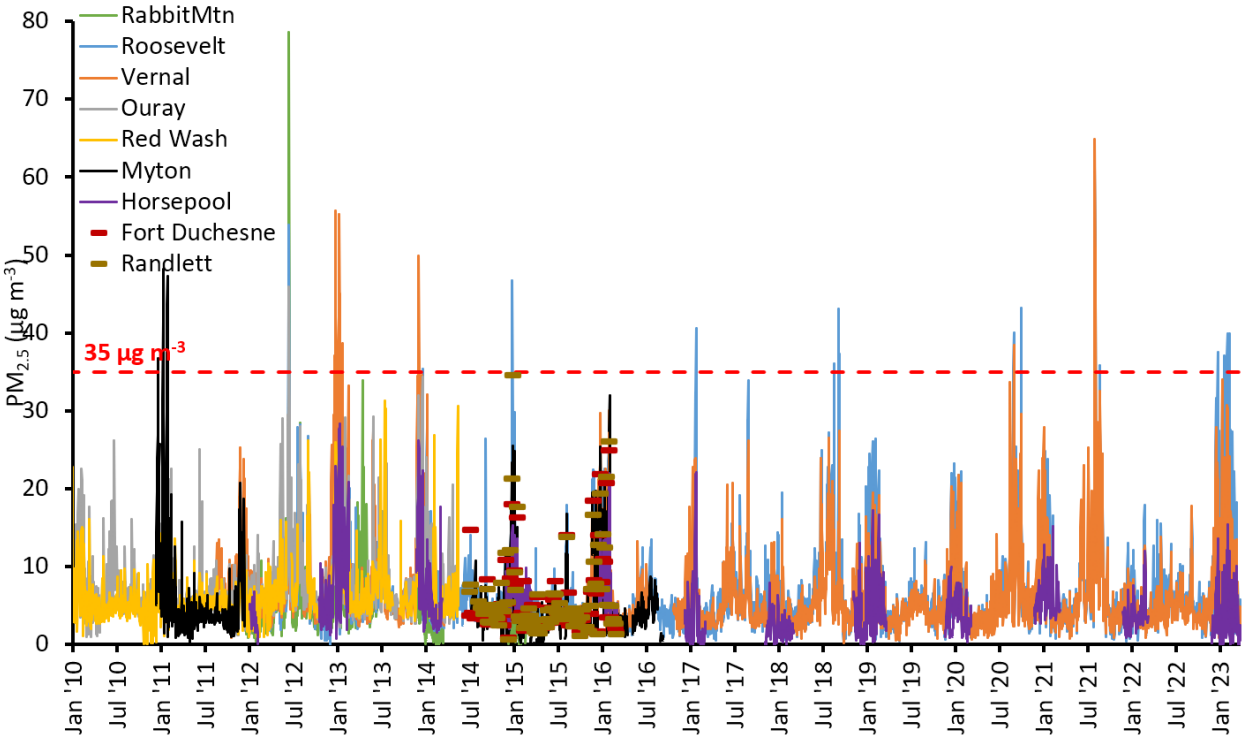

Figure 5-4. Time series of daily 24-hr average $PM_{2.5}$ concentrations at nine sites in the Uinta Basin, October 2009-March 2022. The red dashed line shows 35 µg m^{-3}, the EPA standard for $PM_{2.5}$.

5.4. Trends in the Capacity of Winter Inversion Episodes to Produce Ozone

5.4.1. Ozone Exceedance Days

The number of exceedances of the EPA ozone standard exhibited a decreasing trend (Mansfield and Lyman, 2021) from 2010 through 2022. Figure 5-2 shows all exceedance days by calendar year, including those that occur during summer. The decreasing trend is clearer in Figure 5-5, which shows only wintertime exceedances by winter season. Mansfield and Lyman (2021) showed that NO_X emissions also decreased over the same period, and Lin et al. (2021) showed that methane emissions also decreased over the same period. Section 12 shows that non-methane organic compound emissions also declined over the same period. Mansfield and Lyman (2021) attributed the decline in ozone and its precursors to (1) a decline in energy production (which was driven mostly by a decline in natural gas production) and (2) regulatory and voluntary action by the oil and gas industry to reduce emissions.

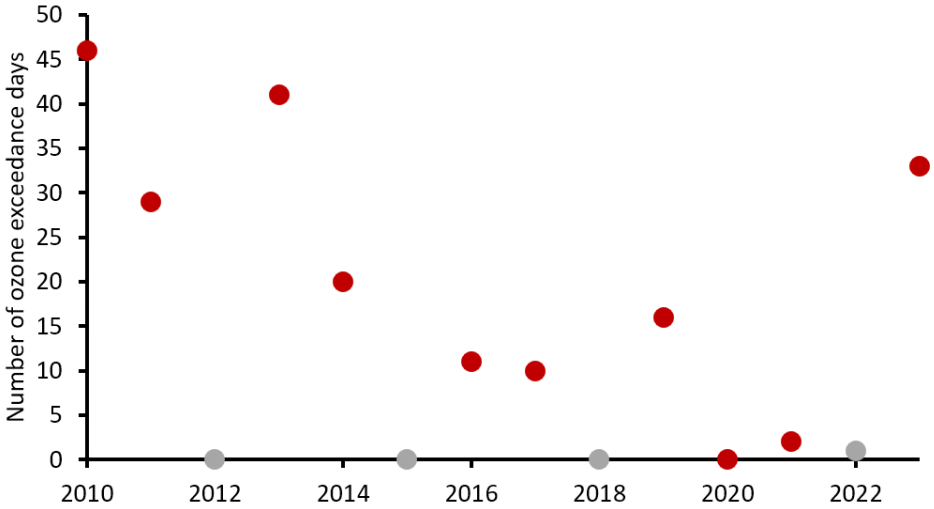

Figure 5-5. Number of ozone exceedance days per winter season. The number of exceedance days at the monitoring station in the Basin with the maximum number in any given winter season is shown. Winters with at least 15 days with snow depth greater than 5 cm are shown in red, and other years are shown in grey.

Figure 5-5 shows that the declining trend in winter ozone reversed sharply in 2023 when deep snow cover and many strong inversions allowed for many exceedance days (also see Section 3). Section 12 shows methane, NO_x, and non-methane organic compound emissions increased in 2021 and 2022, so increased emissions may also be the cause of high ozone in 2023.

5.4.2. Dependence on Meteorological Conditions

As Figure 5-5 shows, significant local production of wintertime ozone has never occurred and cannot occur without significant snow cover across the Uinta Basin (Oltmans et al., 2014). Indeed, the number of wintertime ozone exceedance days is positively correlated with snow cover ($r^2 = 0.49$). The number of winter exceedance days is more strongly correlated with the season-average inversion strength, however (Figure 5-6), since snow cover sometimes exists in stormy or windy conditions that don't allow for strong winter inversion episodes, but strong winter inversion episodes almost never occur without snow cover, and winter ozone needs inversions and snow to form (Mansfield, 2018).

Figure 5-6 plots the number of ozone exceedance days per season against the pseudo-lapse rate. The lapse rate is the inverse of the change in temperature with altitude. The lower the lapse rate, the stronger the inversion. Typically, lapse rates are measured by releasing temperature sensors attached to helium balloons, but these measurements are expensive and have rarely been performed in the Uinta Basin. As an alternative, Mansfield (2018) used temperature measurements from surface stations at different elevations to approximate the lapse rate (a "pseudo" lapse rate). We follow Mansfield's method of determining pseudo-lapse rates in this section.

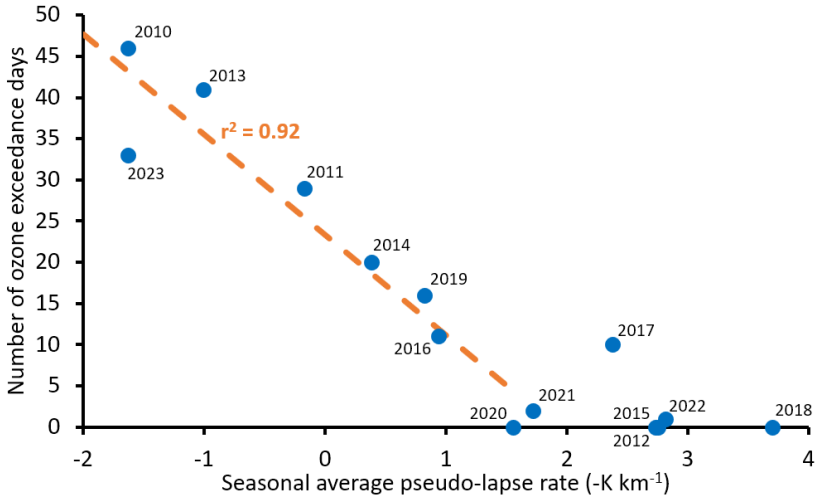

Figure 5-6. Number of ozone exceedance days per winter season versus seasonal average pseudo-lapse rate. Pseudo-lapse rate is a measure of inversion strength (more negative value indicates stronger inversion) and is discussed at length by Mansfield (2018). The orange dashed line is a linear regression that only includes seasonal average pseudo-lapse rates less than 2 K km^{-1}.

Figure 5-7 shows the difference between actual ozone exceedance days per winter season and the number of exceedance days expected from the relationship shown in Figure 5-6. The figure shows an apparent decreasing trend over time, meaning that fewer exceedance days than expected have occurred in recent years. This could indicate that, for similar seasonal conditions, the capacity of the Uinta Basin atmosphere to produce ozone has decreased.

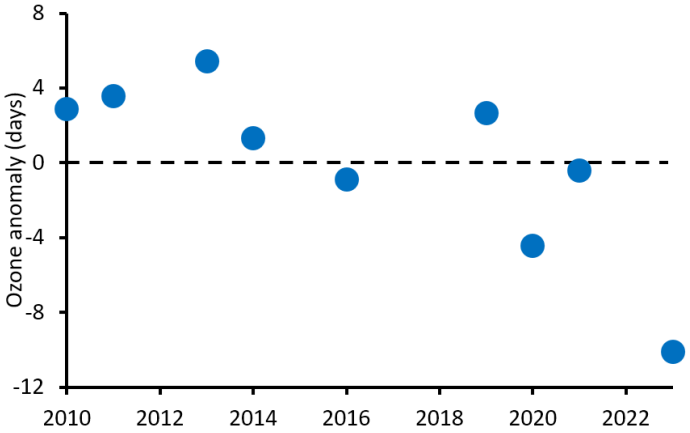

Figure 5-7. Number of excess ozone exceedance days per winter season relative to the amount expected from the relationship shown in Figure 5-6. Only years with seasonal average pseudo-lapse rates less than 2 K km^{-1} are shown.

5.4.3. Trends in Ozone Precursors

Mansfield and Lyman (2021) used a linear regression of daily maximum 8-hr average ozone against daily pseudo-lapse rate to "correct" ozone for inversion strength. Mansfield and Lyman (2021) found that the

daily pseudo-lapse rate and the daily maximum 8-hr average ozone for most winter seasons were correlated. They used the linear regression for each season to calculate the daily maximum 8-hr average ozone value that would be expected for a pseudo-lapse rate of -15 K km^{-1}in that season, and they called this metric $\langle[O_3]\rangle_{-15}$. Since the $\langle[O_3]\rangle_{-15}$ normalizes for the influence of inversion strength on ozone production, they assumed that year-to-year differences in $\langle[O_3]\rangle_{-15}$ were due to differences in ozone-forming emissions, not differences in meteorology. Mansfield and Lyman showed that $\langle[O_3]\rangle_{-15}$ declined from 2010 to 2020, and they attributed this decline to declines in NO_X and organic compound emissions.

Section 12 provides additional evidence that methane, NO_X, and non-methane hydrocarbon emissions decreased from 2010 through 2020, and it shows that emissions increased in 2021 and 2022. We applied the method of Mansfield and Lyman (2021) to these same compound groups in an attempt to track their emissions by a simpler means than those described in Section 12. We calculated linear regressions of the pseudo-lapse rate versus daily average methane, NO_Y (as a proxy for NO_X, since NO_Y is the sum of NO_X and its photochemical degradation products), and total non-methane hydrocarbons measured at Horsepool and Roosevelt. We calculated separate regression equations for each site for each year for which data were available. We omitted days with relatively uncertain pseudo-lapse rates ($r^2 < 0.3$ for the relationship between temperature and elevation).

The pseudo-lapse rate was predictive of the majority of the variability in methane, NO_Y, and non-methane hydrocarbons (r^2 or 0.58 ± 0.21, 0.60 ± 0.22, and 0.56 ± 0.17, respectively; average ± standard deviation). We determined residuals by subtracting predicted daily concentrations from measured concentrations. Daily average concentrations of methane, NO_Y, and non-methane organics were significantly correlated with temperature, wind speed, the number of consecutive inversion days, and the number of days since the winter solstice. The residuals, however, were not significantly correlated with any of these variables, which indicates that regression against the pseudo-lapse rate was adequate to account for the influence of these other variables on daily average concentrations.

Following Mansfield and Lyman (2021), we applied site-and-year-specific regression equations to determine daily average concentrations that would be expected in each winter season at a pseudo-lapse rate of -15 K km^{-1}. The results are shown in Figure 5-8 through Figure 5-10. Since this method takes into account the propensity of methane, NO_Y, and non-methane hydrocarbon concentrations to increase under inversion conditions, and since no other significant meteorological correlations existed after inversion strength was taken into account in this way, we attribute the temporal trends in the figures to changes in emissions. We acknowledge that the trends for Horsepool and Roosevelt shown in the figures may be local. More work is needed to verify whether these trends hold true for the Uinta Basin as a whole.

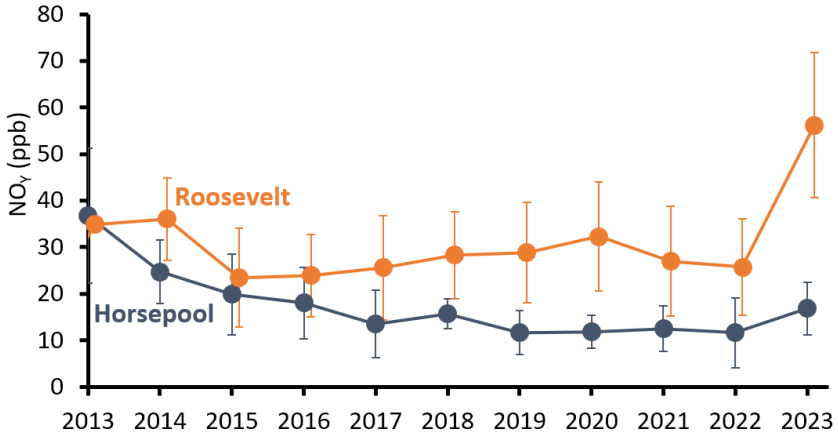

Figure 5-8. Daily average NO_Y (a proxy for NO_X) at a pseudo-lapse rate of -15 K km^{-1}, as predicted from year- and site-specific linear regressions of NO_Y against the pseudo-lapse rate. Whiskers show the combined uncertainty of the pseudo-lapse rate calculation and the NO_Y measurement.

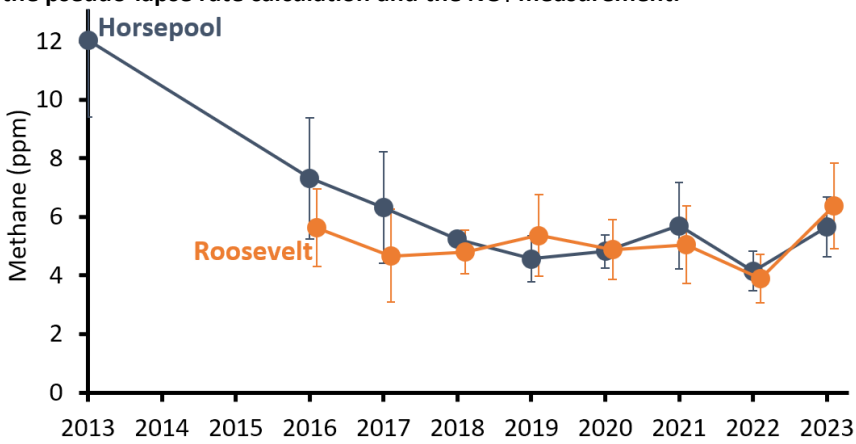

Figure 5-9. Daily average methane at a pseudo-lapse rate of -15 K km^{-1}, as predicted from year- and site-specific linear regressions of methane against the pseudo-lapse rate. Whiskers show the combined uncertainty of the pseudo-lapse rate calculation and the methane measurement.

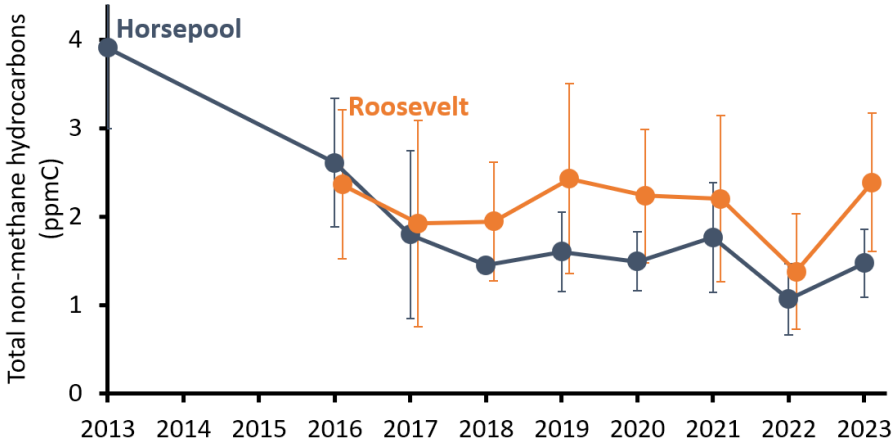

Figure 5-10. Daily average total non-methane hydrocarbons at a pseudo-lapse rate of -15 K km^{-1}, as predicted from year- and site-specific linear regressions of non-methane hydrocarbons against the pseudo-lapse rate. Whiskers show the combined uncertainty of the pseudo-lapse rate calculation and the non-methane hydrocarbons measurement.

The results for Horsepool are similar to the findings in Section 12, the findings of Mansfield and Lyman (2021), and the findings of Lin et al. (2021), which all show that emissions of methane, NO_X, and non-methane hydrocarbons have declined since 2013. As in Section 12, the results for Horsepool show an increase in methane and non-methane hydrocarbons in 2021, though the increase is smaller than in Section 12. Figure 5-8 through Figure 5-10 do not show a meaningful trend in any of the compounds at Horsepool after 2017, even though energy production and oil and gas activity changed considerably over that time (see Section 12 and the full report to which it links).

No clear trend exists for methane and non-methane hydrocarbons at Roosevelt, perhaps because of the site's shorter hydrocarbon measurement record. The NO_Y trend at Roosevelt is dominated by a strong upswing in winter 2023. Several large flares at oil wells were active near the Roosevelt site during winter 2023, and these could be the cause of high NO_Y in 2023.

5.4.4. Searching for Trends in the Capacity for Ozone Production

As mentioned above, Mansfield and Lyman (2021) used linear regression to predict daily maximum 8-hr average ozone at a pseudo-lapse rate of -15 K km^{-1}, and they assumed that year-to-year variations in ozone predicted by this method were the result of changes in emissions of NO_X and organic compounds. We followed the method of Mansfield and Lyman, and Figure 5-11 shows the results. Figure 5-11 is similar to Figure 8 in Mansfield and Lyman, except that we did not use all of the monitoring stations they used, and our figure extends to three additional years.

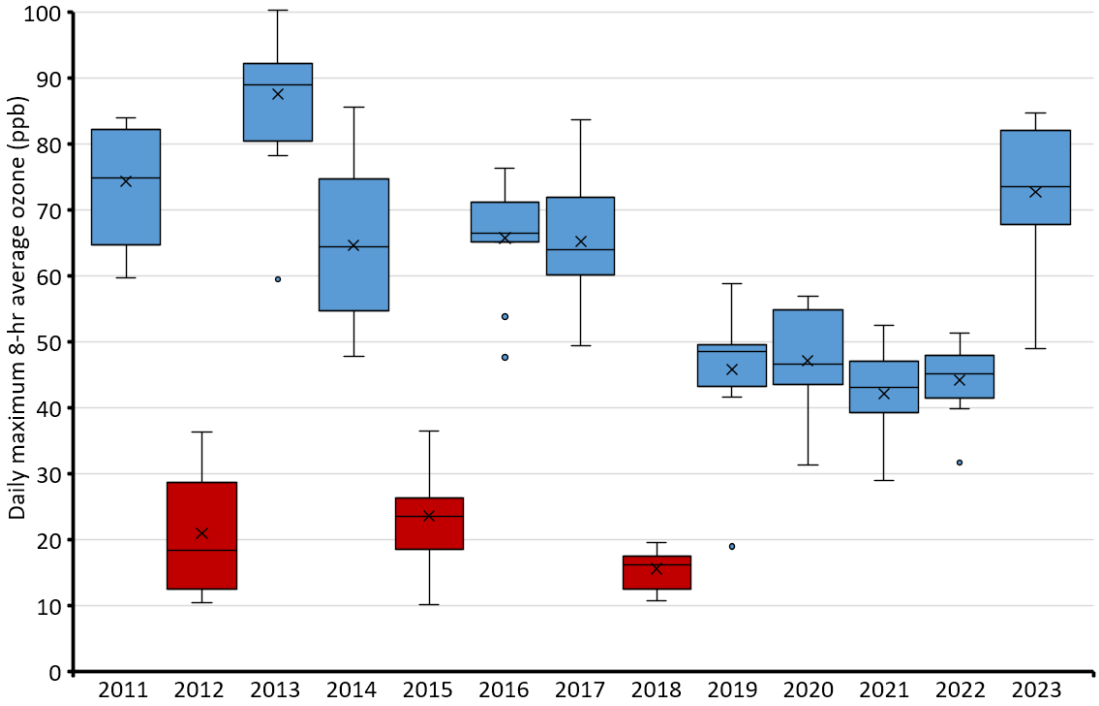

Figure 5-11. Box and whisker plot of daily maximum 8-hr average ozone at a pseudo-lapse rate of -15 K km^{-1}, as predicted from year- and site-specific linear regressions of ozone against the pseudo-lapse rate. The box and whiskers for each year show the variability in predicted ozone for the stations listed in Table 3-1. The extents of the boxes show 25th and 75th percentiles, the whiskers show the full extent of the data (except outliers), the lines within the boxes show medians, the X's in the boxes show averages, and the small circles are outliers. Years 2012, 2015, and 2018 are shown in red because they had significant inversion periods without snow cover, leading to a reversal of the typical regression slope. See additional discussion of these years in Mansfield and Lyman (2021).

Like Figure 8 in Mansfield and Lyman (2021), Figure 5-11 shows a decreasing trend through 2020. It also shows a continuation of the trend through 2022 and then a large increase in predicted ozone in 2023. If, as asserted by Mansfield and Lyman, the ozone trends in the figure were due to trends in emissions, a large increase in ozone precursor emissions in 2023 would be needed to account for the increase in predicted ozone. With the exception of NO_Y at Roosevelt, however, Figure 5-8 through Figure 5-10 do not provide any evidence for such an increase. What is more, Figure 3-14 shows that high NO_X at Roosevelt very likely led to lower, not higher, ozone because the site is NO_X-saturated. We conclude from this that formation of winter ozone is dependent on more than just the pseudo-lapse rate and that a more sophisticated approach is needed to separate the influence of meteorological conditions on ozone production from the influence of emissions. We also note that the trend in Figure 5-11 is opposite to the trend in Figure 5-7. Both figures use pseudo-lapse rate to factor out the influence of meteorological conditions on winter ozone production, but they use the metric in different ways and come to opposite conclusions for winter 2023.

We determined residuals by subtracting ozone predicted via the relationship with pseudo-lapse rate from measured concentrations. The residuals were significantly correlated with the number of days

since the winter solstice (r^2 = 0.42 ± 0.03), the number of consecutive inversion days (r^2 = 0.42 ± 0.05; calculated as the number of consecutive days with pseudo-lapse rate less than zero), and the amount of total ultraviolet radiation (incoming + outgoing) measured at Horsepool (r^2 = 0.42 ± 0.02). We performed a multiple linear regression to account for the influence of pseudo-lapse rate and these additional variables. This method predicted daily maximum 8-hr average ozone more accurately (R^2 = 0.62 ± 0.08) than when only pseudo-lapse rate was used as a predictor (R^2 = 0.22 ± 0.03). The multiple linear regression method predicted site-specific annual average daily maximum ozone (on days with pseudo-lapse rate less than zero only) with high accuracy (R^2 = 0.98). Figure 5-12 shows measured versus linear regression-predicted ozone for all days and sites for which data are available.

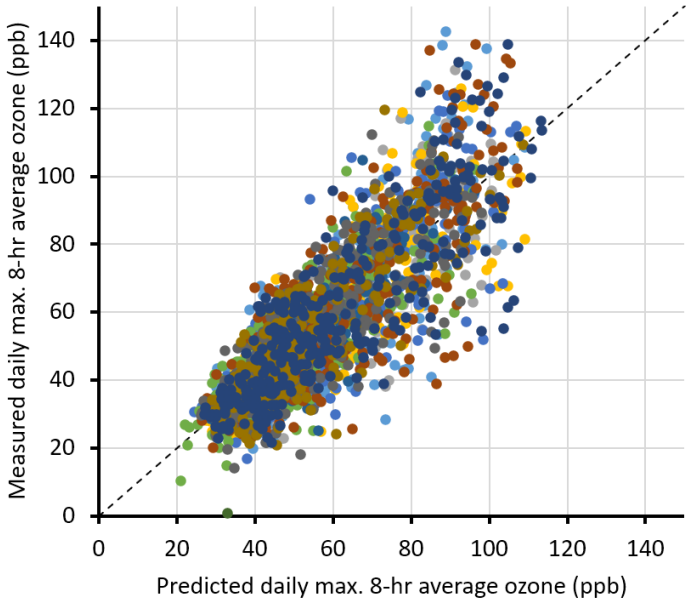

Figure 5-12. Measured daily maximum 8-hr average ozone at all the stations listed in Table 3-1 versus ozone predicted by multiple linear regression. The dashed line shows a 1:1 relationship.

Figure 5-13 shows annual average residuals (measured ozone minus predicted) for the multiple linear regression. In contrast to Figure 5-7 and Figure 5-11, it doesn't show any interannual trend. The residual for year 2023 is negative, meaning that measured ozone was lower than predicted, but this is also true for 2013 and 2019, the other two years during which the Uinta Basin had plentiful snow cover throughout the Uinta Basin and many long, strong, inversion episodes. This result appears to indicate that, if meteorological influences are thoroughly accounted for, the capacity of the Uinta Basin atmosphere to form wintertime ozone has not changed since 2013, at least not in a way that is statistically discernable. This appears to contradict Section 5.4.3 and Section 12, which provide evidence that NO_X and organic compound emissions have declined from 2013 until at least 2017.

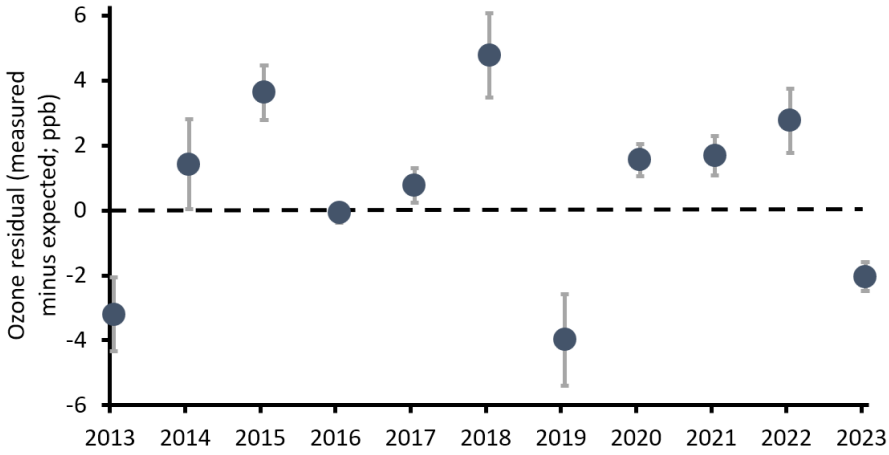

Figure 5-13. Daily maximum 8-hr average ozone residuals, calculated as measured ozone minus ozone predicted via multiple linear regression. Circles are the average of all sites listed in Table 3-1, and whiskers show standard deviations. Values above zero indicate that actual ozone was higher than predicted, and values below zero indicate the opposite.

While we conclude that no statistically discernable change in the capacity of the Uinta Basin atmosphere to produce winter ozone has occurred since 2013, we note the following caveats:

- The evidence for decreasing emissions in Section 5.4.3 and Section 12 is site-specific and may be influenced by local emission sources.
- The response of ozone production to changes in emissions is (1) nonlinear and (2) dependent on meteorology (see Section 9). It is possible that the combination of NO_X and organic compound emissions reductions that have occurred haven't led to a discernable decrease in the capacity to produce winter ozone because of nonlinear chemistry that we have not yet investigated.
- It is also possible that, while total non-methane organics have decreased, the composition of those organics has changed such that recent emissions are more reactive.
- Additional work with more sophisticated statistical methods may result in a different finding.
- The fact that NO_X, methane, and non-methane organics emissions have apparently not increased dramatically in response to the recent increase in oil and gas activity may be taken to mean that the industry has become more efficient over time, even if that increase in efficiency is not yet enough to have a strong impact on the capacity for winter ozone production.

5.5. Acknowledgments

This work was funded by the Utah Legislature and Uintah Special Service District 1.

6. Investigation of Carbonyl Fluxes at the Air-snow Interface

Authors: Seth Lyman, Brant Holmes, Trevor O'Neil

6.1. Introduction

Physical and chemical processes occur in snowpacks and can have a significant impact on the chemistry of the atmosphere (Grannas et al., 2007). Snowpacks act as reservoirs and exchange media, in addition to acting as a photochemical reactor. We presented background information about these processes in our 2019 Annual Report (Lyman et al., 2019a). In previous preliminary work, we showed from field (Lyman et al., 2019a) and lab (Lyman et al., 2020a) measurements that carbonyls, especially acetaldehyde, can be emitted from the Uinta Basin snowpack in the presence of sunlight. Carbonyls are important radical precursors during winter inversions, and they are thus extremely important for winter ozone production (Edwards et al., 2014). To build on our past work, and to understand carbonyl fluxes at the air-snow interface, we built a custom chamber system to observe emissions of organic compounds from snow under controlled conditions.

6.2. Methods

We modified a chest freezer to create the snow chamber apparatus (Figure 6-1). We used styrofoam sheets to divide the chamber into two sections. We cut away a portion of the lid above each section and replaced it with 4 mm ultraviolet light (UV)-transparent acrylic sheeting (91% UV transmission). We used temperature controllers and valves to regulate a flow of liquid nitrogen into each section to maintain the temperature of the freezer at -20° C.

We used FEP or PTFE Teflon bags as the snow chamber. The FEP bags were produced commercially, while we constructed the PTFE bags by cutting and heat-sealing commercially available drum liners. The bags were approximately 30 × 30 cm, with a volume of about 6.5 L when full of air. We connected two lengths of 6 mm outer diameter PFA Teflon tubing to each bag with PFA panel-mount compression fittings that sealed to the bags with the aid of PTFE washers. The tubings for each bag were connected to the inlet and outlet of a PTFE-lined pump. The pump circulated air through the bag at 4 L min^{-1} for the duration of each experiment. The freezer could accommodate one bag in each of its two sections. Throughout this section, we follow established convention by referring to these bags as chambers.

We periodically checked the chambers for leaks by filling them with helium and checking all seams and seals with a laboratory-grade leak detector. The UV transmission of the PTFE chambers was 80% (based on comparisons of measured UVA and UVB light in ambient air with and without the PTFE material covering the light sensor), and the FEP chambers had a rated UV transmission of >90%. All tests were conducted outdoors, away from shade. We continuously measured incoming UVA and UVB radiation inside the chest freezer during all experiments, and the UVA and UVB sensors were covered with a single sheet of chamber material during these measurements.

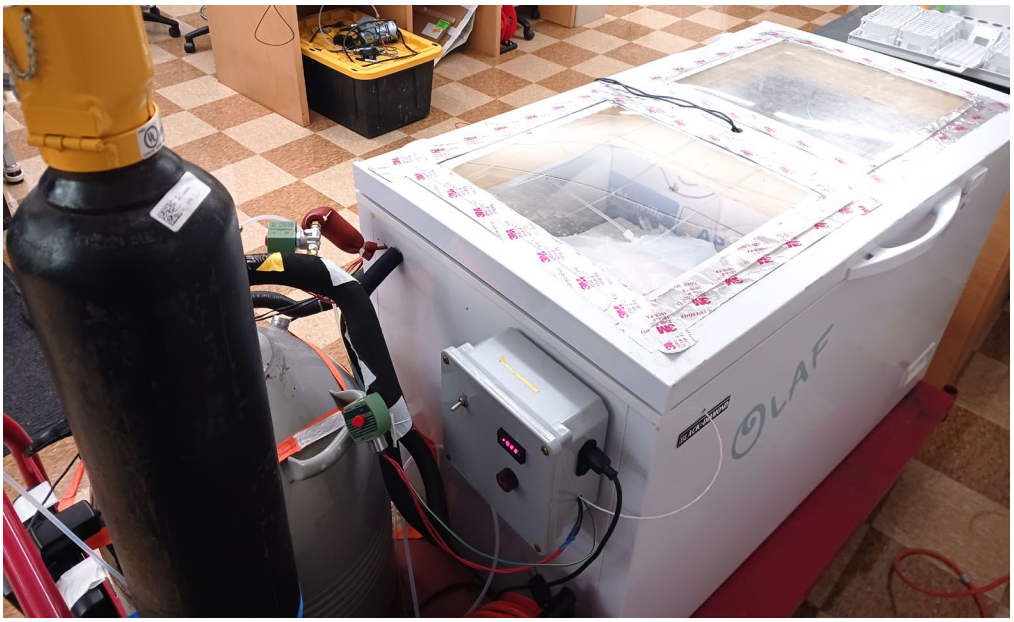

Figure 6-1. Photograph of the snow chamber system.

To test emissions from snow, we filled 10 × 15 × 5 cm (length × width × height) PFA Teflon trays with snow (level with the top of the tray) and placed the snow in the chambers. Since most of the experiments used ambient air in the chambers, we didn't open the chambers or place the trays of snow inside until the chamber system and the chambers were outdoors, so air that entered the chambers was outdoor rather than lab air. After inserting the trays, we sealed each chamber and used the PTFE-lined pump to fill the chamber with ambient air. We filled each chamber completely and then connected the pump to both lengths of tubing to allow it to continuously circulate the air through the chamber.

We carried out each chamber experiment for 2 hr. After each 2-hr period, we plugged one of the lengths of tubing and used the other length of tubing to collect samples for analysis in the laboratory. For a given experiment, we collected either 6-L whole-air canister or dinitrophenylhydrazine (DNPH) cartridge samples. In almost all cases, we performed two identical experiments in immediate succession, with one experiment performed for canister sample collection and another for DNPH cartridge collection. We connected a cleaned and evacuated whole air canister to the tubing and opened the canister valve to pull air from the chamber into the canister. We used KI ozone scrubber cartridges upstream of DNPH cartridges during DNPH sampling, and we used a totalizing mass flow controller to pull the sample at a rate of 0.8 L min^{-1}. We pulled air from the chamber through the cartridge until the chamber was as evacuated as possible with the tray still inside, and we used the flow controller's measurement of sampled volume as an estimate of the chamber volume. We used a 5 µm pore size PTFE filter housed in a PFA filter pack between canisters or DNPH cartridges and the chambers. Using the same sample collection methods, we collected an ambient air sample immediately prior to each experiment.

We analyzed canisters and DNPH cartridges using the methods described in Sections 3.2.4 and 3.2.5. Analyses of DNPH cartridges resulted in a measurement of the mass of individual carbonyls collected.

We divided this mass by the volume of air sampled (determined by the flow controller) to obtain the carbonyl concentration.

We collected the snow used in these experiments at the Horsepool monitoring station or at latitude 40.565 and longitude -109.691 in the Uinta Mountains and stored it in a laboratory freezer until use. We collected snow in liquinox-cleaned high-density polyethylene buckets by scooping snow directly into the bucket and then scooping additional snow with powder-free nitrile gloved hands.

6.3. Brief Summary of Method Development Activities

Our previous snow chamber system (Lyman et al., 2020a) could only accommodate one snow sample at a time, so comparisons of different samples were confounded by differences in ambient air concentrations of organics and oxidants. The new system (Figure 6-1) allows for direct comparisons of different snow or different conditions with identical air. We conducted quality assurance tests to ensure that the data collected with the system were reliable and comparable. We will provide details of those tests in a peer-reviewed publication. We provide a brief summary here:

- *Contamination from DNPH cartridges:* When we began experiments with the snow chamber system, we collected carbonyls on DNPH cartridges by attaching a cartridge to the air being pulled into the circulation pump, so carbonyls were collected continuously during each experiment. We found, however, that the cartridges release organic compounds during sampling, contaminating the chamber air during the experiment. We also tried placing DNPH cartridges upstream of canisters to collect both samples simultaneously, but this resulted in contamination of the whole air canister samples. The chamber volume was too small to fill a whole air canister and a DNPH cartridge from the same chamber, so we decided to conduct two identical experiments each time, collecting canister samples for one and DNPH cartridge samples for the other.
- *Pump and tubing contamination:* We determined that the pumps had drawn in styrofoam while tubing was pushed through holes in the freezer. We cleaned the pumps and tubing with an organic solvent and conducted experiments with and without the pumps in place to show that they did not produce contamination after cleaning.
- *Chamber contamination:* We found that the chambers contained more organic compounds than ambient air, with a different organic compound composition than ambient air, even if no snow was added to the PFA trays. Experiments without the pump attached showed that the cause of these additional organics was not the circulation pump. Cleaning the chambers did not decrease organic compound accumulation. Chambers exposed to light accumulated much higher levels of organics than those kept in the dark. We compared chambers with ambient versus ultra-zero air transferred from a compressed gas cylinder, and we found lower organics in the zero air chambers, but the difference was small. The cause of accumulation of organics in the chambers is unknown. Organics may volatilize from the chamber walls, the PFA trays, or the PFA tubing, or they may diffuse from the freezer through the chamber walls since most plastics, including FEP and PTFE, are porous to gases. Because of this, we conducted comparisons of

chambers with and without snow, which allowed us to subtract background accumulation of organics from accumulation of organics that was due to snow.

- *FEP versus PTFE chambers:* We compared results for FEP and PTFE chambers with no snow in ambient air and ultra-zero air from a compressed gas cylinder. We found that PTFE chambers result in lower accumulation of organics than FEP chambers.

6.4. Emissions from Snow

Most of our work on this project over the past year was focused on the method development tasks described in the previous section. Over the coming year, we will conduct many more experiments, as described in the next section. In the current section, we show the results of a few experiments we conducted to compare chambers containing snow collected at Horsepool with chambers containing empty PFA trays. The chambers were kept at -20°C, filled with ambient air, and exposed to sunlight. Table 6-1 shows the overall results of these experiments, and Figure 6-2 shows the results for individual carbonyls.

We calculated the excess mass of each measured organic compound in the chambers with trays containing snow compared to chambers with empty trays. We also calculated snow-air flux (i.e., the rate of emission from or deposition to the snow surface) by dividing the excess mass in the snow-containing chambers by the surface area of snow and the experiment duration. We also roughly extrapolated the snow-air flux to the entire Uinta Basin by multiplying by hours of sunlight per day (assumed to be eight; evidence exists that emissions only occur in the presence of sunlight) and an approximation of the snow-covered area of the Basin that exists under a typical inversion layer (9,600 km^2). In reality, we don't know enough about snow-air flux of organics to make such an extrapolation. We only do so here to provide a preliminary estimate of the potential importance of snow as an emission source of organics.

Relative to chambers without snow, air in chambers with snow accumulated more organic compound mass. This was true for all of the compound groups shown in the table, though the mass of some individual compounds was lower in the chambers with snow, indicating deposition of those compounds to snow. Total hydrocarbons and alcohols had the largest snow-air fluxes, while alcohols showed the largest percent increase in snow-filled chambers relative to those without snow. Fluxes of aromatics and alkenes were lower than for other compound groups. Carbonyl fluxes were dominated almost entirely by acetaldehyde (Figure 6-2).

We advise against using our rough extrapolation to potential Basin-wide emissions quantitatively. It does, however, provide evidence that snow-air fluxes are significant. For comparison, in a recent project to estimate Basin-wide pollutant emissions (Section 12), we estimated the following Basin-wide emission rates in 2022:

- Hydrocarbons: 237,734 kg day^{-1}
- Alkanes: 230,671 kg day^{-1}
- Alkenes: 1,183 kg day^{-1}

- Alcohols: 14,177 kg day^{-1}
- Carbonyls: 6,364 kg day^{-1}

Thus, snow-air fluxes could account for perhaps 10% of carbonyl and 5% of alcohol emissions but less than 1% of hydrocarbon emissions in the Uinta Basin.

Table 6-1. Average percent increase in organic compound mass in chambers with snow relative to identical chambers without snow for the groups of organic compounds listed. The average snow-air flux (i.e., the rate of emission from or deposition to the snow surface) and a rough extrapolation to Uinta Basin-wide emissions from snow are also shown. Some individual compounds deposit to snow, and others are emitted from it. The net results for the compound groups are shown.

Compound group	Mass increase in chamber air due to snow (%)	Snow-air flux (µg m^{-2} hr^{-1})	Rough extrapolation to Basin-wide emissions (kg day^{-1})
Ethylene and propylene	47%	0.4	31
BTEX (light aromatics)	35%	0.0	0
Isoalkanes	41%	4.2	319
Methanol	64%	5.0	381
Formaldehyde and Acetaldehyde	40%	7.0	540
All alkanes	36%	5.3	404
All alkenes and acetylene	16%	0.3	26
All aromatics	35%	0.0	0
All alcohols	80%	10.6	812
All carbonyls	37%	7.4	571
All hydrocarbons	56%	16.2	1242

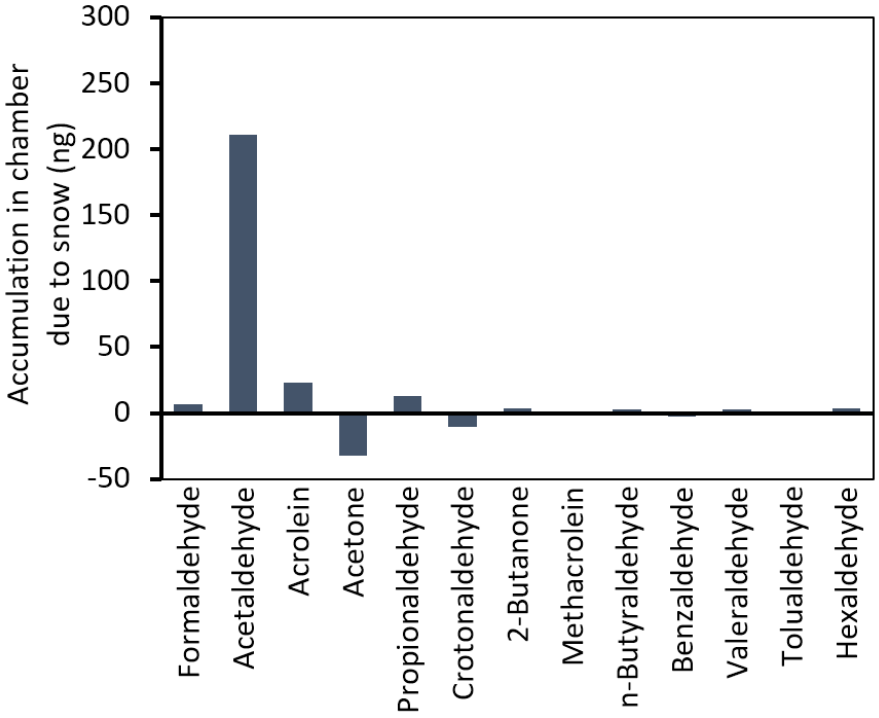

Figure 6-2. Average accumulation of individual carbonyls in the chamber due to snow, determined from the mass difference in the chambers with and without snow.

It is possible that the additional moisture in the chambers with snow, rather than emissions from the snow itself, led to higher organics in the chambers with snow. Experiments to test this possibility are underway. It is also possible that emissions of organics from the snow were simply organics that had been absorbed by the snow at the collection location that were released in the experimental chamber, which would mean that the snow is not an original source but instead merely a short-term reservoir, of the organics. Experiments to test this possibility are also underway.

6.5. Remaining Work

We plan to carry out the following additional experiments:

- Additional comparisons of chambers with snow versus those without snow
- Additional comparisons of snow exposed to sunlight versus snow kept in the dark
- Comparison of snow from Horsepool against snow from the Uinta Mountains
- Comparison of snow versus ultrapure water and shaved ultrapure ice to test whether accumulation of organics in chambers with snow is due to reactions involving organics in the snow or some artifact from having water or ice in the chamber
- Investigation of the impact of snow depth (full tray of snow versus half-full tray)
- Investigation of the impact of snow surface area (two trays versus one)

- Comparison of snow at different temperatures (0, -20, and -40°C)
- Addition to snow of a mixture of hydrocarbons typical of oil and gas emissions to determine whether additional carbonyls are formed
- Addition of a mixture of alcohols to snow to determine whether additional carbonyls are formed
- Additional comparisons of snow exposed to ambient air versus snow exposed to ultra-zero air or N_2
- Experiments at different levels of solar radiation

We anticipate that these experiments will allow us to answer the following questions:

- Are snow-air fluxes from all types of snow similar, or are fluxes from snow in oil and gas-producing areas different from pristine snow?
- Are organic compounds typical of oil and gas emissions converted to carbonyls within the snow?
- Are fluxes dependent on snow surface area or snow depth?
- Do fluxes depend on temperature or solar radiation?

If this study shows that emissions of organics from snow are significant, we will conduct a comprehensive field emissions measurement campaign to verify whether laboratory emissions are representative of emissions from snow in natural conditions. That campaign could occur in winter 2024-25 or winter 2025-26.

6.6. Acknowledgments

This work was funded by the Utah Legislature and Uintah Special Service District 1.

7. Report Summary: Comparison of Chemical Mechanisms in Photochemical Models

Summary by Seth Lyman

Photochemical models that simulate air quality rely on (1) simulations of meteorological and physical conditions, (2) simulations of pollutant emissions, and (3) simulations of chemical reactions that occur in the atmosphere. We have carried out research to improve all three components of models used for winter ozone in the Uinta Basin. Preliminary work completed in 2020 (see Section 5 of our 2020 Annual Report) showed that the chemical mechanism used by air quality models might have a strong impact on model performance. Chemical mechanisms are the lists of chemical reactions that models use to simulate atmospheric chemistry. Atmospheric photochemistry is complex, involving thousands of chemical species and tens of thousands of reactions. Because 3D photochemical models must calculate chemical reactions that occur in thousands of grid cells, explicit modeling of all the species and reactions in the atmosphere would require more computational power than is feasible. Models instead use simplified mechanisms that combine similar compounds and similar reactions together for computational efficiency.

We received funding from the Utah Division of Air Quality and also used funding from the Utah Legislature in a project led by Ramboll to further investigate the importance of chemical mechanisms on photochemical model performance. A full report of the project's outcomes is available at https://www.usu.edu/binghamresearch/files/reports/Ramboll_USU_S4S_RACM2_FinalReport_24Feb2023.pdf.

We compared two simplified chemical mechanisms, version 6 of the Carbon Bond mechanism (CB6r5) and version 2 of the Regional Atmospheric Chemistry Mechanism (RACM2), in a single model (CAMx version 7.1) for a wintertime ozone episode that occurred in February 2019. The CB6 and RACM2 mechanisms simplify atmospheric chemistry in different ways, leading to different abilities of photochemical models to produce ozone. Meteorological inputs were the same for both mechanisms. The emissions inventory inputs were also the same, but because the two mechanisms use different model species, small differences existed in the emissions that were output for use by each mechanism.

Neither of the mechanisms was able to reproduce observed high wintertime ozone values. The meteorological input for the model failed to properly capture the strength of inversion conditions, so simulated levels of organic compounds were much lower in the model than in reality, which probably accounts for the underestimation of ozone. The different chemical mechanisms did result in small differences in simulated ozone levels (Figure 7-1), with RACM2 producing more ozone.

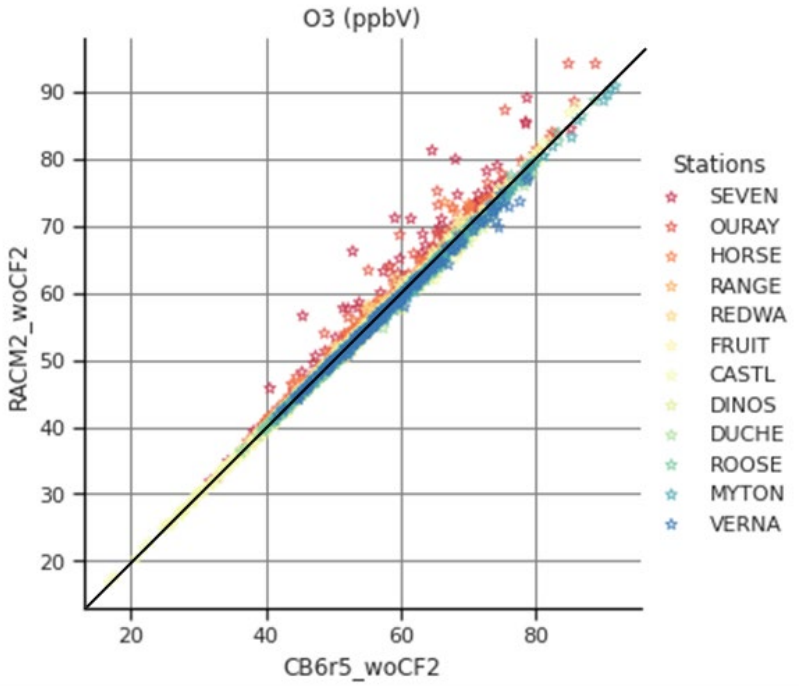

Figure 7-1. CAMx-simulated ozone produced during a 2019 inversion episode with the CB6r5 and RACM2 mechanisms.

The RACM2 mechanism resulted in more organic compounds, especially aldehydes, which are known to be important for winter ozone production (Figure 7-2). The formaldehyde production rate and the production of HO_2 radical from formaldehyde photolysis were both much higher in the RACM2 mechanism (Figure 7-3 and Figure 7-4). Production of formaldehyde and other aldehydes from photodegradation of other organic compounds, followed by photolysis of aldehydes to create radicals, is known to be critical to ozone formation during winter episodes in the Uinta Basin (Edwards et al., 2014).

While these results corroborate our 2020 findings that the RACM mechanism produces more ozone in the wintertime Uinta Basin than the CB mechanism, deficiencies in the meteorological simulation ultimately mean that the extent of the difference between the mechanisms is uncertain, and more work is needed. We plan to continue researching this topic in future years (see Section 20.2.3).

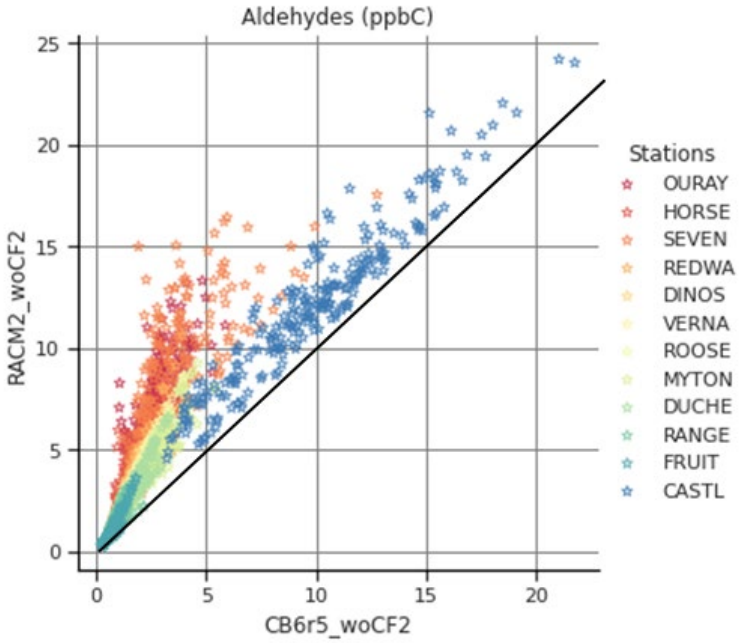

Figure 7-2. CAMx-simulated total aldehydes, in units of parts-per-billion of carbon, produced during a 2019 episode with the CB6r5 and RACM2 mechanisms.

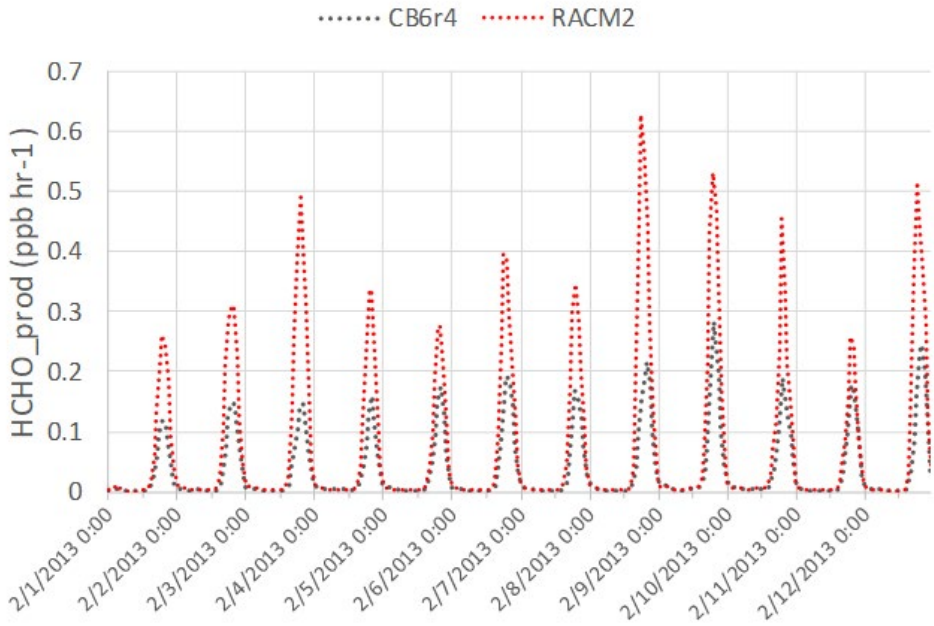

Figure 7-3. Photochemical production rate of formaldehyde (HCHO) at Ouray simulated by CAMx with the CB6r4 and RACM2 chemical mechanisms.

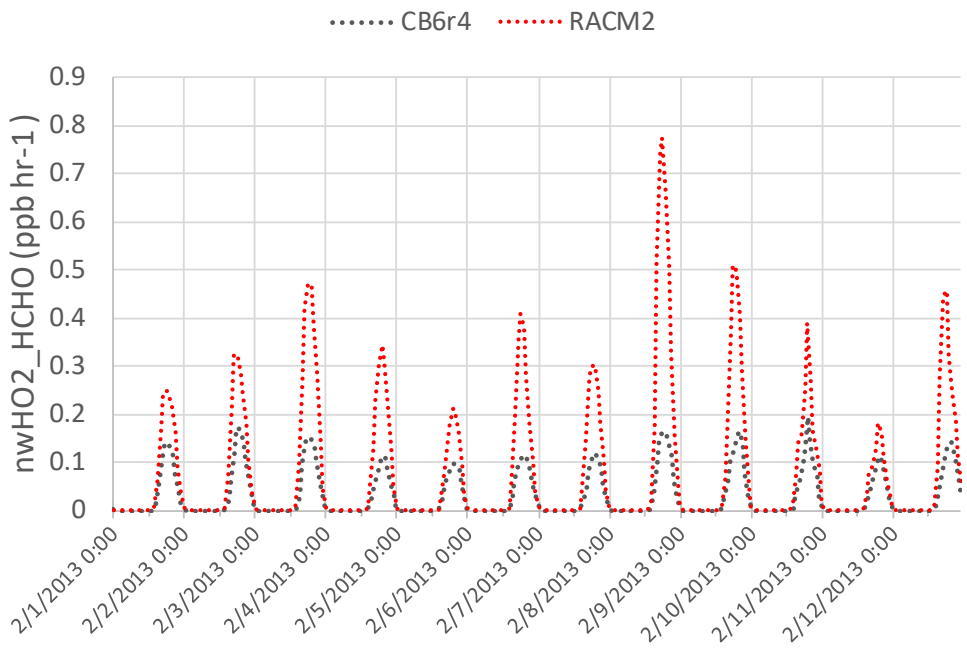

Figure 7-4. Rate of HO_2 radical production from formaldehyde (HCHO) photolysis at Ouray simulated by CAMx with the CB6r4 and RACM2 chemical mechanisms.

7.1. Acknowledgments

This work was funded primarily by the Utah Division of Air Quality. Funds from the Utah Legislature and Uintah Special Service District 1 were also used.

8. Improvements to Methods for Simulation of Wintertime Inversions

Author: Liji David

8.1. Introduction

Inversions are characterized by an inverted lapse rate (i.e., colder temperatures near the surface and warmer temperatures aloft), which leads to suppression of buoyancy-induced vertical motion. Mountainous valleys in the western U.S. can experience inversions in the winter season. The complex terrain in these areas produces cold downslope winds and traps cold air within valleys or basins for days to weeks. Temperature inversions can lead to high pollution episodes because stagnation inhibits pollutants from dispersing out of the region (Silcox et al., 2012). The Uinta Basin's bowl-like topography is conducive to temperature inversions and poor air quality (Neemann et al., 2015). Radiosonde and tethersonde measurements that characterize the vertical structure of the inverted Uinta Basin atmosphere are available for winter 2012 and 2013, but no long-term record exists of the vertical properties of persistent inversions in the Basin.

The Weather Research and Forecasting Model (WRF) is the most-used meteorological model for air quality studies, and previous work has shown that WRF struggles to accurately simulate persistent winter inversions. The objective of this study is to evaluate the effectiveness of new parameterizations of the WRF model for simulating persistent inversion episodes. We use WRF to simulate a persistent inversion episode that occurred in 2019.

8.2. Methods

Simulations were performed for eight days, from 23 February (0000 UTC) to 2 March (2300 UTC) 2019. The WRF model (version 4.3.3) consisted of a single domain (Figure 8-1). There were 37 sigma levels in the vertical domain, reaching a model top of 50 hPa. The vertical levels stretch in size, with a fine resolution near the surface and a coarser resolution in the upper troposphere. The National Land Cover Dataset of 2011 (NLCD 2011) provided land- use information for WRF. Meteorological initial and boundary conditions were taken from the NCEP NAM analysis at 12 km horizontal resolution. Model physics and numerical experiments are summarized in Table 8-1. The purpose of this study is to simulate the three-dimensional structure and evolution of a persistent inversion episode and determine the best set of model physics for accurate simulation.

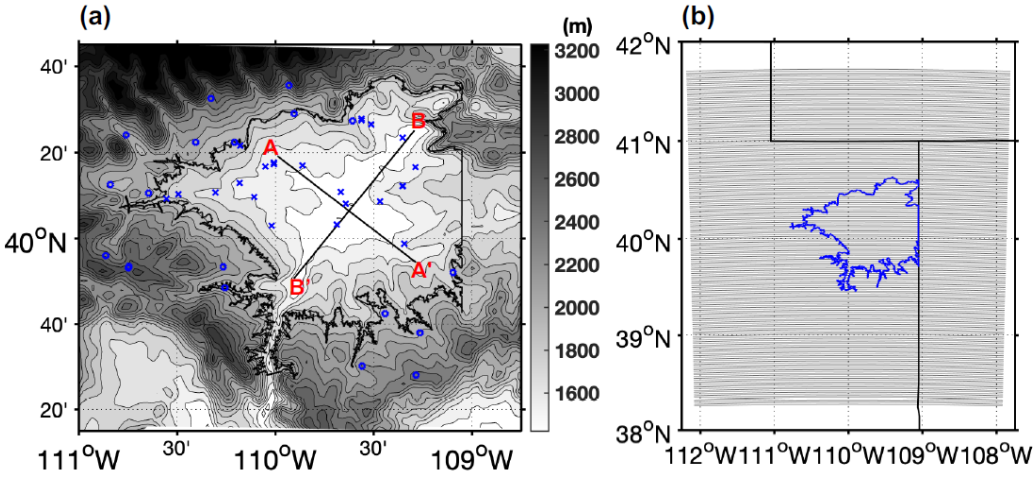

Figure 8-1. (a) Topography of the Uinta Basin. The meteorological sites in the valley (blue crosses; below 1750 m) and non-valley (blue circles) locations are shown, and are taken from MesoWest. The dashed lines A-A' and B-B' are the across-valley and along-valley cross-sections referred to in the text. (b) WRF model domain. The Uinta Basin is marked with a blue line.

Table 8-1. Summary of model physics used for WRF simulation experiments.

Numerical Experiment 1	Numerical Experiment 2	Numerical Experiment 3	Numerical Experiment 4	Numerical Experiment 5
Ferrier, improved Mellor-Yamada, Noah, and no cumulus	Ferrier, improved Mellor-Yamada, RUC, and no cumulus	Ferrier, MYJ, RUC, and no cumulus	Double-moment, improved Mellor-Yamada, RUC, and Kain-Fritsch	Ferrier, improved Mellor-Yamada, RUC, and Kain-Fritsch

8.3. Results

8.3.1. Synoptic-scale Phenomena During the Inversion Episode

Persistent wintertime inversions differ from nocturnal inversions in that they persist throughout the day. Synoptic processes play an essential role in the life cycle of persistent inversions. Figure 8-2 shows the synoptic conditions (potential temperature, geopotential height, and wind vector) from the National Centers for Environmental Prediction (NCEP) North American Mesoscale (NAM) 12 km resolution meteorological analysis dataset at 500 hPa that led to a persistent inversion during the study period. On 23 February (1700 MST), northwesterly winds prevailed over the Intermountain West, transporting cold air from higher latitudes into the Uinta Basin. On the following days (24-25 February), the wind shifted from northwesterly to westerly/southwesterly over the Intermountain West, bringing warm air to the region. By 25 February (1700 MST), there was a region of high pressure over the Uinta Basin that persisted for the next three days. However, the high pressure decreased starting on 28 February (1700 MST), and the advection of cold air (northwesterly wind) on 1 March (0500 MST) broke up the persistent inversion.

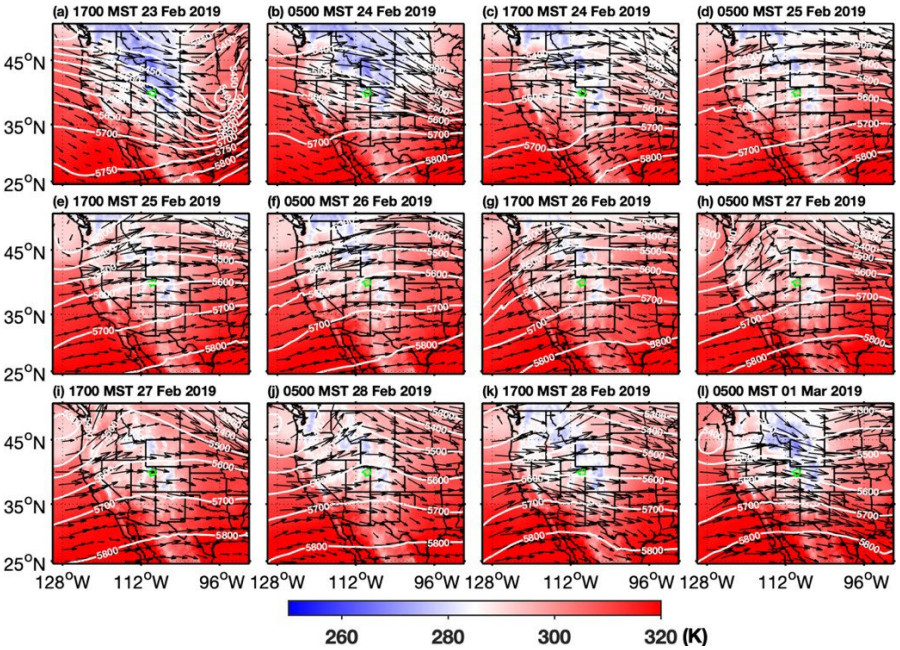

Figure 8-2. NAM 12 km analysis of the 500 hPa potential temperature, geopotential height, and wind for 23 February 2019 to 1 March 2019. The Uinta Basin is marked with a green line. MST is Mountain Standard Time.

8.3.2. Sensitivity Simulations

A statistical analysis of simulated and observed hourly temperature (2 m) and wind speed (10 m) was performed for sites in the valley (below 1750 m) and surrounding mountains (non-valley). The slope, correlation coefficient (R), intercept (c), and mean bias (model minus MesoWest; MB) are given in Table 8-2. For temperature, experiment 5 showed the lowest bias and highest slope and R. All the experiments underestimated the wind speed (except experiment 1 for the valley sites). The correlation between measured and modeled wind was better at non-valley sites than at valley sites. The differences between valley and non-valley sites might be because the model cannot resolve the complex topography of the Uinta Basin or the impacts that topography has on meteorological conditions. In addition, actual wind sensor height varied from 2 m to 7 m (Horel et al., 2002), but all wind sensor data were compared to model wind speed at 10 m.

Table 8-2. The slope, correlation coefficient (R), intercept (c), and mean bias (MB) of simulated and observed (MesoWest) hourly temperature (2 m) and wind speed (10 m) at sites in the valley (V) and non-valley (NV).

Numerical Experiments	Site location	Temperature (°C)				Wind speed (ms^{-1})			
		Slope	R	c	MB	Slope	R	c	MB
1	V	0.641	0.737	4.96	7.51	0.127	0.107	1.32	0.075
	NV	0.705	0.730	1.37	2.70	0.470	0.529	1.61	-0.050
2	V	0.712	0.836	-1.44	0.603	0.160	0.206	0.848	-0.347
	NV	0.747	0.874	-2.16	-1.02	0.474	0.595	1.11	-0.546
3	V	0.606	0.818	-2.15	0.655	0.199	0.240	0.834	-0.307
	NV	0.598	0.873	-2.49	-0.676	0.383	0.594	1.13	-0.810
4	V	0.475	0.704	-3.03	0.701	0.070	0.130	0.732	-0.591
	NV	0.652	0.834	-3.55	-1.98	0.462	0.596	0.963	-0.725
5	V	0.712	0.836	-1.90	0.149	0.153	0.206	0.815	-0.391
	NV	0.786	0.887	-2.14	-1.18	0.478	0.577	1.18	-0.455

WRF output was averaged at 12 km resolution to compare with the IASI satellite vertical temperature profile (Bouillon et al., 2020) at the daytime overpass time (averaged between 1000-1100 MST) on 24 February (beginning of inversion) and 26 February (middle of inversion) 2019, as shown in Figure 8-3. The figure shows that the simulated temperature profile at the beginning of the inversion from the five numerical experiments was comparable to IASI above 800 hPa. There was a discrepancy during the inversion at Myton and Ouray (below 600 hPa) and below 750 hPa at Red Wash. Previous studies have reported that IASI is more accurate for temperatures above 750 hPa (Bouillon et al., 2022). The temperature profiles from numerical experiments 2 and 5 were closest to the IASI observations at multiple sites and days. Based on the surface and profile analysis, we consider numerical experiment 5 to have the best model physics for simulating atmospheric conditions during persistent inversion episodes.

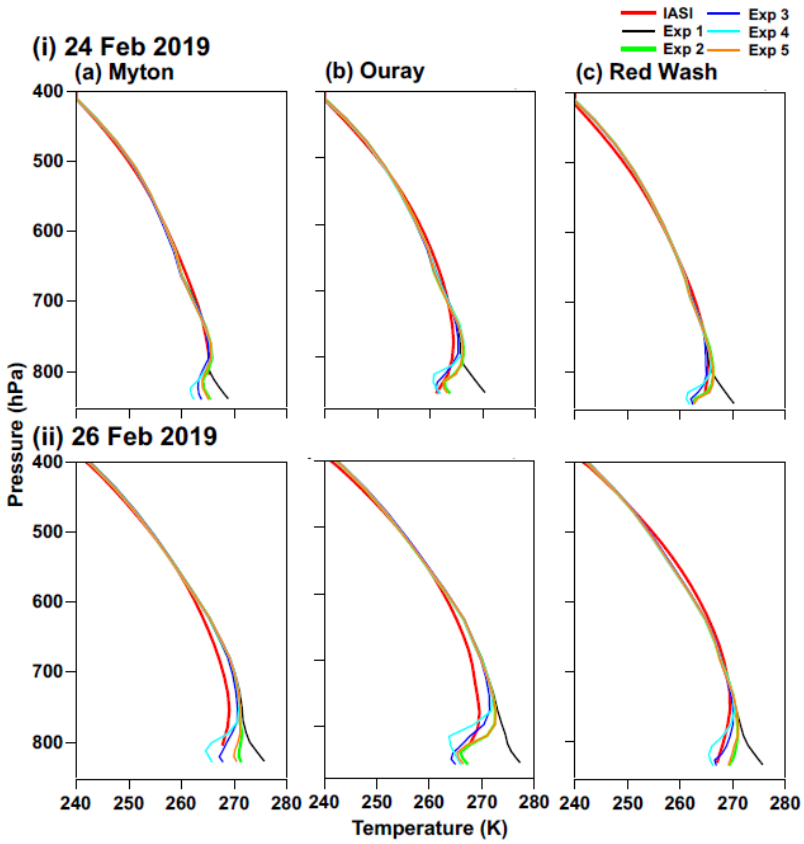

Figure 8-3. Temperature profile from IASI satellite retrievals and WRF experiments for (i) 24 February 2019 and (ii) 26 February 2019 at (a) Myton, (b) Ouray, and (c) Red Wash.

8.3.3. Model Evaluation

WRF results for experiment 5 were used for further model evaluation. The model was evaluated against MesoWest (https://mesowest.utah.edu/) surface observations to understand how well it captures the observed spatial and temporal variation in surface meteorological parameters (temperature and wind). Figure 8-4 shows the simulated and observed (from 53 sites) 2 m temperature in the Uinta Basin and surrounding mountains. A diurnal temperature variation was observed with lower amplitude as the inversion began (24-25 February). The locations below 1600 m (Figure 8-1) showed diurnal variation in temperature with lower amplitude (below 0°C on 25-27 February at 1400 MST). A comparison of the day-to-day variation in temperature showed gradual warming as the inversion progressed, with colder temperatures at the beginning of the inversion. During inversion, the surrounding high terrain (above 1750 m) was warmer than locations within the Uinta Basin. The model reproduced the diurnal cycle, spatial pattern, and warming trend. A statistical analysis of simulated (2 m) and observed hourly temperature was performed for sites in the valley (below 1750 m) and surrounding mountains (outside the valley), and the scatter plot is shown in Figure 8-5. The model was warmer at low temperatures (<-15°C) than the observation within and outside the valley.

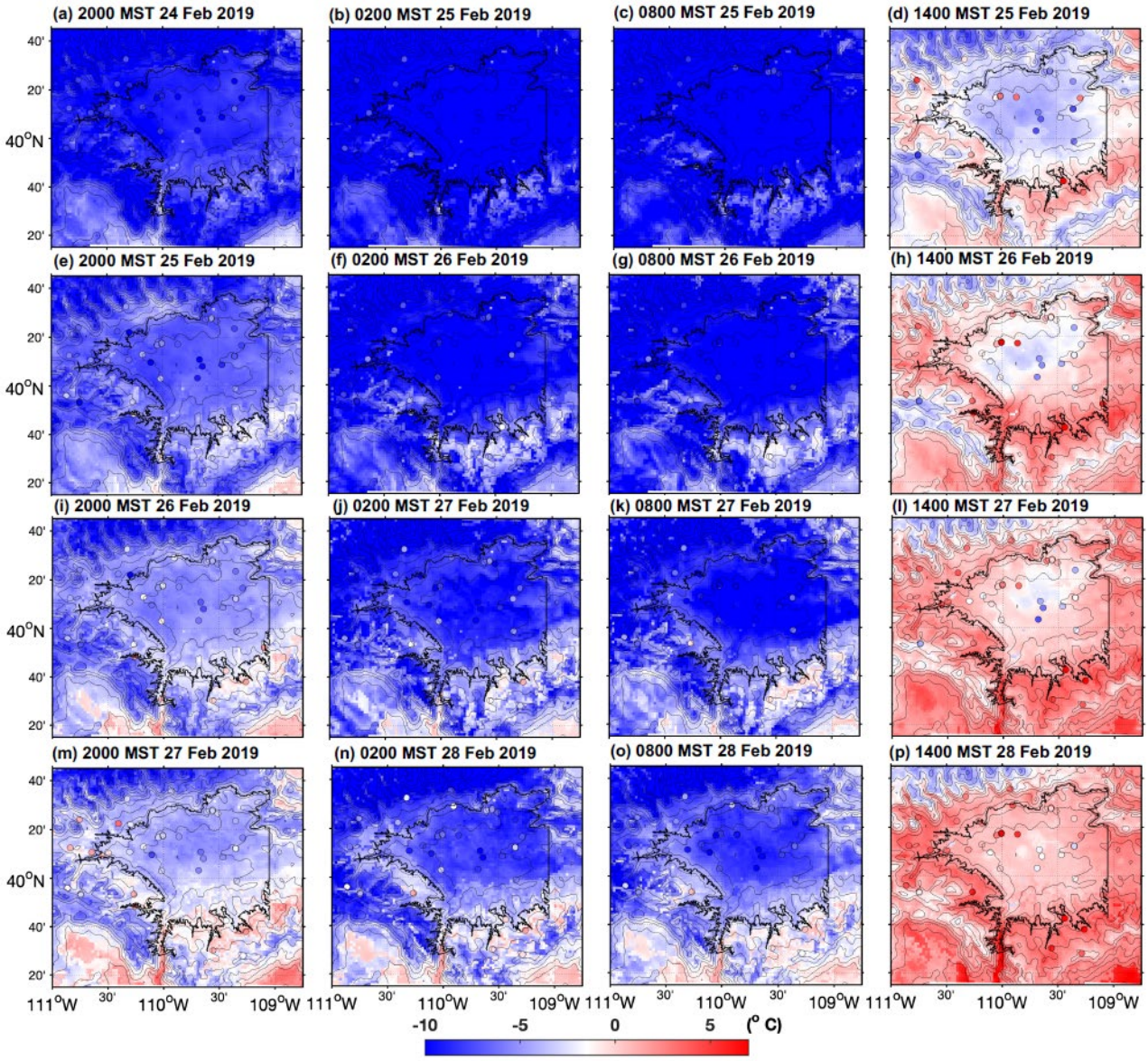

Figure 8-4. Simulated and observed surface temperature in the Uinta Basin and surrounding terrain from 24 to 28 February at 0200, 0800, 1400, and 2000 MST. The contours are the terrain height at 100 m intervals. The dark line is the boundary of the Uinta Basin federal ozone nonattainment area.

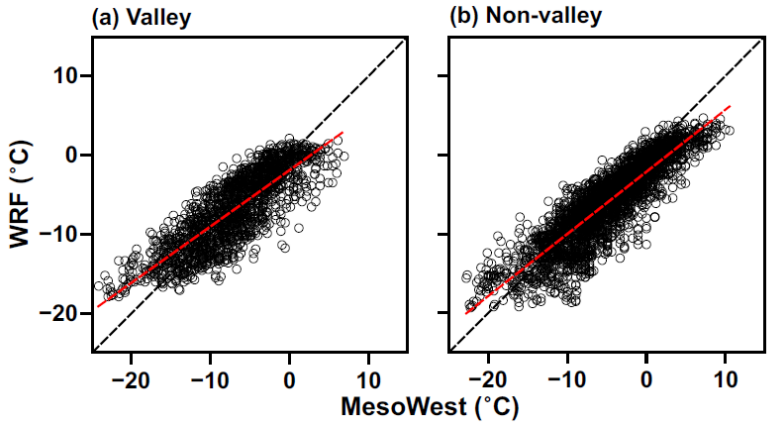

Figure 8-5. Scatter plot of WRF-simulated 2 m temperature versus MesoWest surface observations for the (a) valley and (b) non-valley sites. Linear regression lines are shown in red. The black dashed line corresponds to a slope of one.

Figure 8-6 shows the simulated (experiment 5) 10 m winds compared with the observations for days before (22 to 23 February), during (27 to 28 February), and at the end (1 March) of the inversion episode. There was a daily change in wind vector from mountain wind (2000 MT and 0200 MT) to valley wind (0800 and 1400 MT). Before the onset of an inversion over the region, the wind at 0200 MT and 0800 MT on 23 February was westerly in the western Uinta Basin. Around 110° W longitude, winds were easterly (at 0200 MT and 0800 MT) with lower magnitude, which was simulated and observed. Southerly winds prevailed in the southern Uinta Basin. Once the inversion started building (24 February), the westerly winds became weak, and the easterly/northeasterly winds prevailed during 2000-0200 MT in the western Uinta Basin. There were several distinctive features in the wind observed during the inversion period: (1) the simulated and observed nighttime winds were comparatively stronger than the daytime in the valley and at higher altitudes; (2) a change in the wind direction occurred at 0800 MST; and (3) the model simulated the afternoon (1400 MST) calm winds in the valley and throughout the entire Basin. Toward the end of the inversion period, we observed the intrusion of westerly (in the western Uinta Basin) and southerly winds and stronger winds in the central Uinta Basin (at the lowest altitude).

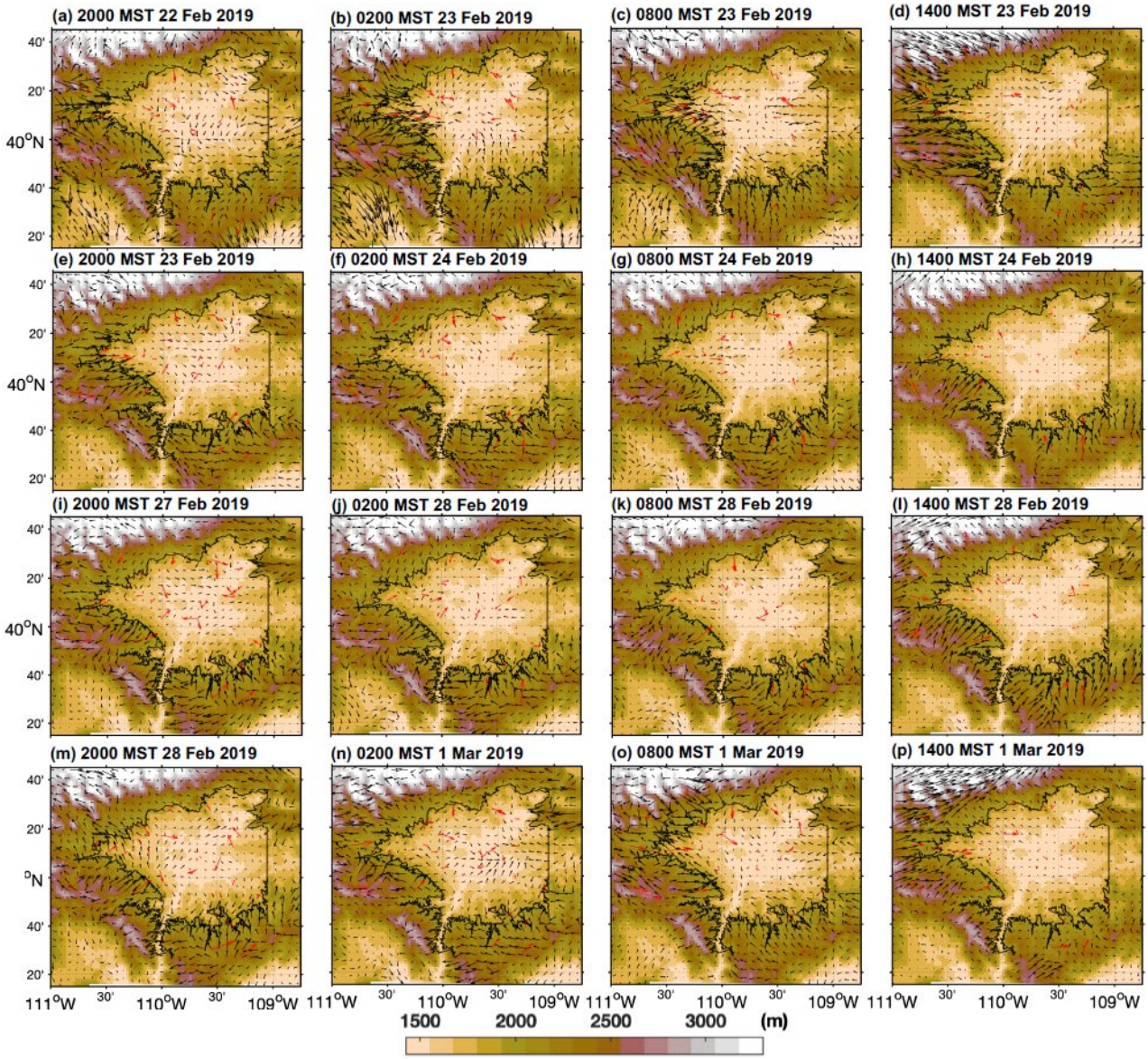

Figure 8-6. Simulated (10 m) and observed wind vectors in the Uinta Basin and surrounding terrain for days before (22-23 February), during (27-28 February), and end (1 March) of inversion. Background coloring represents the terrain height.

Overall, the model could simulate the general wind flow conditions for the study period. A statistical analysis of simulated (10 m) and observed hourly wind speed showed that, while the model generally simulated the correct range of wind speeds, correlation between modeled and measured wind speed was low (Figure 8-7).

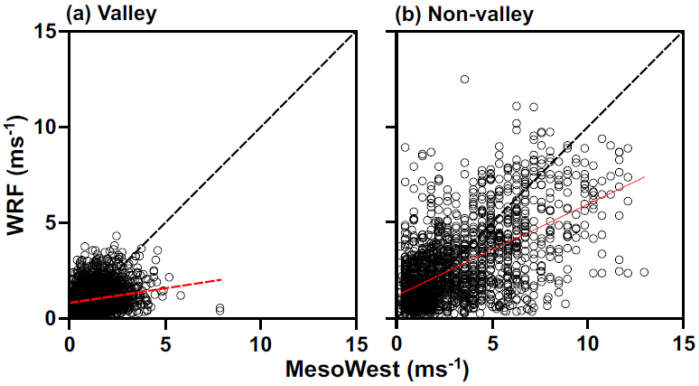

Figure 8-7. Scatter plot of WRF-simulated 10 m wind speed with MesoWest surface observations in the (a) valley and (b) non-valley sites. The linear regression line is shown in red. The black dashed line corresponds to a slope of one.

8.3.4. Evolution of Persistent Inversion Structure

To study the inversion structure and its evolution in the model, the simulated (experiment 5) potential temperature was compared with the ERA5 meteorological reanalysis dataset.

Figure 8-8 shows the ERA5 and WRF-simulated time-pressure cross-section of potential temperature across (AA') and along (BB') the valley. As the inversion began, rapid warming occurred above 750 hPa, and potential temperature increased by more than 10 K in less than 24 hours. From 25 February (1200 MST), a subsidence inversion descended from above 600 hPa to about 725 hPa (the top of the valley, 2600 m). The subsidence descended into the upper part until 28 February (1200 MST). Around 1800 MST (28 February), there was a downdraft followed by the lifting of the subsidence inversion around 1 March (1200 MST). A deep layer of cold air (<285 K) was present at the beginning of the inversion. The layer showed a diurnal cycle during the inversion period (until 28 February). As the inversion proceeded, the depth of the layer reduced and was limited to less than 400 m at night. The atmosphere remained stable above the layer of cold air. Overall, WRF captured the evolution of the persistent inversion across and along the valley, with the only difference seen in the lifting of the inversion on 28 February (~1800 MST), which was not strong in WRF.

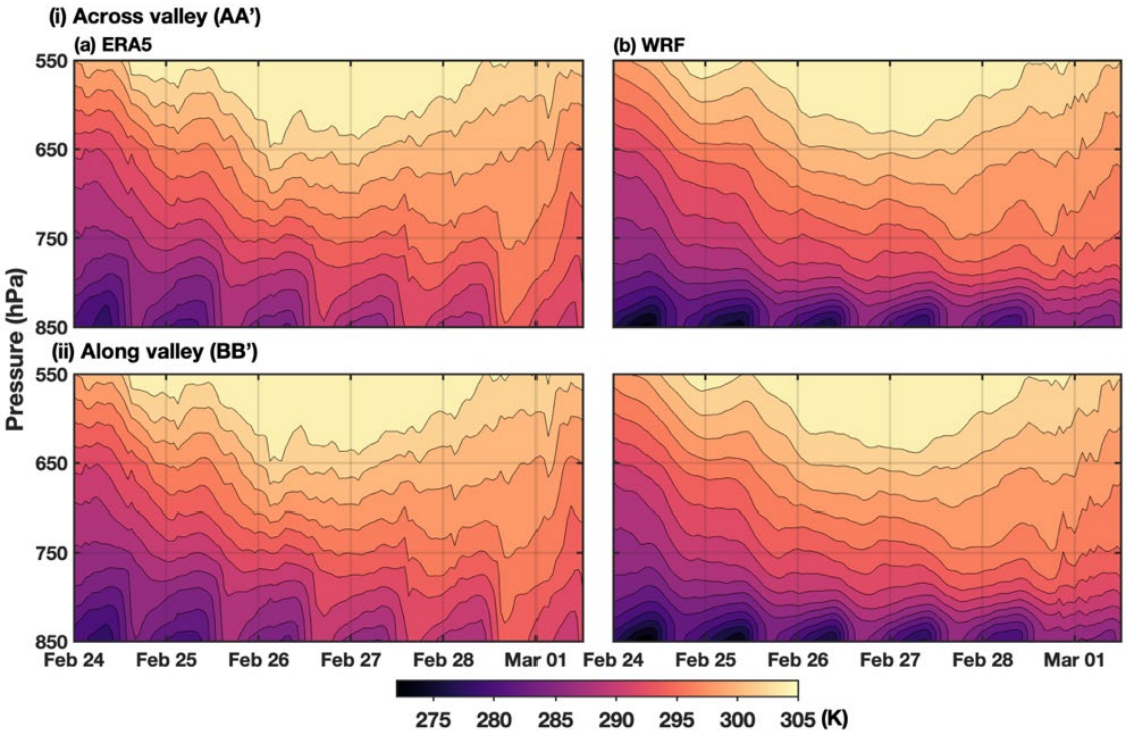

Figure 8-8. Time-pressure cross-section of (a) ERA5 reanalysis and (b) WRF simulated potential temperatures (i) across and (ii) along the valley from 24 February (0000 MST) to 1 March 2019 (1200 MST).

8.3.5. Vertical Motion

The influence of vertical motion on the persistent inversion was analyzed. Figure 8-9 shows the time-pressure cross-section of vertical wind across (AA') and along (BB') the valley from (a) ERA5 and (b) WRF. At the early stage of the inversion, the vertical wind was weak (~0.02 m s^{-1}) across and along the valley at lower levels (below 750 hPa), which favored the formation of an inversion. The vertical wind between 550-600 hPa was downward, resulting in the descent of warmer air; it was strong in WRF compared to ERA5. There was a strong downdraft (>0.05 m s^{-1}) and updraft (>0.04 m s^{-1}) after 28 February (1800 MST) that resulted in mixing and lifting of the inversion. A diurnal cycle in the vertical wind was observed below 800 hPa, with a stronger downdraft during the night. Compared to ERA5, the magnitude of vertical wind simulated by WRF was weaker at lower levels.

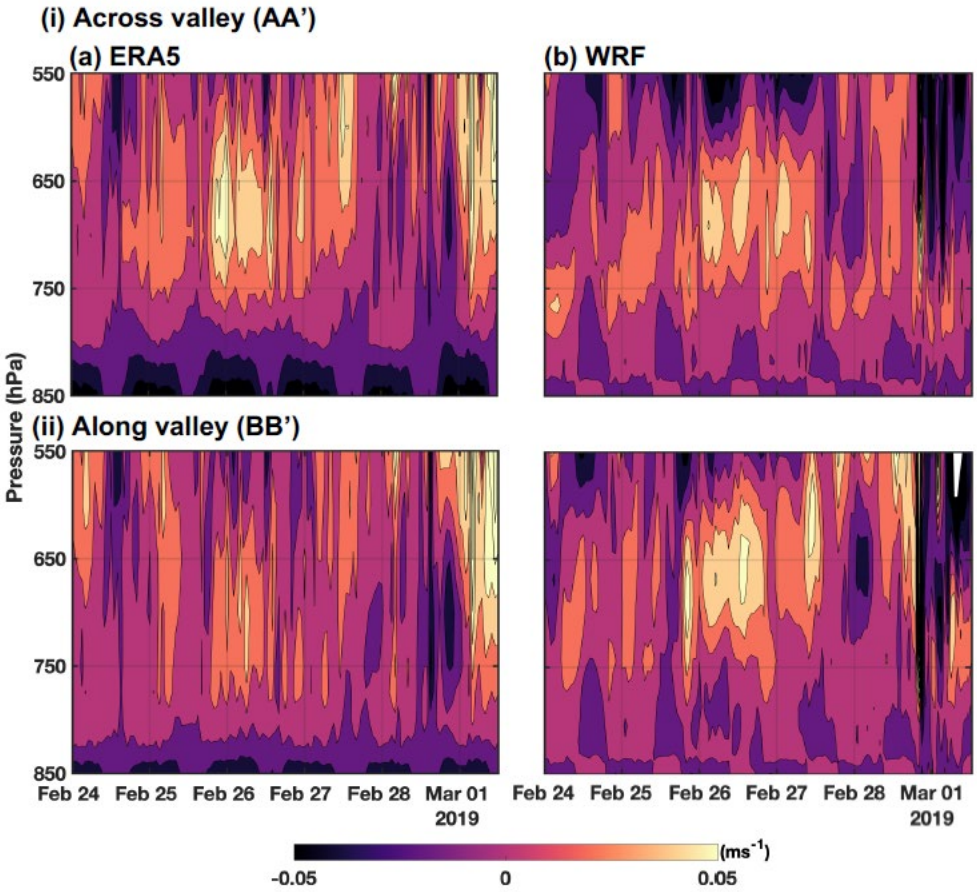

Figure 8-9. Time-pressure cross-section of (a) ERA5 reanalysis and (b) WRF simulated vertical velocity (i) across and (ii) along the valley from 24 February to 1 March 2019.

8.3.6. Horizontal Motion

The spatial and temporal variation in the boundary layer structure from the beginning to the end of the persistent inversion was studied using the simulated potential temperature and wind across (AA') and along (BB') the valley, as shown in Figure 8-10 and Figure 8-11, respectively. At the beginning of the inversion (24 February) in the cross-valley section, the westerly winds aloft were decoupled from the easterly in the valley by a layer of light wind above the mean elevation (~2 km) of the surrounding mountains. By 24 February 1400 MST, the warm air started descending in the upper parts (~2.02 km) of the valley, and winds were northeasterly in the center of the valley (~109.5°W) that brought cold air into the valley, seen as a decrease in the potential temperature. As the inversion progressed (25 February), the warm air descended into the valley, increasing the potential temperature inside the valley, which resulted in a stratified atmosphere. The warming aloft and valley stratification were observed in the along-valley vertical cross-section (Figure 8-11). Accumulation of cold air was observed at 0200 MST and 0800 MST on 24-25 February at the center of the valley in the across and along vertical cross-sections.

During the peak of the inversion (26-27 February), the atmosphere above the valley was warmer, and the inversion was stronger compared to the previous day (25 February; Figure 8-10). A mixed layer was formed within the lowest 400 m at 1400 MST, with the lowest mixing in the center of the valley. By 28 February, the temperature at the lower levels was higher with the intrusion of warm northwesterly wind aloft and southwesterly in the lower levels. The intrusion of warm air and strengthening of the wind aloft and in the lower layers of the valley was observed in the along-valley section. The process of mixing began in the southwest of the Uinta Basin and progressed to the northwest of the basin.

Overall, the life cycle of this persistent inversion depended on a change in the temperature structure and wind pattern in the Uinta Basin. At the beginning of the inversion, warm air aloft and cold air at lower levels led to the intensification of the cold pool. From 28 February, the air aloft started cooling with increased wind speed and a change in wind direction at the lower levels, which led to the weakening of the inversion and eventually lifting up the inversion by 1 March 2019.

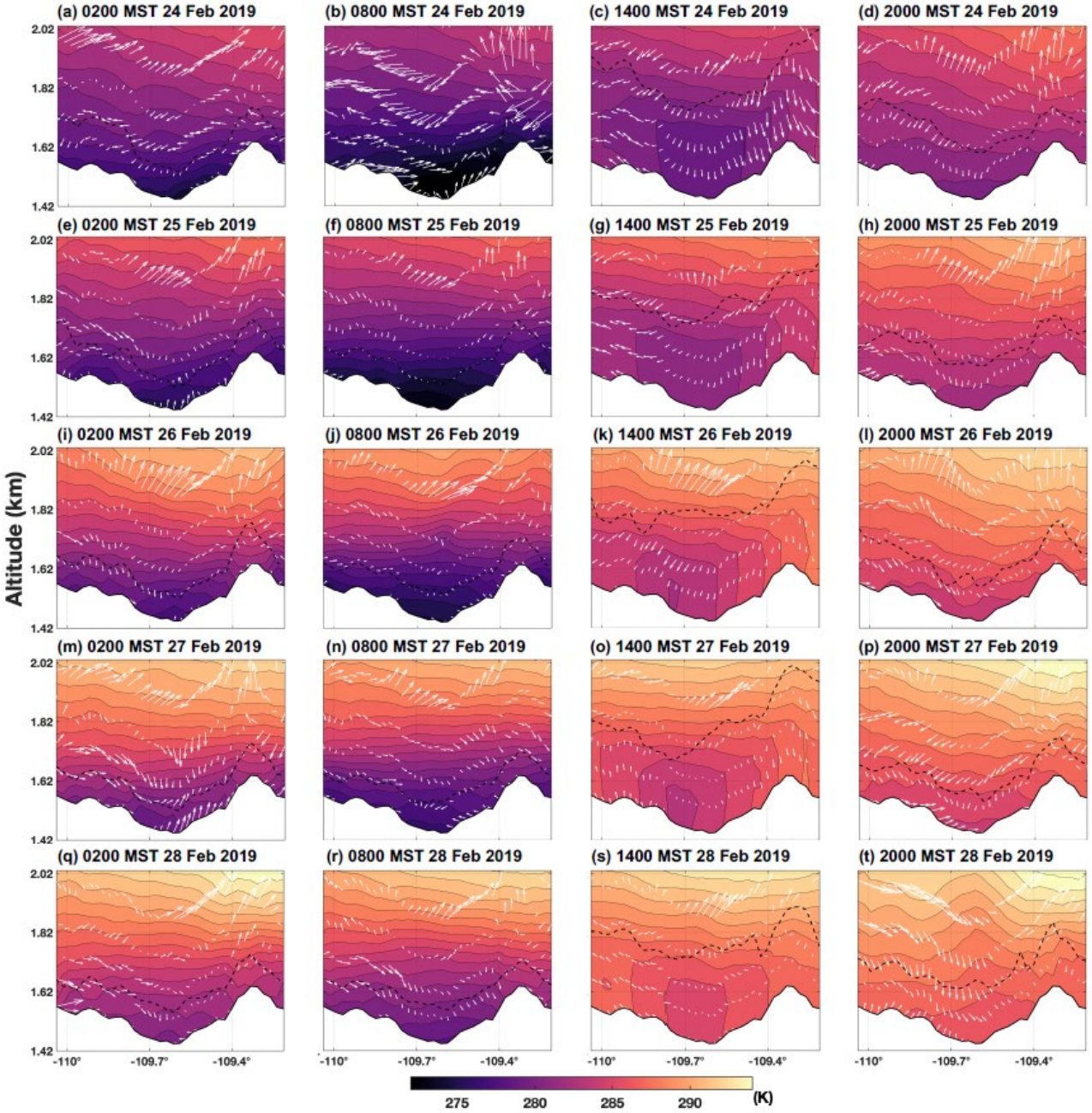

Figure 8-10. Cross-valley (AA') vertical cross-section of simulated potential temperature (contours) and wind from 24 February (0200 MST) to 28 February 2019 (2000 MST). The black dashed line is the simulated planetary boundary layer height.

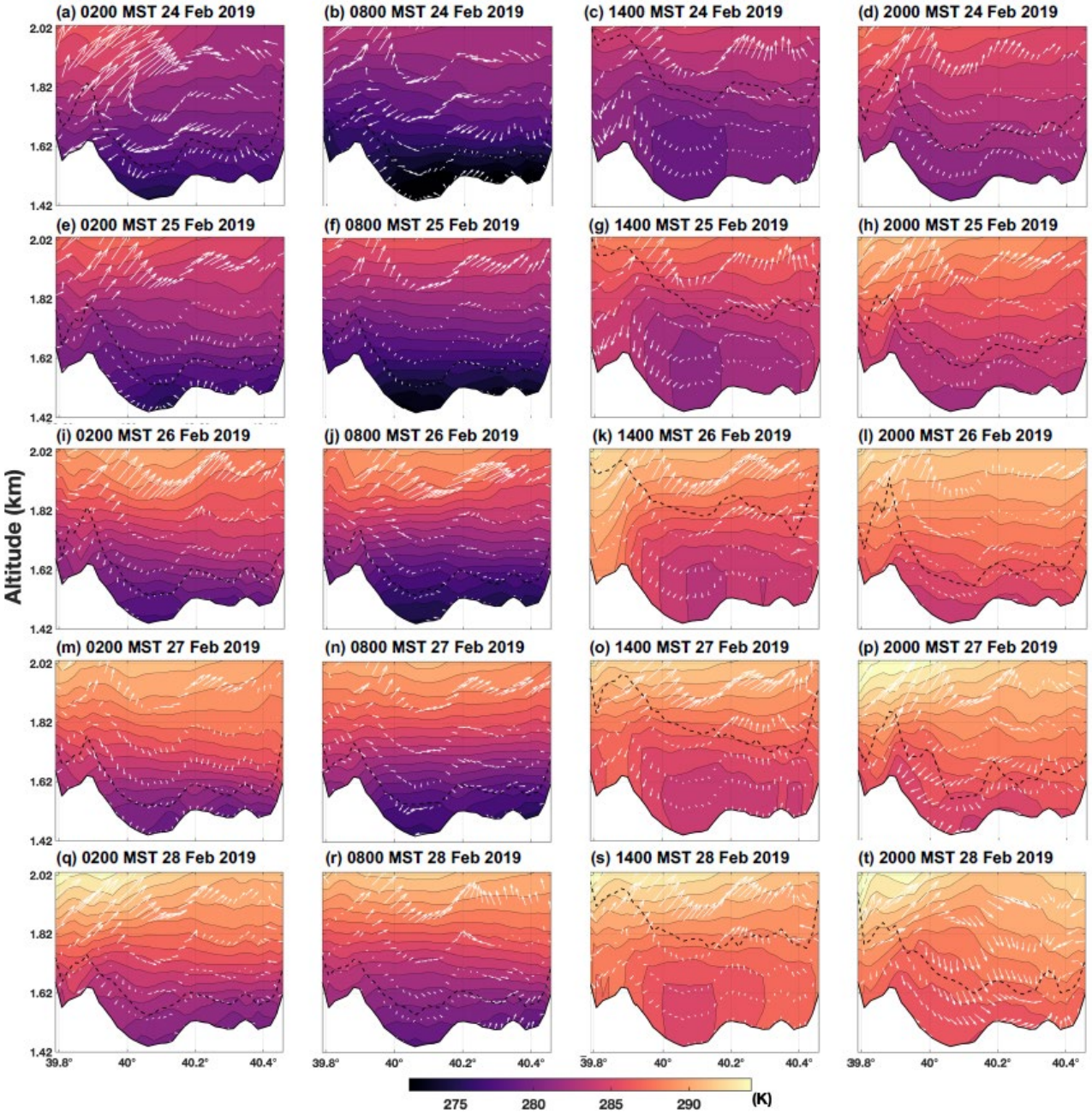

Figure 8-11. Along-valley (BB') vertical cross-section of simulated potential temperature (contours) and wind from 24 February (0200 MST) to 28 February 2019 (2000 MST). The black dashed line is the simulated planetary boundary layer height.

8.4. Acknowledgments

This work was funded by the Utah Legislature and Uintah Special Service District 1.

9. Seasonal Trends in the Wintertime Photochemical Regime

Author: Marc Mansfield

9.1. Note about Terminology

For convenience in this section, we use the acronym VOC to refer to all non-methane organic compounds, including ethane. This is not the regulatory definition of VOC. See Section 2 for more information.

9.2. Introduction

The expression "photochemical regime" refers to the degree to which an ozone system is either nitrogen oxides (NO_X) or volatile organic compound (VOC) sensitive. Knowledge of the regime is important in controlling ozone concentrations. For example, VOC controls would be ineffective if the Uinta Basin airshed is not sensitive to VOC, and likewise for NO_X controls.

Several ozone systems in North America, Europe, and East Asia have been reported to be more NO_X-sensitive in summer and more VOC-sensitive in winter (Jacob et al., 1995; Jin et al., 2017; Kleinman, 1991; Liang et al., 1998; Martin et al., 2004). We reported on a similar trend in the Uinta Basin in our 2013 annual report (Stoeckenius et al., 2014). In the Uinta Basin, the ozone production efficiency, i.e., the number of ozone molecules generated for each NO_X molecule consumed, grows as we progress from the winter solstice to the vernal equinox (Figure 9-1). Larger values of the ozone production efficiency indicate a shift towards relatively higher NO_X sensitivity and vice versa (Chou et al., 2009; Rickard et al., 2002; Sillman, 1995, 1999; Sillman and He, 2002; Sillman et al., 1997; Sillman et al., 1998).

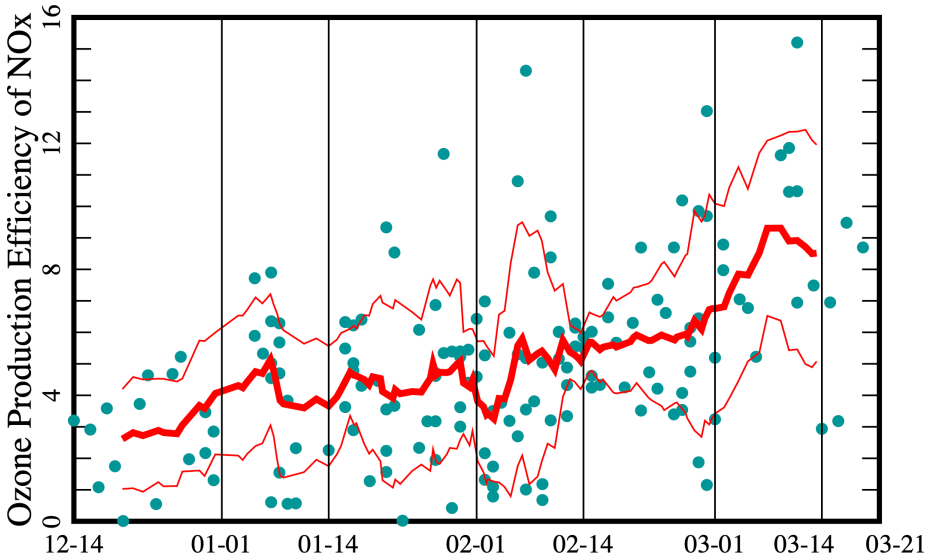

Figure 9-1. Ozone production efficiency at the Horsepool monitoring station in the Uinta Basin. Data from days when the hourly ozone concentration exceeded 60 ppb from 2011 to 2022 and from December 14 to March 20 are shown. The red traces show a ten-point running average plus or minus one standard deviation.

9.3. Methods

We performed box model calculations to better understand this trend in the Uinta Basin. We used the "Framework for 0-D Atmospheric Modeling" (F0AM) platform, version 4.2.1. The chemistry mechanism was a subset of the "Master Chemical Mechanism," MCM v3.3.1 (Saunders et al., 2003; Wolfe et al., 2016).

We define the incremental sensitivity, S_X, of ozone to variable X as follows. Calculate the change in ozone concentration $d[O_3]$ brought about by a small change dX in variable X. The fractional changes are dX/X and $d[O_3]/[O_3]$. S_X is the ratio of these two fractional changes:

$$S_X = \frac{dX}{X} \Big/ \frac{d[O_3]}{[O_3]} = \frac{[O_3]}{X}\frac{dX}{d[O_3]} = \frac{d\ln X}{d\ln[O_3]}$$

Defined in this way, SX is unitless. A 1% increase in X produces an S_X% increase in the daily maximum ozone.

We define three photochemical regimes: NO_X-sensitive when $SNO_X > S_{VOC} > 0$, VOC-sensitive when $S_{VOC} > SNO_X > 0$, and NO_X-saturated when $S_{VOC} > 0 > SNO_X$. The NO_X-saturation regime occurs when a decrease in NO_X produces and increase in ozone. Generally, VOC-sensitivity and NO_X saturation occur when there is an excess of NO_X, while NO_X-sensitivity results from an excess of VOC. It is often useful to consider transitional regimes, e.g., $SNO_X \approx S_{VOC}$. These are generally obvious from the context.

We modeled ozone concentrations on 24 peak-ozone days between 15 December and 15 March and between 2013 and 2021. Maximum one-hour ozone concentrations on these days varied anywhere from 59 to 154 ppb. Observational values of meteorological data and NO_X concentrations were employed as input data. Ambient VOC concentrations were usually not available. Input VOC concentrations were in a proportion determined from independent measurements at the Horsepool station, and to obtain a base-case model for the day, we adjusted the total VOC concentration until the modeled ozone concentration agreed with measurements.

9.4. Results

Figure 9-2 shows the VOC and NO_X sensitivities of each model. In December and January, VOC sensitivities are always larger than NO_X sensitivities, and NO_X sensitivities are often negative. In late winter, NO_X and VOC sensitivities are typically comparable. The three late-winter models (2019-02-27, 2013-03-03, 2019-03-06) have nearly equal sensitivities to NO_X and VOC.

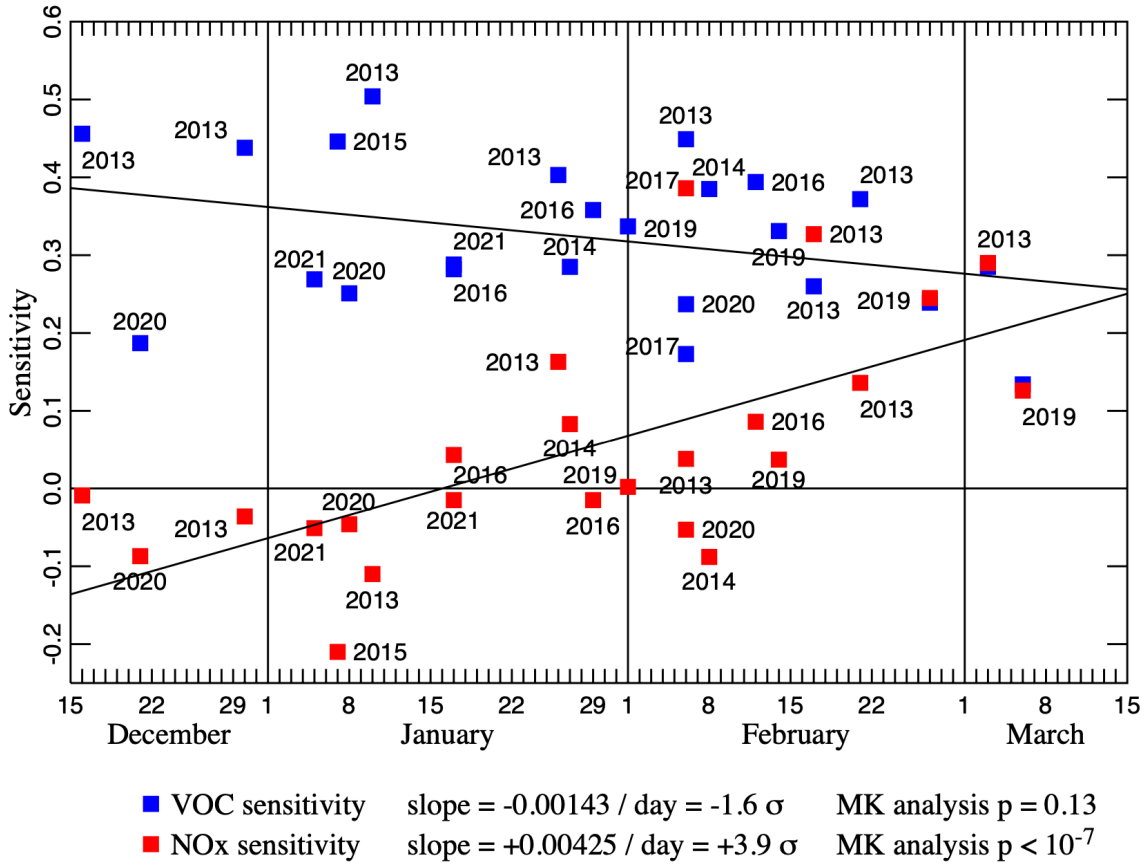

Figure 9-2. *S*VOC and *S*NOX for 24 different box model runs. Slopes of the least-squares trend lines are given both as numerical values and as multiples of the standard deviations of the slopes. The *p*-values from Mann-Kendall trend analyses are also shown.

The late-winter convergence of S_{VOC} and SNO_X results more from an increase in SNO_X than from a decrease in S_{VOC}. The trend line for S_{VOC} has a slope of $-1.6\ \sigma$, for σ the standard deviation of the slope and a *p*-value of 0.13 from a Mann-Kendall trend test (Kendall, 1948; Mann, 1945). Therefore, the downward trend in S_{VOC} may be real, but yet is not statistically significant at the 95% confidence limit. On the other hand, with a slope of $+3.9\ \sigma$ and a very small Mann-Kendall *p*, the upward trend in SNO_X is statistically significant. The models indicate that in early winter, the Basin is either VOC-sensitive ($S_{VOC} > SNO_X > 0$) or NO_X-saturated ($S_{VOC} > 0 > SNO_X$), while in late winter, NO_X and VOC sensitivities are about the same.

We performed additional box model calculations to better understand the drivers for the trends in S_{VOC} and SNO_X. Table 9-1 presents several variables that trend throughout the season and that we considered as candidate drivers. We modulated each of these variables in our box models to appraise their effect on S_{VOC} and SNO_X.

Table 9-1. Variables considered as possible causes of trends in S_{VOC} and SNO_X.

TRENDING VARIABLE	RANGE
Increase in available actinic flux, with noontime solar zenith angle as proxy.	Noontime solar zenith angle varies from 63.6° at the solstice to 40.1° at the equiNO_X.
Decrease in VOC concentrations, with CH_4 concentration as proxy.	Mean [CH_4] is 5.6 ppm in early January, and 2.7 ppm in early March.
Decrease in NO_X concentrations.	Mean [NO_X] is 5.4 ppb in early January, and 1.1 ppb in early March.
Increase in temperature.	The mean varies from –6.6°C to + 8.3°C from early January to early March.
Increase in absolute humidity.	The mean varies from 3.0 mbar to 4.3 mbar from early January to early March.

The trends in actinic flux, temperature, and absolute humidity are, of course, well understood. The trends in VOC and NO_X concentrations result from at least two causes:

1. Weakening inversions. Inversions are typically weaker in late winter and precursors are more diluted because the mixing layer is deeper.
2. Usage patterns. Many studies report that NO_X emissions are greater in winter, due for example, to poorer engine performance, cold starts, and operation of NO_X after-treatment systems (e.g., catalytic converters) outside their optimal temperature range (Bishop et al., 2022; Dardiotis et al., 2013; Grange et al., 2019; Hall et al., 2020; Li et al., 2020; Reiter and Kockelman, 2016; Saha et al., 2018; Suarez-Bertoa and Astorga, 2018; Wærsted et al., 2022; Wang et al., 2019; Weber et al., 2019). We have been unable to find data on temperature trends in the NO_X emissions from drilling rigs, but their cold-weather behavior may be similar to other internal combustion engines. Emissions sources that operate preferentially in winter, for example, well-site and portable natural gas-fueled heaters, glycol dehydrogenators, heat trace pumps, “hot oil” trucks, operations to thaw frozen lines, pipeline venting, and well blowdowns, probably also contribute.

More study is needed to better understand the relative importance of the two causes.

For each of the models, we allowed each of the variables in Table 9-1 to vary throughout its range while holding the other four constant, and we examined the resulting changes in S_{VOC} and SNO_X. The results appear in Figure 9-3. Let ΔS_{VOC} and ΔS_{NOx} represent the change in S_{VOC} and SNO_X, respectively, over the course of the winter. Each bar indicates the contribution to ΔS_{VOC} or ΔS_{NOx} arising from the indicated variable. In both cases, the solar zenith angle is the most important driver, contributing to increases in both S_{VOC} and SNO_X. The decreasing trends in precursor concentrations are the second most important drivers. They exert a negative influence on S_{VOC} and opposing influences on SNO_X. Temperature exerts a weak positive influence on both S_{VOC} and SNO_X. The impact of absolute humidity is negligible. The combined effect of all five variables on S_{VOC} is not statistically significantly different from zero but is net positive for SNO_X, consistent with the results shown in Figure 9-2.

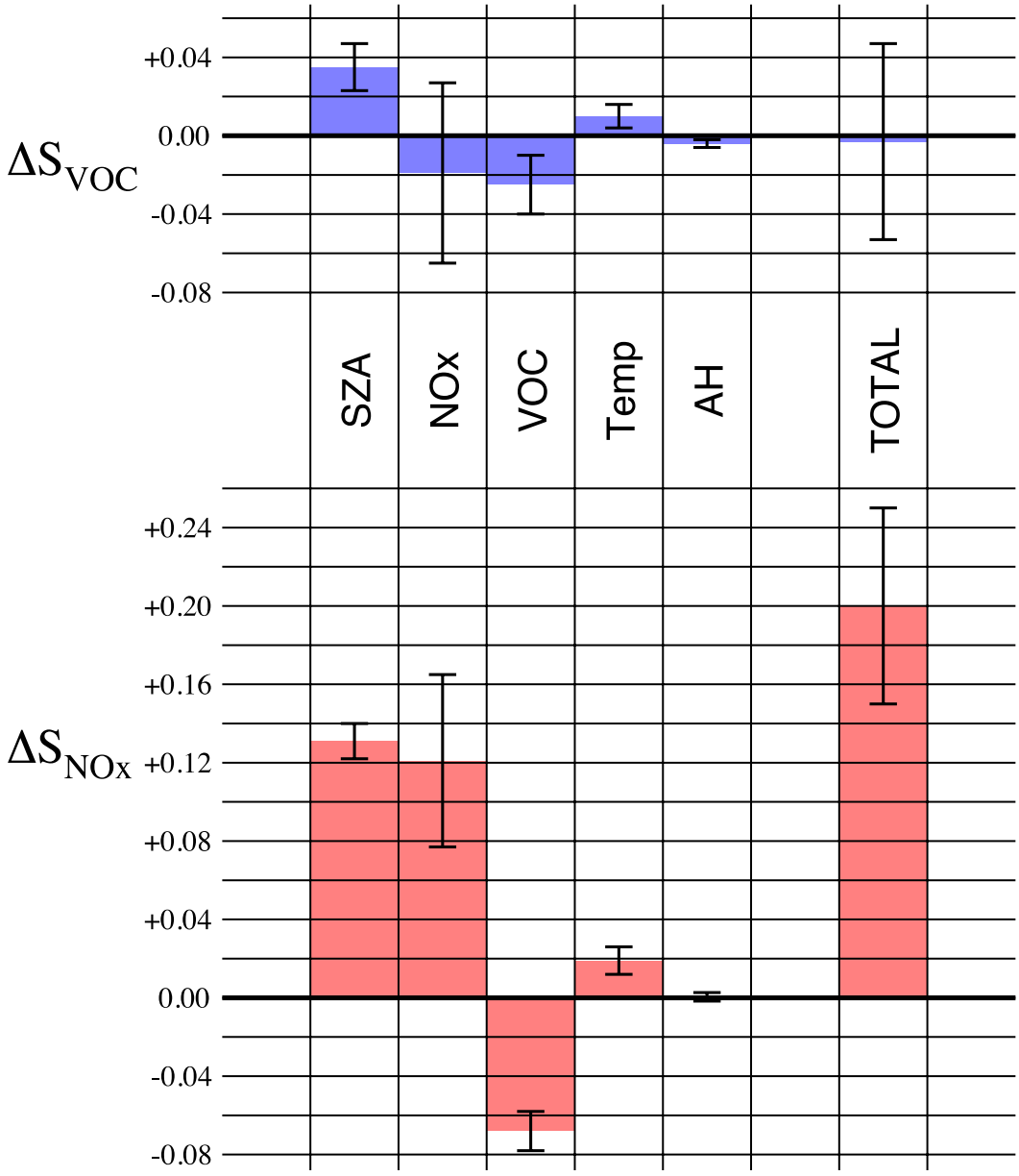

Figure 9-3. Contribution of the seasonal trends in each of the indicated variables to changes in S_{VOC} and SNO_X; decreasing solar zenith angle (SZA), decreasing VOC and NO_X concentrations, increasing temperature (Temp), and increasing absolute humidity (AH); on the seasonal trends in VOC and NO_X sensitivity. The sum of all five contributions is labeled "TOTAL."

It is interesting to document these results in the ozone isopleth plots. We calculated an ozone isopleth diagram for each of the 24 models by scaling NO_X and VOC concentrations relative to the base model. Each F0AM run requires approximately 2 to 4 minutes on a MacBook Pro laptop, and generating the full diagram at high resolution proved to be too time-consuming. Rather, we calculated pixels at high

resolution only around the boundary of the diagram and in the vicinity of the "indicator curves," defined below, and at lower resolution throughout the remainder of the plot. The ozone isopleth surface at all remaining pixels was generated by kriging interpolation (Kerry and Hawick, 1998).

We found that any two isopleth diagrams generated from nearby calendar dates are approximately superposable. This superposability allows us to generate six composite isopleth diagrams corresponding to each half-month from December 15 to March 15 (Figure 9-4). The white and pink squares define "indicator curves:" The white squares give the locus of points at which $SNO_X = 0$ so that the NO_X-saturation domain, $SNO_X < 0$, lies above them. Pink squares define the locus of points at which $SNO_X = S_{VOC}$. Therefore, the VOC-sensitive domain lies between the white and pink squares, and the NO_X-sensitive domain lies below the pink squares. Discontinuities in the contour curves occur because the diagrams of the individual models were not constructed with the same boundaries and because the individual models are not perfectly superposable. The indicator traces fail to line up exactly for the same reason. Nevertheless, these discontinuities are generally not large, validating the approximate superposability of the individual models. The domains defined by the 25th and 75th percentiles of VOC and NO_X appear in Figure X.4 as white boxes.

Three trends are obvious in Figure 9-4: (1) The calculated ozone concentration grows through the season. The maximum ozone concentration in the upper right corner doubles from about 110 ppb in December to about 220 ppb in March. As explained below, the primary driver for this trend is the change in solar zenith angle. (2) The indicator curves shift upward as winter progresses. As documented in Figure 9-3, this is due predominantly to the change in solar zenith angle. (3) The decrease in typical values of precursor concentrations, described above, is observed as the white boxes drift downward and to the left. The net effect is that in early winter, the white boxes lie in the NO_X-saturation and VOC-sensitive regimes, and they shift over the course of the winter to the NO_X-sensitive and VOC-sensitive regimes.

Although our primary focus is the trend in SNO_X and S_{VOC}, we also calculated the sensitivity of ozone to solar zenith angle, S_θ, to temperature, S_T, and to absolute humidity, S_{AH}. Over the 24 models, solar zenith angle contributes to a +36% to +53% (25th to 75th percentiles) change in ozone concentration from December to March. The contributions from temperature and absolute humidity are weaker: +4% to +10% and +1% to +2%, respectively.

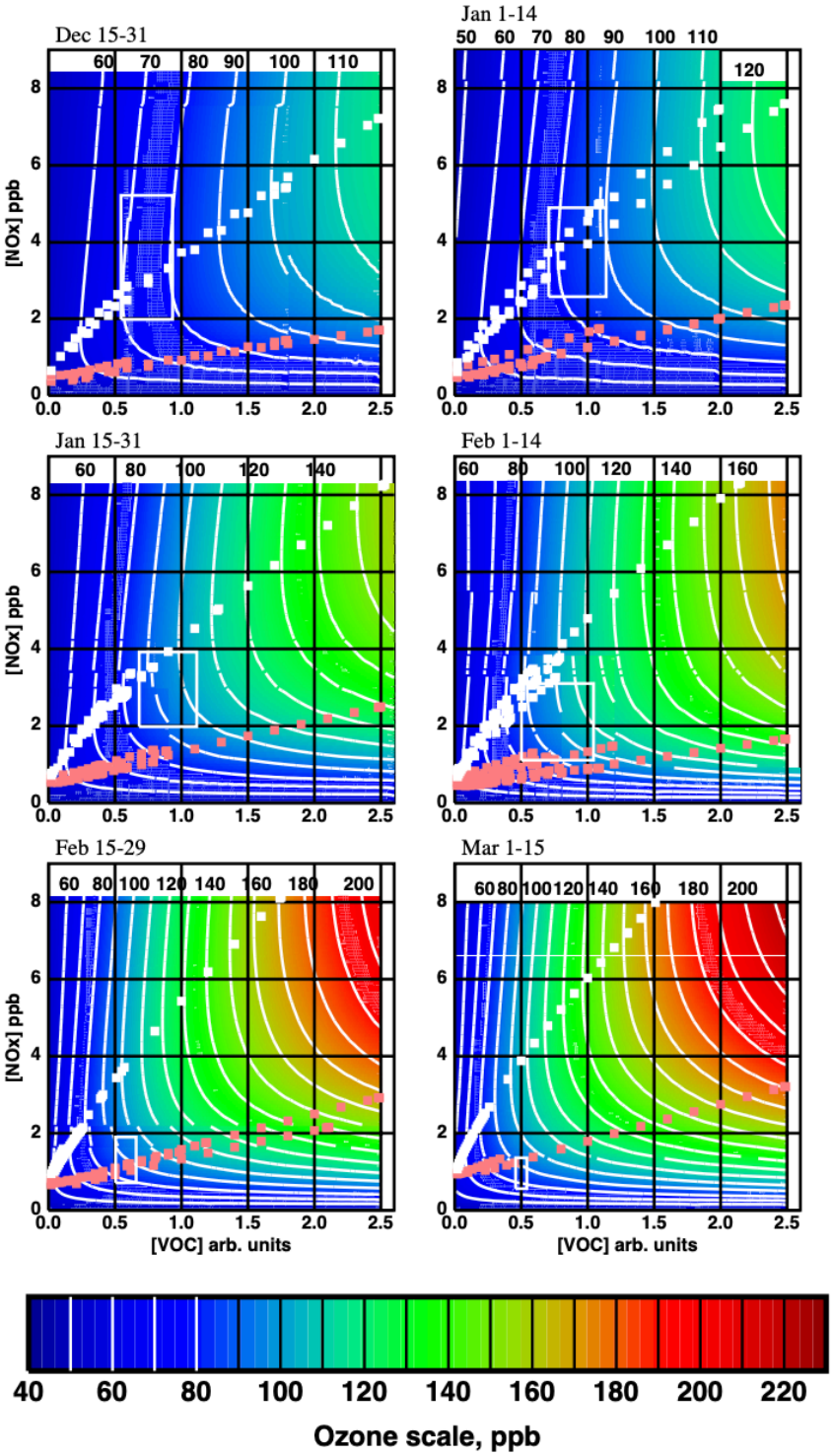

Figure 9-4. Composite ozone isopleth surfaces. White squares define the locus of points at which $SNO_X = 0$. Pink squares define the locus of points at which $SNO_X = S_{VOC}$. White boxes enclose the 25th-to-75th percentiles of VOC and NO_X concentrations.

9.5. Conclusions

Seasonal trends in the photochemical regime are very common throughout the Northern Hemisphere. This study identifies the primary drivers for the trend in the Uinta Basin from late December to early March. No doubt these drivers have a similar effect elsewhere, but we should be cautious in extending these results to other regions. For example, biogenic emissions may be an important driver in many regions than they are in the arid Uinta Basin. However, the fact that such trends are ubiquitous may result from the importance of actinic flux as a driver in all regions.

On the basis of these results, we recommend that ozone mitigation be focused on controlling both NO_X and VOC. NO_X controls in early winter might stimulate higher ozone (whenever $SNO_X < 0$), but then there are fewer daily exceedances with lower ozone on average. Any early-winter ozone increases will probably be more than offset by decreases in February and March.

9.6. Acknowledgments

This work was funded by the Utah Legislature and Uintah Special Service District 1.

10. Sensitivity of Winter Ozone to Individual Organic Compounds

Author: Marc Mansfield

10.1. Introduction

Carter and Seinfeld (2012) used a box model to determine incremental sensitivities for individual organic compounds during a winter ozone episode in the Upper Green River Basin, Wyoming. An incremental sensitivity is a measure of the change in ambient ozone caused by a change in atmospheric concentrations of an organic compound. Carter and Seinfeld found incremental sensitivities that were quite different from those developed for urban summertime ozone by Carter (2009). Winter ozone precursor concentrations and composition in the Upper Green River Basin during the episode modeled by Carter and Seinfeld were different from those currently experienced in the Uinta Basin. Notably, their modeled NO_X concentrations were about an order of magnitude higher than those currently typical of oil and gas-producing areas in the Uinta Basin. Also, their model used erroneously high concentrations of nitrous acid. Thus, incremental sensitivities for Uinta Basin winter ozone episodes may be different from those produced by Carter and Seinfeld.

Incremental sensitivities specific to Uinta Basin winter ozone episodes are needed to better understand how changes to various emission sources may impact winter ozone production. Different emission source types have very different organic compound compositions, such that a kg of organics emitted from a raw gas leak will have a lower capacity to produce ozone than a kg of organics emitted from a glycol dehydrator, for example, since dehydrator emissions are richer in reactive aromatics. Incremental sensitivity data will allow for a comparison of the ability of emissions from different sources to produce ozone.

10.2. Methods

We used the F0AM box model to determine incremental sensitivities for individual organic compounds. Details about the model and its implementation for this study are available in Section 9. We carried out the same reactivity calculation for 24 different models – the same 24 considered in Section 9.

Let y represent the maximum ozone concentration in the F0AM run, and x the concentration of any one organic compound. The incremental sensitivity is defined as the ratio of the fractional change in y, dy/y, to the fractional change in x, dx/x. In other words, if S = 1, and if x changes by 1%, then y will also change by 1%. The second equality shows that S is the slope of the tangent on a log-log plot.

$$S = \frac{x}{y}\frac{\partial y}{\partial x} = \frac{\partial \ln y}{\partial \ln x}$$

We estimated the derivatives as

$$\frac{\partial y}{\partial x} \cong \frac{1}{2}\left[\frac{\Delta_1 y}{\Delta_1 x} + \frac{\Delta_2 y}{\Delta_2 x}\right]$$

Where Δ_1 represents the change in the concentration when x is increased by 5% and Δ_2 represents the change in the concentration when x is decreased by 5%. We calculated the sensitivity of winter ozone production to 41 different organic compounds and carbon monoxide (CO).

In each model run, we changed concentrations of one compound while forcing other measured organic compounds to match measured values. This is equivalent to having all sources and sinks in balance during the run. This gives questionable results for compounds that form from photochemical reactions in the atmosphere, like aldehydes. It is most reasonable in cases where the compound is in enough excess that its concentration changes imperceptibly.

10.3. Results

The box-whiskers plots in Figure 10-1 show the calculated sensitivity values for each of the analyzed compounds. Each box-whisker construction corresponds to the distribution of sensitivity values over each of the 24 models. The sensitivities vary so widely that four different scales have been used. Formaldehyde sensitivity is an order of magnitude larger than any others. Most sensitivities are positive, but a few are negative, namely, acrolein, acetaldehyde, and benzaldehyde. A negative sensitivity occurs when an increase in the particular compound produces a DECREASE in ozone.

The figures at the end of this section show the sensitivity of each individual compound in each individual model. Because the method we used shows the change in ozone per fractional change in an organic compound, rather than the mass change in an organic compound, the magnitude of the sensitivity value depends both on the reactivity of the compound and its abundance. For example, methane and ethane are less reactive than alkanes with six or more carbon atoms, but their sensitivities, as determined by this method, are greater because they are much more abundant than alkanes with six or more carbon atoms (Figure 10-3).

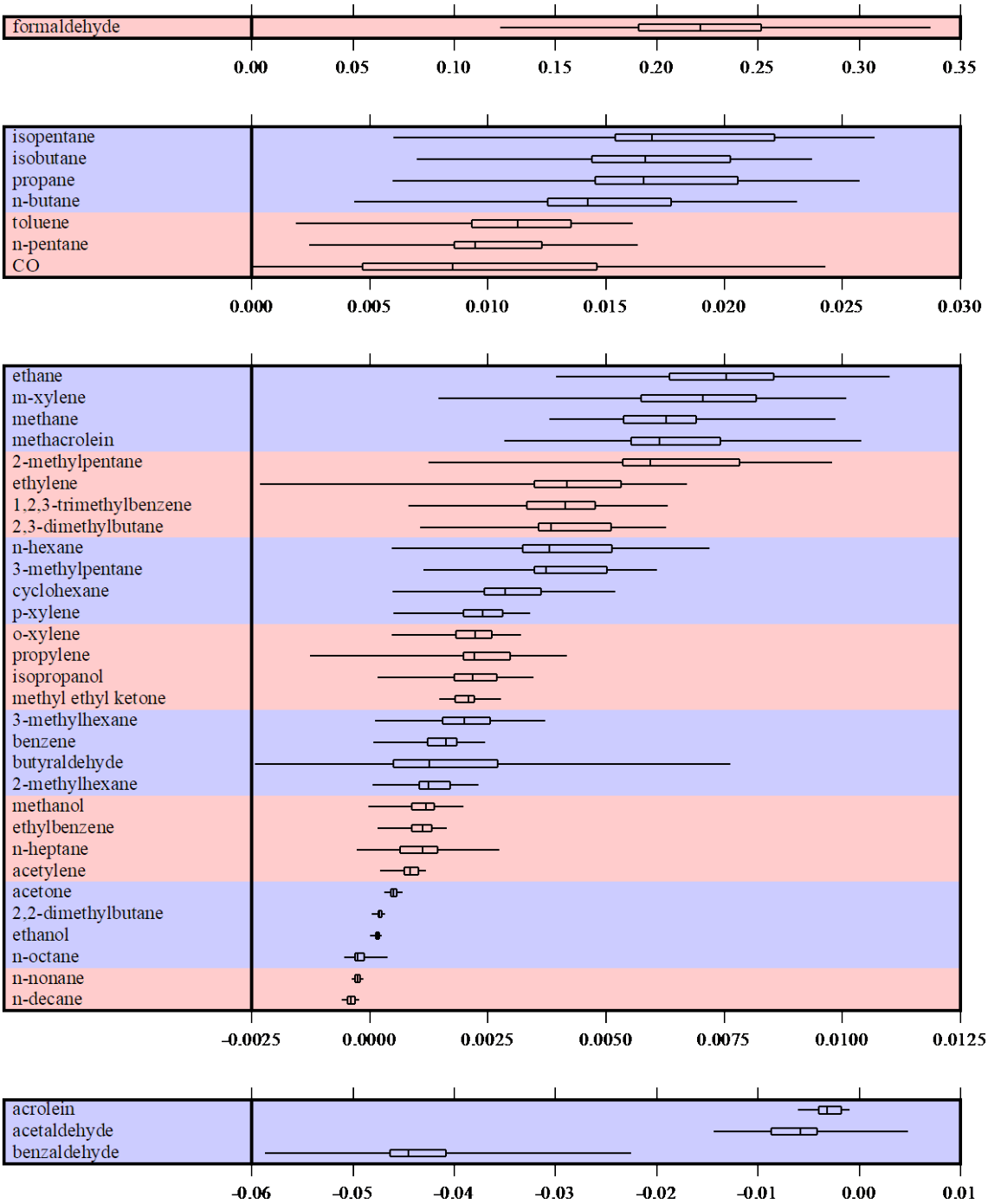

Figure 10-1. Box and whisker plots of winter ozone sensitivity to individual organic compounds and CO. Units are the fractional increase in ozone in response to an equivalent fractional change in the indicated compound. The line segmenting each box is the median value for the 24 model runs, and the limits of each box are the 25th and 75th percentiles of the data. The whiskers show the full extent of the data.

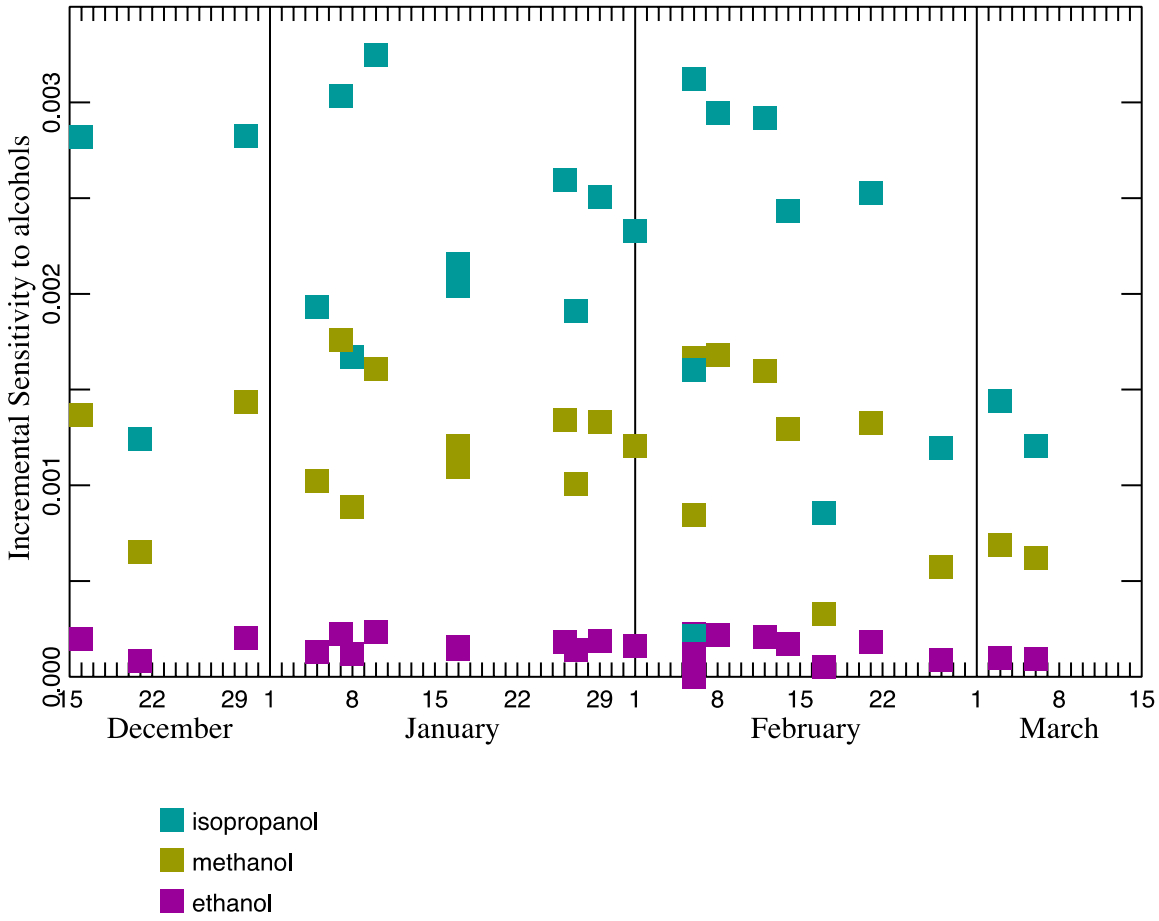

Figure 10-2. Incremental sensitivity of daily maximum ozone to light alcohols in each of the 24 modeled episodes.

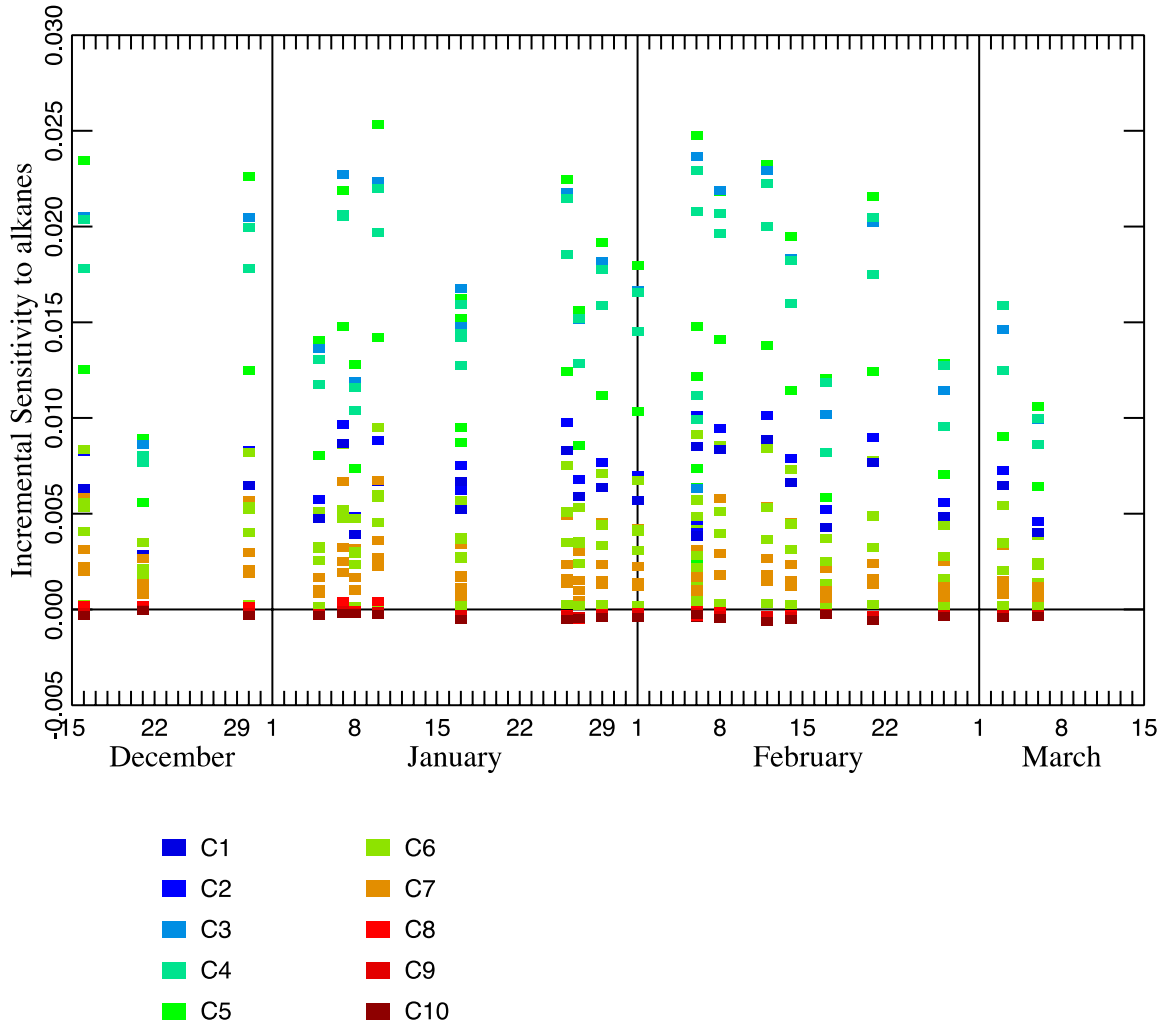

Figure 10-3. Incremental sensitivity of daily maximum ozone to methane (C1) and alkanes in each of the 24 modeled episodes. Compounds are grouped by the number of carbon atoms in each compound (C1 compounds have one carbon, C2 have two, etc.)

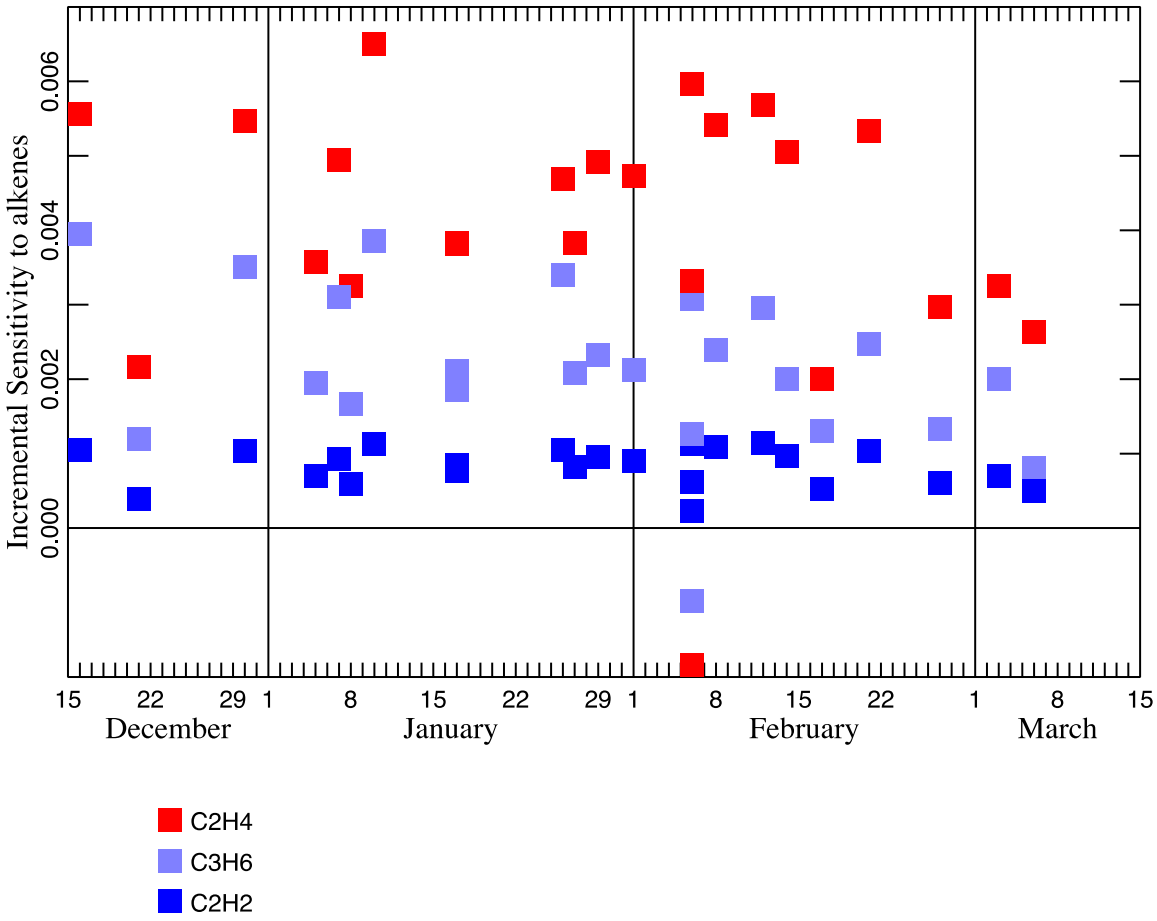

Figure 10-4. Incremental sensitivity of daily maximum ozone to ethylene (C2H4), propylene (C3H6) and acetylene (C2H2) in each of the 24 modeled episodes.

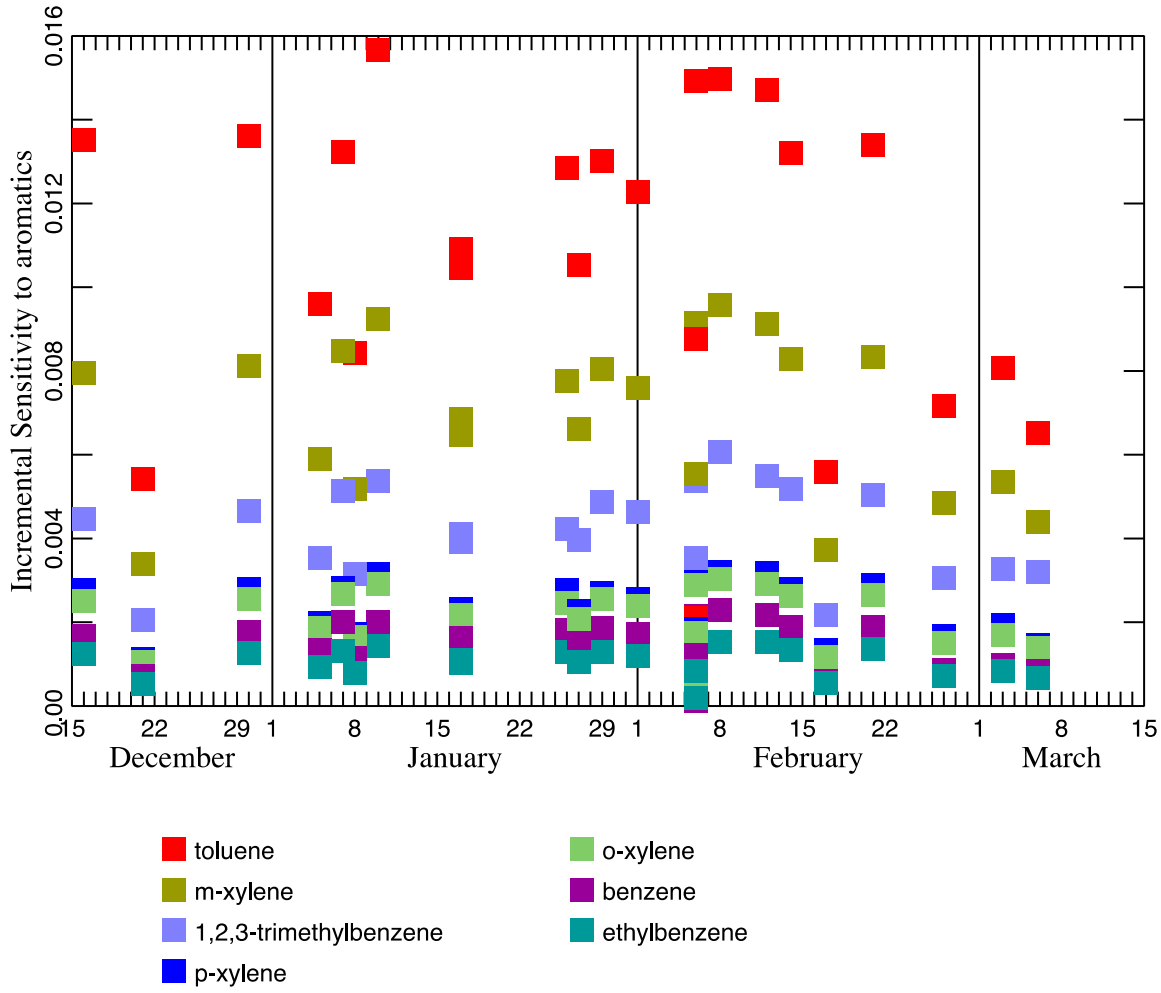

Figure 10-5. Incremental sensitivity of daily maximum ozone to aromatics in each of the 24 modeled episodes.

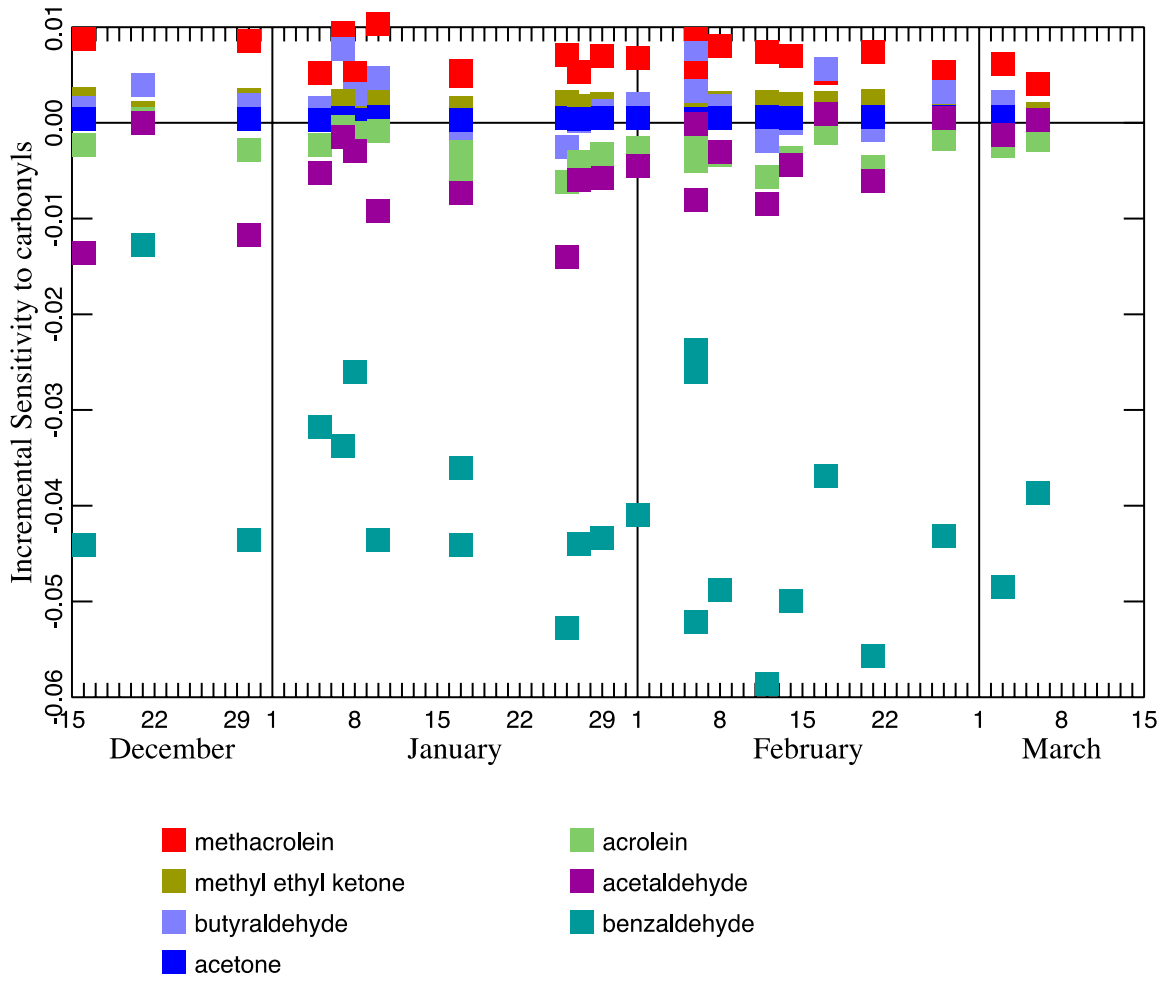

Figure 10-6. Incremental sensitivity of daily maximum ozone to carbonyls (except formaldehyde) in each of the 24 modeled episodes.

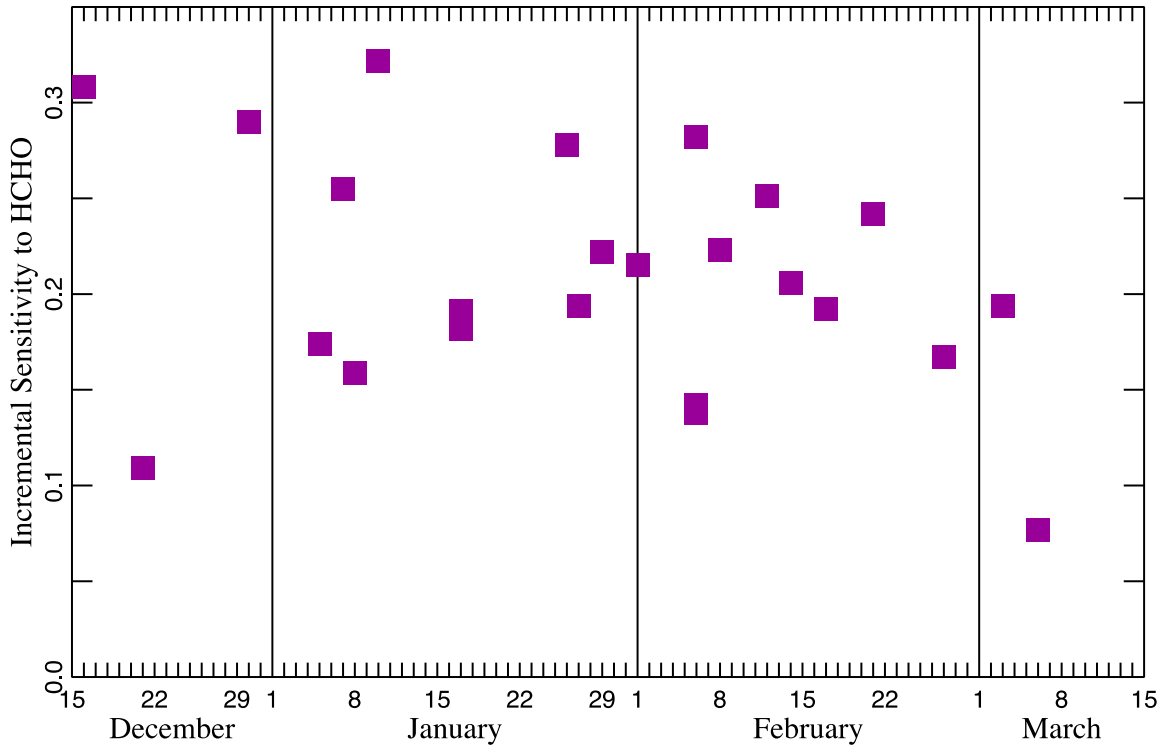

Figure 10-7. Incremental sensitivity of daily maximum ozone to formaldehyde (HCHO) in each of the 24 modeled episodes.

10.4. Acknowledgments

This work was funded by the Utah Legislature and Uintah Special Service District 1.

11. Estimates of Emissions by Pumpjack Engines

Author: Marc Mansfield

11.1. Introduction

There are about 3,000 natural-gas-fueled pumpjack engines in the Uinta Basin of Eastern Utah. The emission inventory prepared by the Utah Division of Air Quality (UDAQ) for calendar year 2017 (UDAQ, 2023) and an independent fuel-based estimate by Gorchov Negron et al. (2018) both peg the NO_X emission from pumpjack engines in the Uinta Basin at about 5,000 ton/year or 41% of all oil-and-gas NO_X emissions. However, Lyman et al. (2022c) measured emissions from pumpjack engines in the Uinta Basin and found that their NO_X emissions were only 9% of the value reported in the UDAQ inventory. We also consulted several other inventories prepared by state agencies and found that all followed the identical protocol for estimating pumpjack emissions. Lyman et al. also found that organic compound emissions by pumpjacks were about a factor of 15 larger than in the UDAQ inventory. We performed mining and analysis of several databases to better understand the discrepancy between estimates of NO_X emissions by such engines.

Three datasets on pumpjack engines informed our work.

1. Laboratory measurements performed at Texas A&M University (TAMU) on NO_X emissions from an Ajax E-565 engine are available (Brown, 2017; Griffin, 2015; Griffin and Jacobs, 2015). Here, we refer to their data as the TAMU database.
2. Researchers from Utah State University measured emissions from 58 pumpjack engines in the Uinta Basin between January and May 2021, with a few follow-up measurements in January 2022 (Lyman et al., 2022c). We refer to their measurement campaign as the USU Engine Study and to their data as the USU database.
3. Federal regulations (Code of Federal Regulations/Title 40/Chapter I/Subchapter C/Part 60/Subpart JJJJ) require owners to perform and report measurements of emissions from natural-gas-powered internal combustion engines installed after 2008. Results are on file with the State of Utah (http://eqedocs.deq.utah.gov). We culled data from 261 reports on natural-gas-fueled engines and refer to the database we constructed as the JJJJ database. Our database includes 248 engines rated by the manufacturer at less than 100 hp, for which the owners are only required to report NO_X and CO emissions. The vast majority of these are pumpjack engines. The remaining 13 engines, rated greater than 100 hp, are almost always compressor engines, i.e., engines used to compress natural gas, and for these organic compound emissions were also reported.

11.2. NO_X Emissions by Pumpjack Engines are Highly Non-Linear with Load and are Overestimated in Typical Emissions Inventories

Measurements found in the TAMU database consistently indicate that NO_X emissions by pumpjack engines are highly non-linear functions of the load on the engine. The NO_X emission, even at 70% to 80% load, is much lower that the emission at 100% load. In Figure 11-1, the average NO concentration in the exhaust reported in the TAMU database is shown as a function of engine load. Of course, concentration is not the same as emission, but since all measurements occurred at the same engine speed (450 RPM) we expect the two to be strongly correlated.

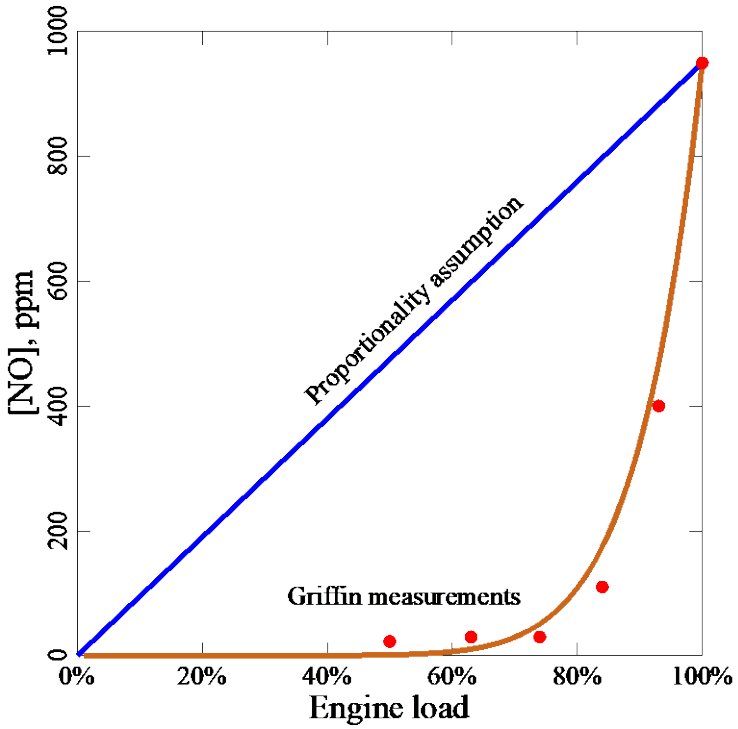

Figure 11-1. NO concentration in engine exhaust as a function of engine load for an Ajax E-565 engine at 450 revolutions per minute (rpm). NO concentration is highly non-linear in the load. The blue diagonal represents the expected concentration from an assumption of linearity. Adapted from Griffin (2015), Figure 19.

Engine emissions are usually reported as the "specific emission rate," SER, i.e., the emission in g/hr normalized by the engine load in horsepower (hp), resulting in units of g/(hp-hr). There are large discrepancies between SER values employed in preparing inventories and those determined in the JJJJ certification measurements. We consulted inventories prepared for Oklahoma, Texas, Minnesota, Utah, and the Western Regional Air Partnership. All follow the same approach to estimating pumpjack engine emissions. They use an appropriate SER value at 100% load, thereby ignoring the non-linear dependence on the load documented above. Some inventories apply a load factor of around 70%, but this is equivalent to using the blue line in Figure 11-1. Figure 11-2 compares SER values employed in the UDAQ inventory against those reported in the JJJJ certification tests. The median SER from the JJJJ

database is about an order of magnitude lower than the SER values used to estimate emissions in the inventory.

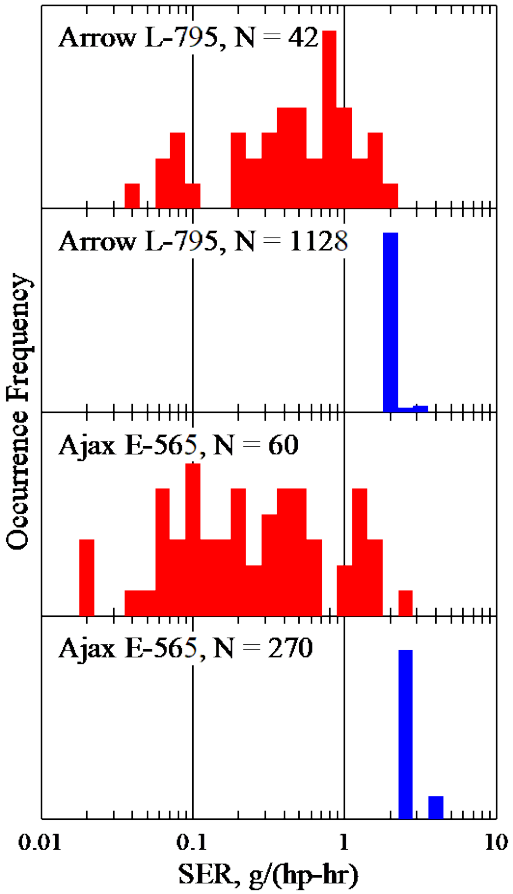

Figure 11-2. Distribution in NO_X SER values for the indicated engine make and model. Red bars are the results from a selection of JJJJ-mandated field tests, and blue bars indicate the SER values used to develop the UDAQ inventory.

New wells are high producers, represented by the far right of Figure 11-1 and Figure 11-2, and they must be fitted with engines capable of lifting large volumes. Typical production rates decline significantly over about a year, but the engines typically are not replaced. Therefore, most engines run at partial loads, well below their rated horsepower capacity, following the tan trace in Figure 11-1 rather than the blue, and their NO_X emissions are significantly overestimated in the inventory. During February 2017, according to production data provided by the Utah Division of Oil, Gas, and Mining (https://oilgas.ogm.utah.gov/oilgasweb/live-data-search/lds-prod/prod-lu.xhtml), over one-half of the Uinta Basin wells produced less than 14 barrels of water and oil per day. According to our estimates summarized below, this corresponds to a time-averaged power requirement of 1 to 2 hp or less using engines rated between 25 and 65 hp and to stroke times of around a minute or longer. Of course, peak loads over the cycle are larger. These results are consistent with the pumpjack measurements reported by the USU Engine Study.

11.3. Modified Estimates of Pumpjack Emissions in the Uinta Basin

We used an industry-standard software product, Echometer QRod 3.1 (https://www.echometer.com/Software/QRod), to develop new estimates of the NO_X emissions by pumpjacks. QRod takes the number of barrels of oil and water lifted daily and computes the necessary power requirement. We applied it to about 3000 wells reported to have produced oil and water in February 2017.

The results of our QRod calculation are compared with other emissions estimates in Figure 11-3. Figure 11-3 parts a and b give the distribution in emissions estimates from two state inventories. Part c gives the distribution obtained from the QRod calculation. Part d shows the distribution obtained from the TAMU database, and Part e shows the results from the USU Engine Study. The total estimated emission over all engines in the QRod calculation is 13 kg/hr. In contrast, the total emission estimate from the same engines in the UDAQ inventory was 586 kg/hr, a factor of 45 times larger.

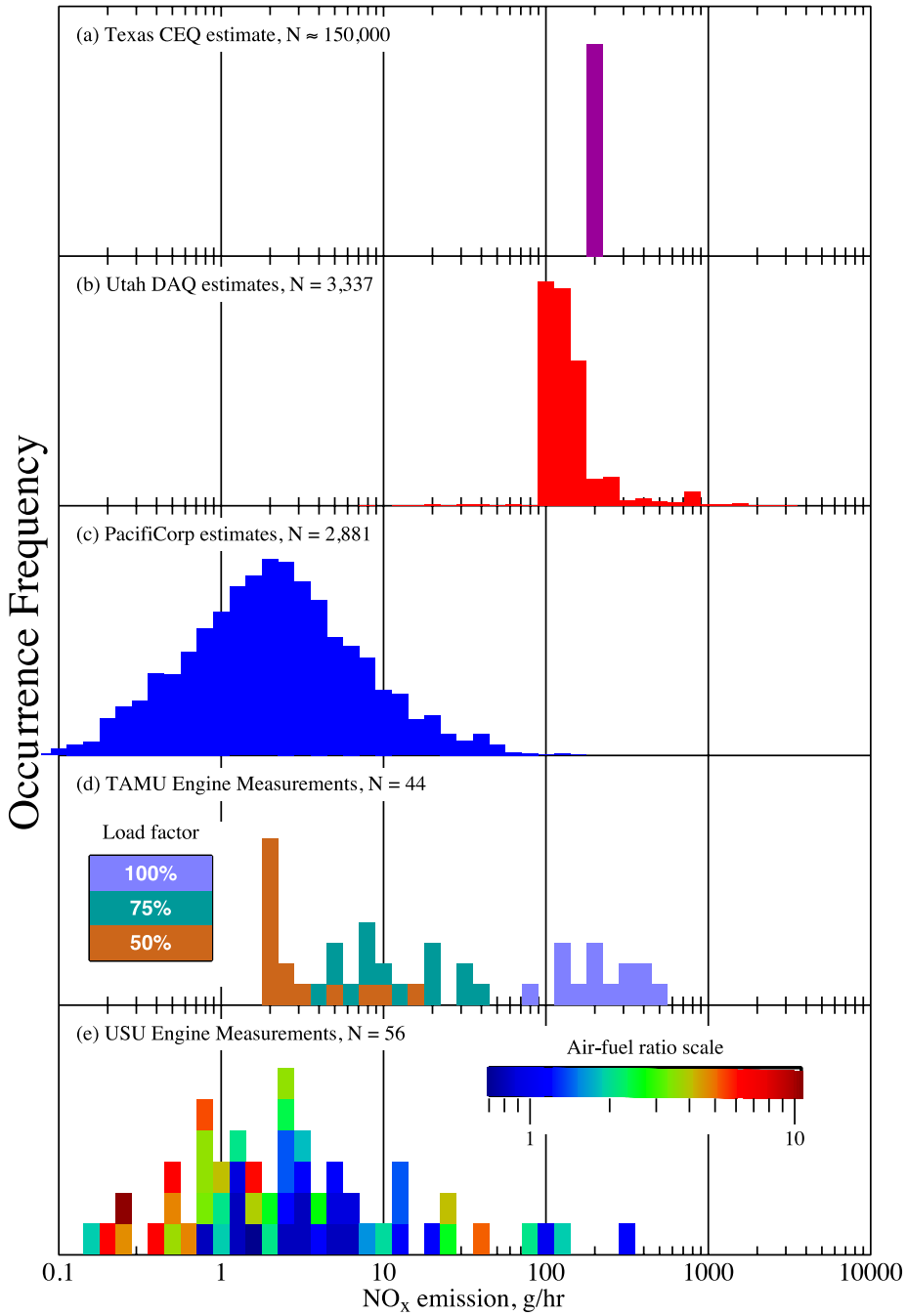

Figure 11-3. NO_X emissions from pumpjack engines, either estimates or measurements. N is the number of engines or independent measurements. (a) An emissions inventory for the Texas Commission on Environmental Quality [TCEQ] applies a blanket average 215 g/hr to all engines in the inventory. (b) The distribution of NO_X emission estimates from pumpjack engines from the UDAQ 2017 inventory. (c) Distribution of estimates obtained in our study. (d) Laboratory results from Texas A&M University for NO_X emissions from

an Ajax E-565 engine, broken down by engine load. (e) Measurements by Utah State University in the Uinta Basin, color code indicates the air/fuel ratio (λ).

11.4. Conclusions

An important finding of this study and of the USU Engine Study is that NO_X and organics emissions from pumpjack engines are severely over- and under-estimated, respectively. NO_X emissions by pumpjacks in the Uinta Basin had been estimated to constitute about 40% of all NO_X emissions from the oil and gas sector, whereas now they appear to be negligible. Organic compound emissions by pumpjacks were thought to be negligible, but the USU Engine Study indicates that they are not. NO_X emissions by natural-gas-fired engines appear to be a highly non-linear function of the load on the engine. Estimates of pumpjack NO_X emissions are most accurate for new wells when the engines work at near 100% load, but production from wells drops off quickly, and after about a year, the same engines are lifting a much lighter load. About one-half of all pumpjack engines in the Uinta Basin lift fewer than 14 barrels of oil and water a day and operate well below 100% load. Organic compound emissions estimates seem to be predicated upon manufacturers' recommendations and do not adequately consider engine adjustments (e.g., the air-fuel ratio) made by operators in the field. For example, the USU Engine Study found many wells with unburned fuel in the exhaust.

A spreadsheet containing the JJJJ database will be made publicly available in the near future.

11.5. Acknowledgments

This work was funded by the Utah Legislature and Uintah Special Service District 1.

12. Report Summary: Top-Down Estimates of Emissions from Oil and Gas Production

Author: Seth Lyman

We recently completed a Basin-wide emissions estimation study, and a final report of our work is available at https://www.usu.edu/binghamresearch/files/reports/Topdowninventory_finalreport_2023.pdf. The following is a brief summary.

We used measurements at monitoring stations in the Uinta Basin to estimate Basin-wide emissions of methane, NO_X, and speciated non-methane organics across multiple years. Figure 12-1 shows Basin-wide emissions estimates determined by this method for methane, total non-methane organics, and NO_X. Estimates for 2013 are from Ahmadov et al. (2015), and methane estimates from 2015 through 2020 are from Lin et al. (2021). Lin et al. first reported the decline in methane emissions through 2020 shown in Figure 12-1, and Mansfield and Lyman (2021) demonstrated a decline in wintertime ozone over a similar time period. Mansfield and Lyman also showed evidence of a decline in NO_X.

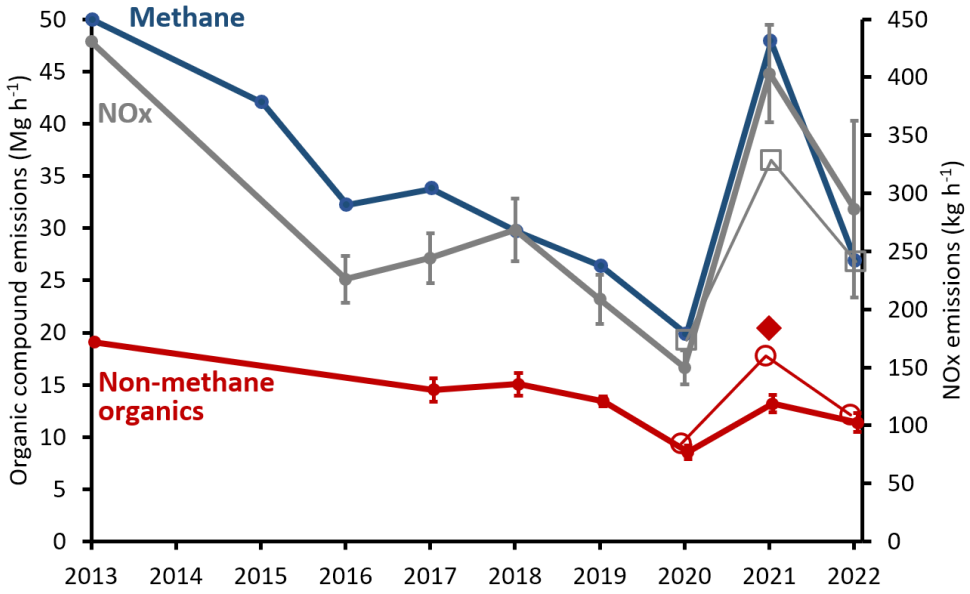

Figure 12-1. Uinta Basin-wide annual emissions estimates for methane, NO_X, and total non-methane organic compounds. 2013 estimates are from Karion et al. (2013) and Ahmadov et al. (2015). Closed circles show estimates derived from Horsepool measurements. Open symbols show estimates derived from Castle Peak measurements. The diamond shows the estimate derived from measurements at portable stations. Whiskers show 95% confidence intervals.

The results shown in Figure 12-1 also show that emissions have increased since 2020, with an anomalous spike in 2021. The low point for pollutant emissions in the Basin was 2020, when the COVID-19 pandemic led to extremely low oil and gas prices. Drilling of new wells also reached its lowest point

in 2020, as did total energy production in the Uinta Basin, and a rebound in oil and gas activity in 2021 and 2022 corresponds with the increase in emissions. We are not certain as to the cause of the 2021 emissions spike. Methane and non-methane organics emissions correlate with several indicators of natural gas extraction activity in the Uinta Basin. NO_X emissions, in contrast, correlate with construction of new wells, perhaps indicating the importance of drilling and well completions to Basin-wide NO_X emissions.

The 2017 Utah Division of Air Quality oil and gas emissions inventory contains several times more NO_X emissions than were estimated in this study, even when overestimates of inventoried NO_X emissions from engines were accounted for (Table 12-1). Inventoried VOC emissions were similar to those observed in this study.

Table 12-1. Basin-wide emissions of NO_X and VOC emissions from the 2017 Utah Division of Air Quality oil and gas emissions inventory, modifications of that inventory as explained in the full report, and the 2017 top-down emissions estimate from this study. Values for this study are shown with ± 95% confidence intervals.

	2017 Utah DAQ emissions inventory version 1.89	2017 Utah DAQ inventory, Modification 1	2017 Utah DAQ inventory, Modification 2	2017 emissions estimate from this study
NOx (tons/yr)	12,284	8,049	5,686	2,357 ± 209
VOC (tons/yr)	102,728	101,584	110,333	104,237 ± 10,085

High NO_X in the 2017 Utah Division of Air Quality inventory enhances the ability of photochemical models to simulate winter ozone (at least in late winter; see Section 9), and the composition of organics in an application of the inventory in a photochemical box model appears to be as able to produce as much ozone as the estimates produced in this study. Thus, the inability of recent 3D photochemical model simulations to reproduce observed high wintertime ozone ((Matichuk et al., 2017; Tran et al., 2023; Tran et al., 2018)) is likely not caused by inaccuracies in the Division of Air Quality inventory. Instead, the study provides evidence that meteorological simulations used for 3D models underrepresent winter inversion conditions, allowing too much pollution to escape from the inverted layer. Inadequacies in model chemical mechanisms may also play a role. This doesn't mean that VOC emissions in the inventory are correct. It means that total VOC emissions for the entire Uinta Basin are probably similar to reality. The full report provides examples of inaccuracies for several specific source types.

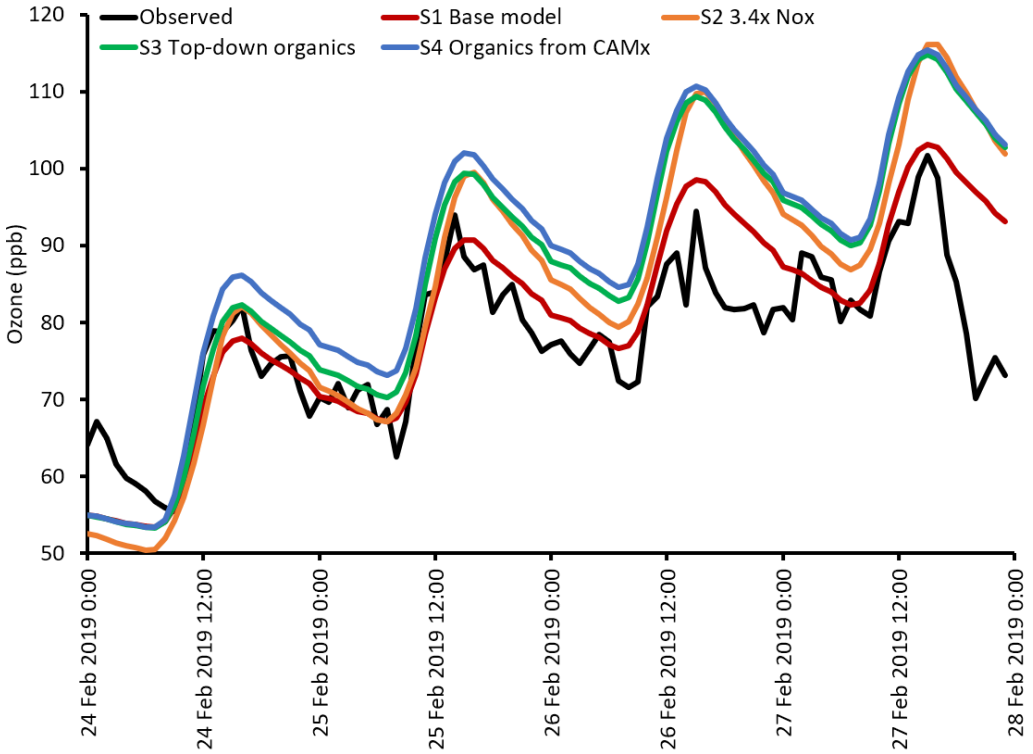

Figure 12-2. Observed ozone at Horsepool from 24 through 27 February 2019, along with F0AM box model outputs for several model scenarios. S1 forces the box model NO_X and organic compound mixing ratios to match measurements. S2 increases NO_X to correspond with artificially high NO_X in the Division of Air Quality emissions inventory. In S3, the speciation of organics is changed to match speciation from this study rather than measurements. In S4, the speciation is changed to match a photochemical model application of the Division of Air Quality inventory.

12.1. Acknowledgments

This work was carried out with funding from the Utah Division of Air Quality, the Utah Legislature, and Uintah Special Service District 1.

13. Atmospheric Mercury

Authors of the summary: Seth Lyman and Colleen Jones

This report covers all work carried out at the Bingham Research Center, not just work related to wintertime ozone. The Bingham Research Center has carried out many studies of mercury in the atmosphere (see https://www.usu.edu/binghamresearch/papers-and-reports#reviewed). For the most part, the Center's atmospheric mercury work is not specific to the Uinta Basin, and the work is separate from our Uinta Basin winter ozone research. Here, we report on a few recent developments in our atmospheric mercury work, which is funded entirely by the U.S. National Science Foundation.

13.1. Mercury Measurements at Storm Peak in Steamboat Springs, Colorado

We developed a dual-channel mercury measurement system and an automated mercury calibration system, and we deployed these at Storm Peak Laboratory in Colorado from March 2021 through September 2022 (Figure 13-1). The dual channel system is designed to overcome mercury measurement biases that are known to exist in commercial instrumentation (Lyman et al., 2020b) and was able to achieve a measurement sensitivity for elemental and oxidized mercury of about one part per quadrillion. Figure 13-2 shows time series of the collected data.

The purposes of this work were to improve measurement and calibration methods for atmospheric mercury (see information about mercury calibration in the next section) and to learn about how mercury behaves in the high elevation atmosphere. We detected several periods when air contained elevated oxidized mercury and depleted elemental mercury, and we used a variety of methods to show that these conditions occurred when air sampled at Storm Peak originated from the free troposphere. We showed that available 3D photochemical models of mercury were not able to predict these high oxidized mercury episodes, probably because the atmospheric oxidation and reduction chemistry used in the models is inaccurate. Additional information about this work is available in Tyler Elgiar's Master's thesis, which can be downloaded at https://www.usu.edu/binghamresearch/files/reports/Thesis_Elgiar_FinalApproved.pdf, and several peer-reviewed publications are in preparation.

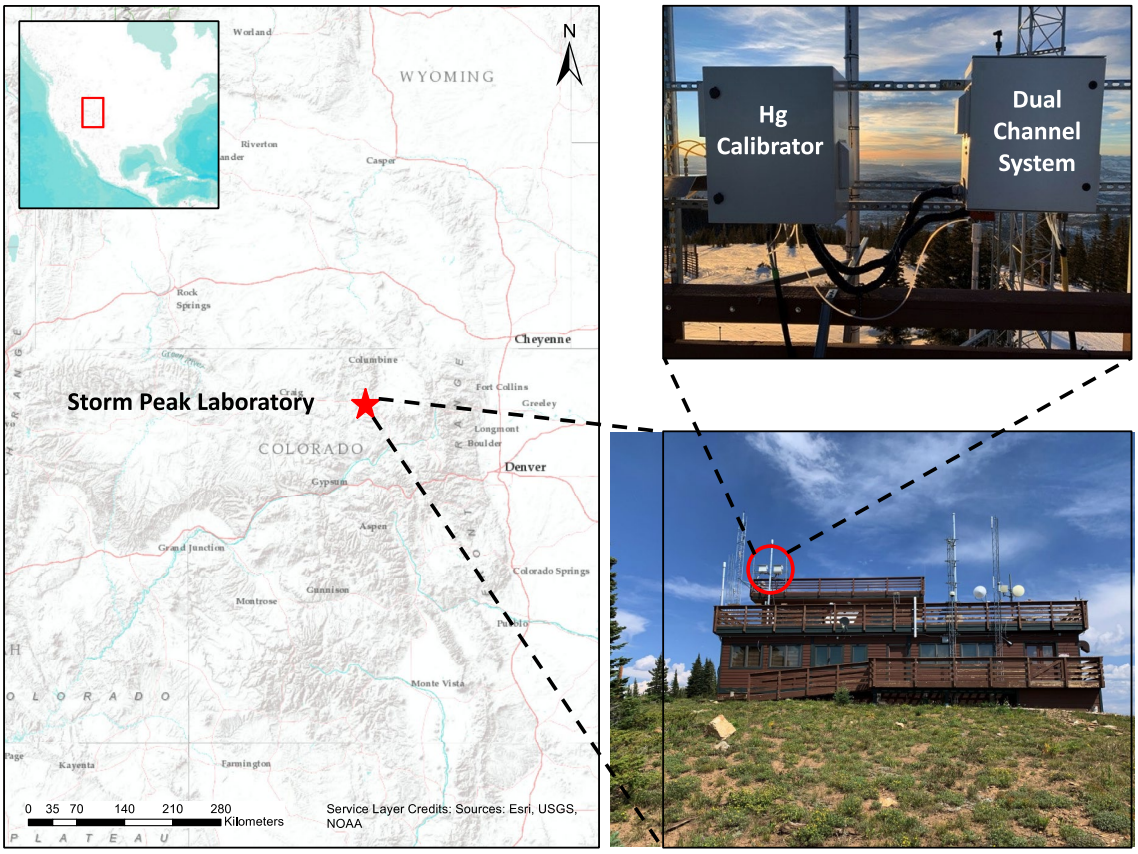

Figure 13-1. Location of Storm Peak Laboratory and the location of the dual channel system and automated calibrator on the laboratory's roof.

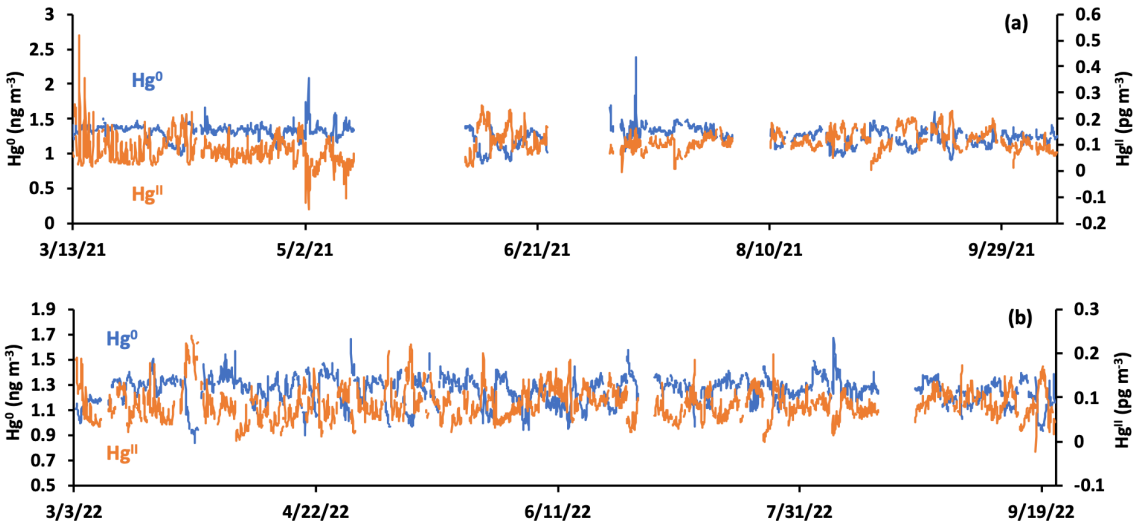

Figure 13-2. Dual channel mercury measurements during the 2021 (a) and 2022 (b) measurement periods.

13.2. Advancements in Mercury Calibration Techniques

We have been working with collaborators at the University of Nevada, Reno, Reed College, and the Jozef Stefan Institute in Ljubljana, Slovenia, to develop methods to calibrate atmospheric mercury measurements. These methods rely on permeation tubes containing elemental mercury or mercury compounds. We build the permeation tubes in our laboratory and maintain them in ovens with careful temperature control. Mercury or mercury compounds slowly permeate through the tubes at a rate that is constant for a given temperature, and an inert carrier gas sweeps the emitted mercury along an outlet tube and into a mercury analyzer like the one mentioned in the previous section. We characterize the total mercury mass lost from the tubes with a microgram-sensitivity balance and with a custom-built gas chromatography-mass spectrometry system. Details are available in Tyler Elgiar's Master's thesis (https://www.usu.edu/binghamresearch/files/reports/Thesis_Elgiar_FinalApproved.pdf) and peer-reviewed papers in preparation.

A key outcome of this work is the demonstration, shown in Figure 13-3, that our laboratory determination of the emission rate from our permeation tubes matched recovery of mercury from the tubes by our dual channel measurement system at Storm Peak Laboratory. This shows that (1) mercury emissions from our calibration system are stable and well characterized, and (2) our dual channel system measures elemental and oxidized mercury accurately. In fact, our mercury measurements at Storm Peak are the first to ever have been calibrated with a calibration system that is traceable to NIST standards.

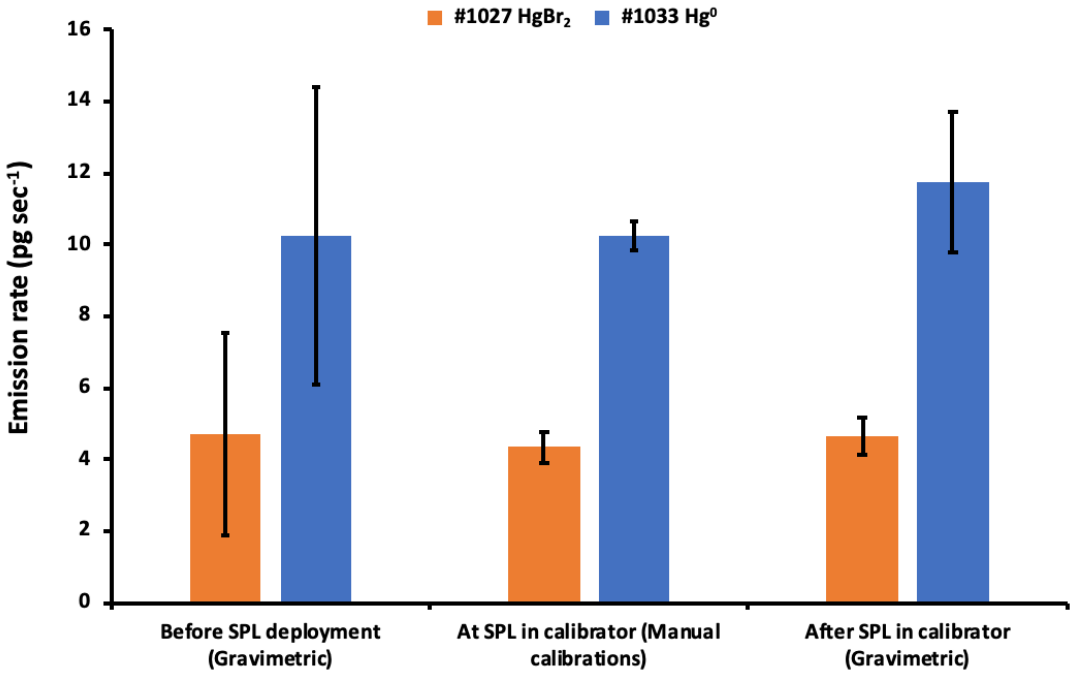

Figure 13-3. Emission rates determined gravimetrically and as detected by the dual channel system at SPL for #1027 $HgBr_2$ and #1033 Hg^0 permeation tubes.

13.3. Atmospheric Mercury Measurement Methods Workshop

We co-organized a workshop on atmospheric mercury measurement methods, which was held in Reno, Nevada, in October 2023 (https://naes.unr.edu/mercury-2023/). The workshop brought 26 scientists from four continents together to talk about how measurement and calibration methods for atmospheric mercury are made, problems with them, and what needs to be done to improve them. A peer-reviewed paper about the workshop's outcomes is in preparation.

13.4. Mercury Chemistry Project at the Great Salt Lake

We received funding for a project to measure and model atmospheric mercury in the Great Salt Lake area this year, and we are currently preparing for the field campaign portion of the project. We will use a well-validated technique to measure atmospheric mercury in the vicinity of the U.S. Magnesium plant on the west side of the Great Salt Lake. The plant is a large source of halogens, which are known oxidants of elemental mercury. We will also measure halogens, ozone, NO_X, OH radical, aerosol scattering, and meteorological parameters. With these ancillary measurements, we will characterize plume conditions and assess the influence of other potential oxidants on Hg redox chemistry. We will use trajectory modeling and the Framework for 0-D Atmospheric Modeling (F0AM) box model to assess mercury reaction mechanisms and rates. Accurate, comprehensive atmospheric measurements in this unique environment, combined with detailed chemical modeling, will allow us to improve scientific understanding of Hg chemistry and atmospheric cycling.

Specific contributions of the proposed project to the body of atmospheric Hg research include:

- A comprehensive dataset of atmospheric Hg and other relevant species (halogens, ozone, NO_X, NO_Y, aerosols, and OH radical) in an area with some of the highest Hg^{II} ever measured in North America (Lan, 2012).
- Improvements to and further measurements with the only Hg measurement and calibration system that has ever been shown to quantitatively measure Hg^{II} compounds.
- Decrease in the uncertainty of Hg-halogen reaction rates, which are key to Hg^0 oxidation, and will help constrain estimates of when, where, and how atmospheric Hg impacts ecosystems.

13.5. Acknowledgments

All atmospheric mercury research at the Bingham Research Center is funded by the U.S. National Science Foundation.

14. Report Summary: The Salt Lake Regional Smoke, Ozone, and Aerosol Study

Authors of the summary: Seth Lyman and Colleen Jones

We worked with collaborators at the University of Washington and the University of Montana on a project to investigate the causes of summertime ozone production in Salt Lake City, and that project was completed this year. A final report is available at https://www.usu.edu/binghamresearch/files/reports/Samoza_finalreport.pdf. The project was funded by the Utah Division of Air Quality and several companies that operate oil refineries in the Salt Lake City area. The following is a reproduction of the executive summary from the final report:

The Salt Lake City region is one of approximately 50 metropolitan regions around the U.S. that do not meet the 2015 8-hour ozone National Ambient Air Quality Standard (NAAQS). To better understand the causes of high ozone days in the region, a group of scientists from the University of Washington, Utah State University and the University of Montana developed and proposed the Salt Lake regional Smoke, Ozone and Aerosol Study (SAMOZA). The primary goals of SAMOZA are:

1. Make observations of a suite of organic compounds, including many oxygenated organic compounds by Proton Transfer Reaction Mass Spectrometry (PTR-MS) and the 2,4-dinitrophenylhydrazine (DNPH) cartridge method.
2. Evaluate whether UDAQ ozone measurements show a positive bias during smoke events.
3. Quantify the range of concentrations of NO_X, organic compounds, CO and PM2.5 on smoke-influenced vs non-smoke days.
4. Conduct photochemical modeling and statistical modeling/machine learning analyses to improve our understanding of the sources of ozone and PM2.5 photochemistry (NOx vs organic compound sensitivity) on both smoke-influenced and non-smoke days during the summer of 2022.

Key results:

- We found no significant difference in the ozone measurements from the “scrubber-less” UV instrument compared to the standard ozone measurements made by UDAQ with a Teledyne T400 instrument at $PM2_{.5}$ concentrations up to 60 µg m^{-3}.
- For formaldehyde, which was measured by two different methods, there is a generally good correlation in the data from the two methods, but the PTR-MS measurements are approximately 50% greater than the DNPH measurements on smoky days. The cause for this difference is not yet known.
- On days with smoke, we found that $PM_{2.5}$, CO, ozone and nearly all organic compounds were significantly enhanced. On average, NO_X was also enhanced on days with smoke, but this was complicated by day of week effects on NO_X concentrations (higher on weekdays).
- Photochemical modeling of ozone production rates at the Utah Tech Center for both smoke influenced and no smoke days demonstrates a strong sensitivity to organic compound

concentrations and less sensitivity to NO_X. For non-smoke days, reductions in organic compounds of ~30% result in significantly reduced ozone production. Reductions in NO_X of ~60% are needed to get a significant reduction in ozone production for non-smoke days.

- The photochemical modeling shows that formaldehyde and other oxygenated organic compound, along with alkenes, were the most important ozone precursors.
- Generalized Additive Modeling (GAM) gave similar MDA8 ozone enhancements on smoky days as the photochemical modeling. Analysis of the GAM results show that 19-31% of the smoke days have GAM residuals that exceed the EPA (2015) criteria for statistical analysis of ozone data, and thus this method could be used as support for exceptional event cases for those days.

14.1. Acknowledgments

This work was funded by the Utah Division of Air Quality, Big West Oil, Chevron, Holly Frontier, and Tesoro.

15. Report Summary: Post-Wildfire Vegetation and Soil Assessment

Author: Colleen Jones

We are engaged in a project to assess recovery from wildfires using drone-based spectrometric techniques. A report of the work completed for this project thus far is available at https://www.usu.edu/binghamresearch/files/reports/wildfire_veg_nov2023.pdf. The following is a reproduction of the report's executive summary:

Wildfires significantly alter vegetation composition, soil stability, and water quality, as well as substantial economic and social impacts. In 2023, the Department of Interior received $2.1 billion for fire preparedness, suppression, fuels management, and wildlife adjustment. Part of the funding goes toward post-fire reformation. The major focus of post-fire restoration has typically been to reduce erosion. Broadcast seeding has been the method of choice, as roots stabilize soil while vegetation reduces raindrop impacts. However, research shows that seeded plants rarely produce enough cover the first year post-fire and even have the same cover as non-seeded areas. Mulch treatments can be cost-effective in reducing erosion on hillslopes but can also introduce weeds. Burned Area Emergency Response (BAER) assessment teams identify additional risks but are mostly focused on short-term mitigation. Once site stabilization is no longer a concern (1-3 years post-fire), the goal shifts to focusing on long-term ecological restoration.

One of the limitations of long-term ecological restoration management is monitoring to assess the success or effectiveness of the restoration project. The monitoring phase of a project is often not funded as well as labor-intensive. The Bingham Research Center (BRC) of Utah State University in conjunction with the Utah Watershed Restoration Initiative, Bureau of Land Management, and other partners are collaborating to find solutions to the limitations of monitoring by using remote sensing as a tool to assist land managers with post-project monitoring by reducing the time spent collecting vegetation and cost over time.

The use of remote sensing with orthomosaics in post-fires is more time and cost-efficient. Using remote sensing and spectral analysis can help understand the impacts of wildfires on vegetation, but also monitor the return of vegetation to the landscape after wildfires. Remote sensing has been in use in post-fire monitoring, but also for ascertaining burn severity, current fire activity, fire risk assessments, and potential fuel quantities for fires. There is no one 'silver bullet' sensor or method. However, by using a variety of multispectral sensors, post-fire data on severity, revegetation, and soil erosion will improve the limitations of monitoring projects over time.

In Year 1 of a two-year project, BRC collected aerial multispectral imagery, vegetation transects, and soil sample data to assess watershed-scale impacts of wildfire management practice efficiencies for vegetation response monitoring and soil stability of post-fire management response to the Snake John 2021 Fire, Richard Mountain 2020 Fire, and Bear 2020 Fire with the supervised classification of the vegetation accuracy of 96% with 0.137m resolution, average accuracy 55% with 0.157m resolution, and average accuracy 45% with 0.28m resolution respectively.

Future work includes another season of collecting aerial imagery and plant cover transects from the Snake John, Richard Mountain, and Bear fires. BRC will continue to investigate improvements in remote sensing multispectral cameras with higher resolution and more spectral bands to improve the accuracy as well as incorporating satellite data into data analysis. BRC is also looking into vertical take-off and landing (VTOL) UAS and working with USU's Price Campus's UAS Certification program to address terrain issues encountered during the Bear Fire 2023 collection.

15.1. Acknowledgments

This work was funded by the Utah Division of Wildlife Resources.

16. Ozone Alert Program

Author: Seth Lyman

At the request of oil and gas industry representatives and with input from the Utah Division of Air Quality, TriCounty Health, and several oil and gas companies, we created a program in 2017 to alert oil and gas companies when high winter ozone is expected. The program includes a web page (https://www.usu.edu/binghamresearch/ozone-alert) to describe the program and allow individuals to sign up to receive alerts. When individuals sign up, we collect their name, company name, and email.

We send everyone on the list an email when local ozone formation is expected, if an ozone episode extends longer than expected, and when episodes end or are expected to end. We attempt to forecast ozone episodes up to six days in advance. The purpose of this program is to provide users with information that allows them to reduce ozone-forming pollution when it matters most.

Winter 2022-23 had more than 30 days during which at least one monitoring station exceeded the EPA standard, and we sent many alerts, updates, and explanations. Periods during which we alerted subscribers that high ozone was likely are indicated in Figure 16-1.

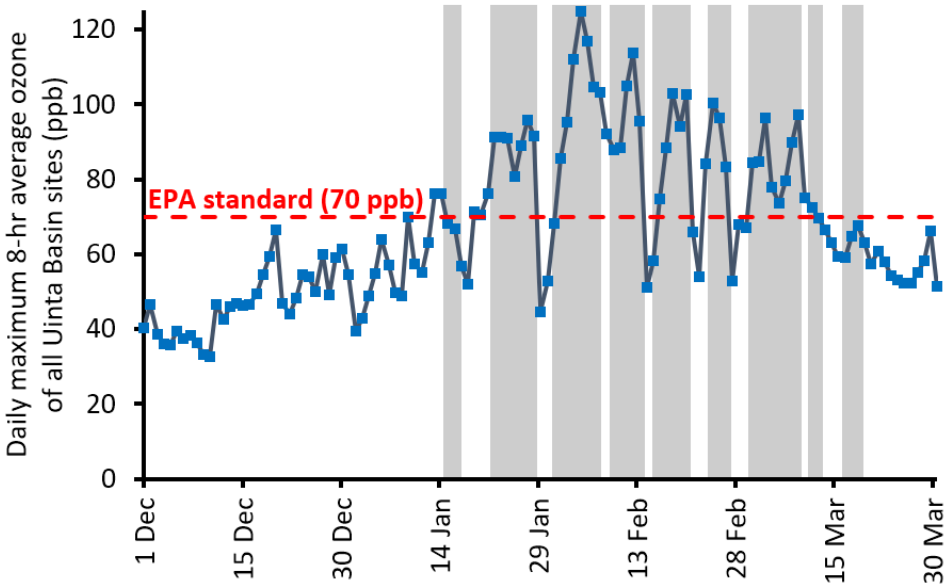

Figure 16-1. Time series of the highest daily maximum 8-hr average ozone the site observed at any monitoring site in the Uinta Basin during winter 2022-23. The EPA ozone standard is shown as a red dashed line. Periods during which USU issued ozone alerts are shown as grey shading.

The program currently has 146 subscribers, among which 38% represent the energy industry, 25% are affiliated with government entities, 21% are members of the local public, 10% are academics, 3% are representatives of the media, and 2% are from environmental groups.

The Utah Petroleum Association has created a list of actions the oil and gas industry can take to reduce ozone-forming emissions when we send an ozone alert email (Figure 16-2) and is actively promoting the ozone alert program and their emissions reductions list to energy companies.

Reducing Emissions During Wintertime Ozone Alerts

- ☐ Before a winter ozone alert:
  - o Review information about ozone and the need to reduce emissions.
  - o Update worn or missing "Latch the Hatch" signs.
  - o Clean and maintain thief hatch closure surfaces and replace worn gaskets.
- ☐ Refresh VOC and NOx reduction ideas when an alert starts. Agree on a plan for the alert.
- ☐ Double-check thief hatches to ensure they are closed. Latch the Hatch!
- ☐ Ensure flare/combustor pilots are lit. Double check to ensure that any flares in use are lit.
- ☐ Minimize liquid hauling from well sites other than sites equipped with a LACT unit.
- ☐ Conduct OGI and/or AVO inspections of components. Repair leaks.
- ☐ Postpone or avoid maintenance that could lead to emissions.
  - o Consider avoiding liquids unloading, blowdowns, pigging, venting.
- ☐ Limit vehicle idling. Maintain speed limits. Combine trips (work, shopping, errands, etc.).
- ☐ Delay refilling methanol and chemical tanks.
- ☐ Use only paints, chemicals, cleaning, and personal care products with low VOC emissions.
- ☐ Reduce production as needed to eliminate or minimize flaring.
- ☐ Postpone flowback and completion activities.
- ☐ Postpone or avoid gas releases associated with compressor startups and shutdowns.
- ☐ Reduce circulation rates of glycol dehydrators.
- ☐ Capture/control emissions from equipment.

Figure 16-2. Flier created by the Utah Petroleum Association that lists actions industry can take to reduce emissions when USU issues an ozone alert.

16.1. Acknowledgments

This work was funded by the Utah Legislature and Uintah Special Service District 1.

17. Report of 2023 Performance

Author: Seth Lyman

This section contains information about our performance on overall goals for Uinta Basin air quality research and performance for annual project objectives for the 2023 reporting period. Our management plan, which describes our group's overall goals and objectives, is available here: https://usu.box.com/s/877z4o8nwynu3uwcze8uxj8jaant7auw.

17.1. Research Output

The most basic outcomes of our research are publications and presentations that describe our work and make it available to other academics, stakeholders, and the public. Here, we list the publications and presentations we have produced during the reporting period. This list includes some publications and presentations that are not directly related to Uinta Basin air quality. All the peer-reviewed publications and significant technical reports we have authored are available on our website at https://www.usu.edu/binghamresearch/papers-and-reports.

17.1.1. Peer-reviewed Publications

Ninneman M., Lyman S., Hu L., Cope E., Ketcherside D., Jaffe D., 2023. Investigation of Ozone Formation Chemistry During the Salt Lake Regional Smoke, Ozone, and Aerosol Study (SAMOZA). ACS Earth and Space Chemistry, accepted.

Stratman D.R., Yussouf N., Kerr C.A., Matilla B.C., Lawson J.R., Wang Y., 2023. Testing stochastic and perturbed perturbation methods in an experimental 1-km Warn-on-Forecast system using NSSL's phased-array radar observations, Monthly Weather Review, https://doi.org/10.1175/MWR-D-23-0095.1.

Gustin M.S., Dunham-Cheatham S.M., Allen N., Choma N., Johnson W., Lopez S., Russell A., Mei E., Magand O., Dommergue A. and Elgiar T., 2023. Observations of the chemistry and concentrations of reactive Hg at locations with different ambient air chemistry. Science of The Total Environment, 904, 166184.

Roy C., Ravishankara A.R., Newman P.A., David L.M., Fadnavis S., Rathod S.D., Lait L., Krishnan R., Clark H. and Sauvage B., 2023. Estimation of stratospheric intrusions during Indian cyclones. Journal of Geophysical Research: Atmospheres, 128(3), 2022JD037519.

Veenus V., Das S.S. and David L.M., 2023. Ozone Changes Due to Sudden Stratospheric Warming-Induced Variations in the Intensity of Brewer-Dobson Circulation: A Composite Analysis Using Observations and Chemical-Transport Model. Geophysical Research Letters, 50(13), 2023GL103353.

17.1.2. Reports

Lyman S., Mansfield M.L., David L.M, O'Neil T., 2022. 2*022 Annual Report: Uinta Basin Air Quality Research*. Utah State University, Vernal, Utah. https://www.usu.edu/binghamresearch/files/reports/UBAQR_2022_AnnualReport.pdf.

Elgiar T., 2022. *Atmospheric Mercury at Storm Peak Laboratory: Development of Methods to Calbirate Ambient Oxidized Mercury Measurements and Comparisons to a 3-D Photochemical Transport Model*. Master's Thesis, Utah State University, Logan, Utah. https://www.usu.edu/binghamresearch/files/reports/Thesis_Elgiar_FinalApproved.pdf.

Jaffe D., Hu L., Lyman S., 2023. *The Salt Lake regional Smoke, Ozone and Aerosol Study (SAMOZA): Final Report*. University of Washington Bothell, Bothell, Washington. https://www.usu.edu/binghamresearch/files/reports/Samoza_finalreport.pdf.

Lyman S., Lin J., Tran H., 2023. *Top-down Estimates of Emissions from Oil and Gas Production in the Uinta Basin: Final Project Report*. Utah State University, Vernal, Utah. https://www.usu.edu/binghamresearch/files/reports/Topdowninventory_finalreport_2023.pdf.

Ramboll, 2023. *Assessing Wintertime Ozone Prediction Sensitivity to Photochemical Mechanism*. Ramboll, Salt Lake City, Utah. https://www.usu.edu/binghamresearch/files/reports/Ramboll_USU_S4S_RACM2_FinalReport_24Feb2023.pdf.

Allred J., Jones C., 2023. *Post-wildfire Vegetation and Soil Stability Monitoring Assessment: 2023*. Utah State University, Vernal, Utah. https://www.usu.edu/binghamresearch/files/reports/wildfire_veg_nov2023.pdf.

ILWA, 2022. 2022 *Report to the Governor and Legislature on Utah's Land, Water, and Air*. Institute for Land, Water, and Air, Utah State University, Logan, Utah. https://www.usu.edu/ilwa/reports/2022/.

ILWA, 2023. 2023 *Report to the Governor and Legislature on Utah's Land, Water, and Air*. Institute for Land, Water, and Air, Utah State University, Logan, Utah. https://www.usu.edu/ilwa/reports/2023/.

17.1.3. Presentations

Lyman S., November 2022. Uinta Basin air quality has improved: What we can do to continue the trend. Utah Division of Oil, Gas and Mining Collaborative Meeting, Duchesne, Utah.

Gratz L., Lyman S., Elgiar T., et al., January 2023. Trace gases & aerosol observations in smoke plumes at the high-elevation Storm Peak Laboratory in the U.S. Intermountain West. American Meteorological Society Annual Meeting, Denver, Colorado.

Lyman S., February 2023. Exploration of some interesting features of 2022-23 winter ozone. Uinta Basin Ozone Working Group Meeting, Vernal, Utah.

Lyman S., March 2023. What is going on with winter ozone right now and when will it end? Uinta Basin Ozone Working Group Meeting, Vernal, Utah.

Lyman S., Lin J., March 2023. Decoupling of Methane, NO_X and Non-methane Organics Emissions in the Uinta Basin. Air Quality: Science for Solutions Conference, Salt Lake City, Utah.

Jones C. P, Lyman S. N., O'Neil T., Jaffe D., and Hu L., March 2023. Comparison of PTR-MS and DNPH-HPLC Carbonyl Measurements in Salt Lake City. Air Quality: Science for Solutions Conference, Salt Lake City, Utah.

Lyman S., April 2023. Uinta Basin air quality research. Uintah Special Service District 1 board meeting, Vernal, Utah

Emery C., Tran H., Tran T., Lyman S., Yarwood G., June 2023. Comparing the chemical mechanisms:CB6r5 and RACM2s21 for a winter ozone episode in Utah. International Technical Meeting on Air Pollution Modeling and its Application, Chapel Hill, North Carolina.

Lyman S., Jones C., Mansfield M., June 2023. Bingham Research Center. United States Forest Service Regional Climate Conference, Vernal, Utah.

Allred J., Jones C.P., June 2023. Richard Mountain and Snake John Multispectral Imagery of 2023. Utah Watershed Restoration Indicative Northeastern Region Field Trip.

Lyman S., Lin J., Tran H., August 2023. Basin-wide pollutant emissions estimates. Uinta Basin Ozone Working Group Meeting, Vernal, Utah.

Lyman S., August 2023. Uinta Basin air quality. Uintah Basin Energy Summit, Vernal, Utah.

Jones C. P., Taylor E., Burger B., August 2023. Get "FIT" (Free Interactive Text) for student success with OER. Utah State University-ETE Conference, Logan, Utah.

Lyman S., September 2023. The chemical and political science of wintertime ozone. Utah State University Department of Chemistry and Biochemistry seminar series, Logan, Utah.

Lyman S., October 2023. Addressing Inconsistencies in Tekran Elemental Hg Measurements. Atmospheric Mercury Measurement Workshop, Reno, Nevada.

Lyman S., O'Neil T., Elgiar T., et al., October 2023. NIST-traceable, Automated, Field-ready, Permeation Tube-based Calibration of Hg^0 and Hg^{II}. Atmospheric Mercury Measurement Workshop, Reno, Nevada.

Lyman S., O'Neil T., et al., October 2023. Using GC/MS for oxidized Hg detection. Atmospheric Mercury Measurement Workshop, Reno, Nevada.

Lyman S., Mansfield M., October 2023. Atmospheric emissions from produced water. Utah Petroleum Association Lunch and Learn, Salt Lake City, Utah.

Jones C. P., October 2023. Is the Uinta Basin a Density Tank? Uinta River High School Language Arts Class, Fort Duchesne, Utah.

Lyman S., November 2023. Uinta Basin air quality: Where we are now. Utah Division of Oil, Gas and Mining Collaborative Meeting, Duchesne, Utah.

Lyman S., November 2023. Mercury in the atmosphere. University of Utah Department of Atmospheric Sciences seminar series, Salt Lake City, Utah.

Lyman S., November 2023. Air quality in Utah's oil country: Problems, impacts, and progress. Utah State University Research Landscapes series, Salt Lake City, Utah.

Allred J., Jones, C. P., November 2023. Aerial Imagery for Vegetation Monitoring Post-Wildfire. Utah Watershed Restoration Indicative Northeastern Region Annual Meeting, Vernal, Utah.

Lawson J., November 2023. There's a Good Chance I Should Care About Probabilities. USU Faculty Spotlight, Vernal, Utah.

Lawson J., November 2023. Reducing Surprise. Uinta Basin Ozone Working Group meeting, Vernal, Utah.

17.2. Media Appearances

The following are news articles from the reporting period that mention our work. A complete list of media mentions of our research is available at: https://usu.box.com/s/5s0busf524npd935mqfecsnvhn4cep52.

- Utah's Air Quality, Energy Production Discussed at Latest Research Landscapes. November 2023. USU Today.
- Funding for Bingham Research Center. November 2023. Uintah Basin Standard.
- Bingham Research Center Hosts Celebratory Open House. September 2023. USU Today.
- Gen Z's Road to Clean Energy Runs Through Flyover Country. September 2023. RealClear Energy.
- Air quality update. September 2023. Article by Seth Lyman in Profiles in Energy, a supplement to the Vernal Express.
- Elizabeth Cantwell: My vision for a land-grant university in the 21st century. September 2023. Salt Lake Tribune.
- The Uinta Basin, Petroleum Country: Part 1. September 2023. EM.
- Celebration at Bingham Research. September 2023. Uintah Basin Standard.
- Promotions at USU Uintah Basin. June 2023. Vernal Express.
- Great Salt Lake dust events, Utah ozone issues get monitoring money. March 2023. Deseret News.

- What is Ozone and What Can Be Done to Help Improve Levels This Winter? March 2023. USU Today.
- Utah State University Collaborating with Slovenia to Measure Atmospheric Oxidized Mercury. March 2023. USU Today.
- USU studies atmospheric oxidized mercury. March 2023. Vernal Express.
- A Proposed Utah Railway Could Quadruple Oil Production in the Uinta Basin, if Colorado Communities Don't Derail the Project. March 2023. Inside Climate News.
- Improving ozone levels in the Basin. March 2023. Vernal Express.
- USU and You Radio Show: Seth Lyman. February 2023. KVEL 920AM radio program.
- Snow Cover Across The Basin Increases Future Potential For High Ozone. December 2022. Basinnow.com

17.3. Funding

We have received $13,986,258 in research funding between 2011 and the present, including $10,180,100 in funding for research specifically related to Uinta Basin air quality. Figure 17-1 shows the funding we have received, organized by year and type of funding source. In the figure, funds are allocated to the year during which they were first awarded, not the years in which they were spent.

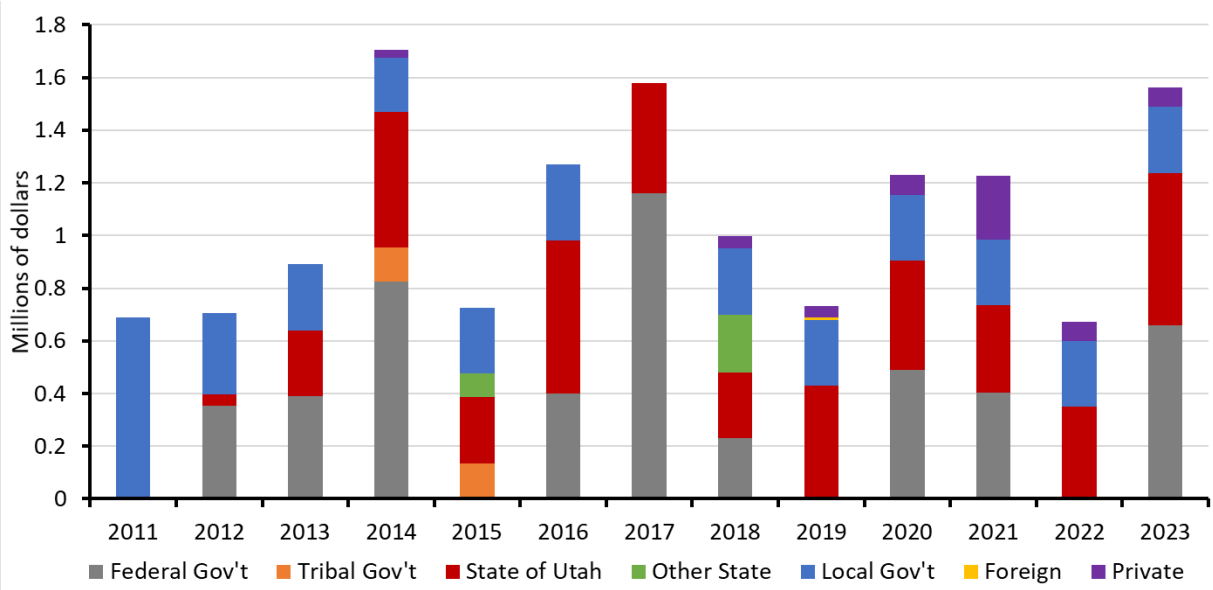

Figure 17-1. Funding awarded to our research group from 2011 to the present, categorized by type of funding source. For grants and contracts, the entire amount of funding awarded is shown in the first year of the award, even though a portion of those funds may have been spent in subsequent years.

Figure 17-2 shows a breakdown of our team's total funding since 2011 by source type. 35% of our funding has come from federal government sources. 32% has come from the state of Utah. 25% has come from local government (entities within Uintah County). 2% and 2% have come from the Ute Indian Tribe and the State of Wyoming, respectively. 4% has come from private companies, and less than 0.1% has come from foreign entities.

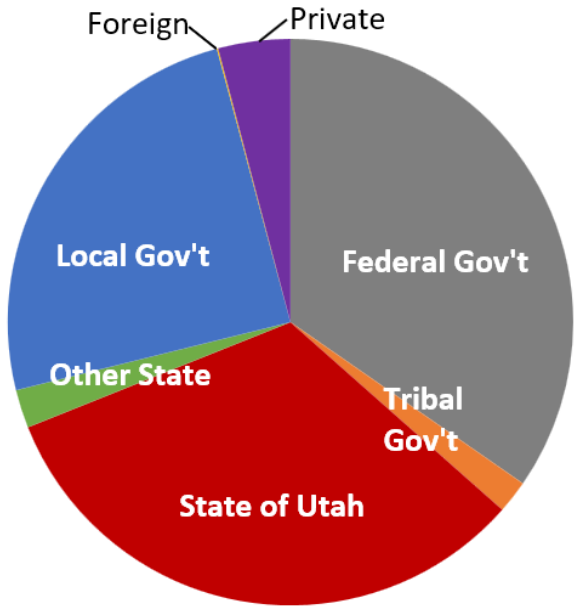

Figure 17-2. All funding sources for our research team from 2011 to the present.

Figure 17-3 shows a breakdown of funding for work specifically for projects related to Uinta Basin air quality. Compared to our research funding as a whole, a greater portion of our winter ozone-specific research has come from the state of Utah (43%) and local government (36%), while less has come from federal government agencies (18%).

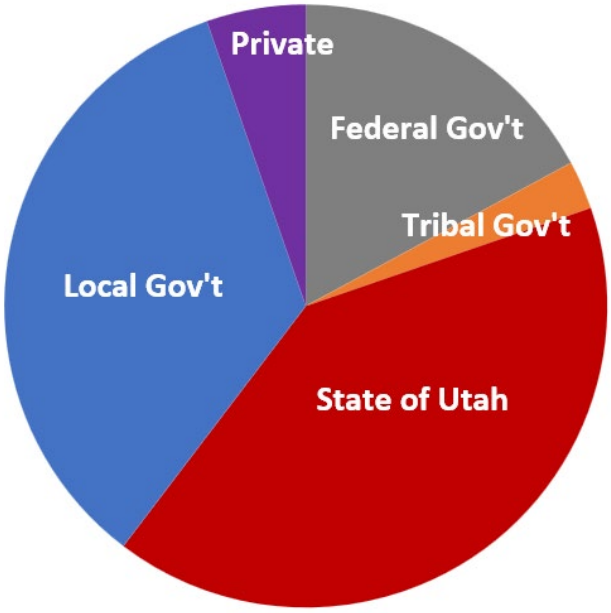

Figure 17-3. Sources of funding for our research team for Uinta Basin air quality projects from 2011 to the present.

Since our inception, we have received funding from the following entities, ranked in order of the total amount of funding received:

- Uintah Special Service District 1 (formerly Uintah Impact Mitigation Special Service District)
- Utah Legislature
- National Science Foundation
- Department of Energy
- USTAR
- Utah Division of Air Quality
- Department of Defense
- Bureau of Land Management
- State of Wyoming
- Ute Indian Tribe
- USTAR Energy Research Triangle
- PacifiCorp
- Utah Division of Wildlife Resources
- Anadarko Petroleum
- National Oceanic and Atmospheric Administration
- SITLA
- Deseret Power
- Chevron Refinery
- Environmental Protection Agency
- Dominion Energy

- Anonymous energy company
- UCAIR
- Anonymous company
- Big West Oil
- Nanjing University
- TriCounty Health

17.4. Student Involvement and Training

17.4.1. Anadarko Student Fellowship

A generous endowment from Anadarko Petroleum Corporation has provided funds for students to participate in Uinta Basin air quality research (https://www.usu.edu/binghamresearch/student-fellowship). The following is a list of the students who have benefitted from this program and other sources of funding for student research during the reporting period.

- Tyler Elgiar worked with our team as an undergraduate researcher from January 2019 through August 2020. Tyler graduated from Utah State University-Uintah Basin with a Bachelor of Science degree in wildlife ecology and management in spring 2020. He performed maintenance and repairs at our field sites and participated in several field campaigns. He also worked to build and test instrumentation to measure mercury in the atmosphere and has presented his research at international conferences. He was the USU-Uintah Basin Undergraduate Researcher of the Year in 2020. Tyler completed a Master's degree in toxicology in 2023 and now works as an Air Resources Specialist with the Vernal office of the Bureau of Land Management.

- Brant Holmes has worked with us since May 2021. He has participated in field measurements of oil and gas emissions and is now working to understand how organic compounds in the air interact with snowpack. Brant will receive an Associate's degree from USU in spring 2024.

- Rachel Merrell has worked with us since April 2023. She has worked in the laboratory to develop and test instrumentation for atmospheric mercury and is now analyzing a dataset of wintertime pollutants in the Uinta Basin while pursuing her education at USU's Logan campus.

- Loknath Dhar has worked with us since May 2023. He is a PhD student in USU's Chemistry and Biochemistry Department and is based in Logan. Loknath is researching the chemical pathways that lead to secondary formaldehyde formation during wintertime ozone episodes and how chemical mechanisms used in photochemical models represent those pathways.

- KarLee Zager has worked with us since August 2023. KarLee is pursuing a bachelor's degree in Biology at the USU Vernal campus. She is involved in ozone measurement and development and testing of atmospheric mercury instrumentation.

- Justin Allred worked with the Bingham Research Center as an undergraduate and now is pursuing a PhD in Soil Science with Colleen Jones. He is using drone-based multispectral imaging to evaluate the effectiveness of wildfire reclamation techniques.

- Lisa Boyd is pursuing a PhD in Ecology with Colleen Jones and is employed at the Vernal office of the Bureau of Land Management. She is studying the life cycle of endangered plants and ecological reclamation.

17.4.2. All Students and Postdoctoral Researchers

The following is a list of all students and postdoctoral researchers that have worked at the Bingham Research Center. The year the person first worked at the Center is also listed.

1. Emily Smith, undergraduate, 2012
2. Chad Mangum, undergraduate, 2013
3. Cathy Crawford, undergraduate, 2013
4. Jordan Evans, undergraduate, 2013
5. Trevor O'Neil, undergraduate, 2013
6. Trang Tran, postdoctoral researcher, 2013
7. Huy Tran, postdoctoral researcher, 2014
8. Colleen Jones, postdoctoral researcher, 2015
9. Cody Watkins, master's student, 2014
10. Tate Shorthill, undergraduate, 2014
11. Tanner Allen, undergraduate, 2014
12. Lena Morgan, undergraduate, 2015
13. Felito Martinez, undergraduate, 2015
14. Sheree Meyer, graduate, 2015
15. Eric Hacking, undergraduate, 2016
16. Sandra Young, undergraduate, 2017
17. Justin Allred, undergraduate and graduate, 2017
18. Makenzie Holmes, undergraduate, 2018
19. Tyler Elgiar, undergraduate and graduate, 2018
20. Krystal White, undergraduate, 2019
21. Brant Holmes, undergraduate, 2020
22. Keirra Tolbert, undergraduate, 2021
23. Jackson Liesik, undergraduate, 2021
24. Davis Smuin, undergraduate, 2021
25. Lisa Boyd, graduate, 2022
26. Kristin Miller, undergraduate, 2023
27. Rachel Merrell, undergraduate, 2023
28. Loknath Dhar, graduate, 2023
29. KarLee Zager, undergraduate, 2023

17.5. Data Management, Quality, and Dissemination

17.5.1. Data Management

As described in our management plan, all measurement data we have generated during the reporting period has been stored on a cloud-based data storage server, with regular backups to local, removable hard drives. We have collected field and laboratory notes using a secure, cloud-based electronic note-taking software that complies with 21 CFR part 11 of the U.S. Federal Code. We stored all instrument

maintenance, calibration, and repair information within this archival structure. We used established standard operating procedures for our work. These are publicly available here: https://www.usu.edu/binghamresearch/team_pages/standard-operating-procedures.

17.5.2. Atmospheric Data Quality

Table 17-1 shows a summary of data quality results for ambient air measurements we collected during the reporting period. The maximum uptime possible for most measurements shown in the table is approximately 95% due to maintenance and calibration periods.

Table 17-1. Data quality summary for ozone, oxides of nitrogen (NO_X), carbon monoxide (CO), and organic compound data collected during 2022-23. Results are shown as averages ± 95% confidence intervals for all locations at which the indicated measurements were collected (confidence intervals are shown if the number of data points is three or more). For a list of measurements collected and sites of collection, see Table 3-1. Percent uptime indicates the percent of the measurement period for which valid measurements were obtained. NMHC indicates non-methane hydrocarbons. N/A means not applicable.

Measurement	Zero calib. (ppb)	Span calib. (% recov.)	Percent uptime
Ozone	-0.4 ± 0.4	102 ± 1	96 ± 6
NO	-0.0 ± 0.0	99 ± 1	71 ± 103
NO_X (NO calib.)	-0.1 ± 0.1	100 ± 1	71 ± 103
NO_Y (NO calib.)	0.0 ± 0.1	100 ± 1	93
NO_X (GPT calib.)	N/A	99 ± 1	71 ± 103
NOy (GPT calib.)	N/A	100 ± 1	93
CO	-1 ± 8	100 ± 3	97
Methane	34 ± 13	102 ± 1	86
Total NMHC	55 ± 24	97 ± 1	86
Speciated NMHC	0.1 ± 0.0	101 ± 0	100 ± 0
Speciated Carbonyls	0.0 ± 0.0	98 ± 1	97 ± 10
$PM_{2.5}$ (BAM)	N/A	N/A	96

17.5.3. Data Dissemination

We have uploaded the winter ozone dataset (Section 3) for the most recent winter and an updated air chemistry and meteorology dataset for the Roosevelt, Castle Peak, and Horsepool monitoring stations to the data access page of our website, https://www.usu.edu/binghamresearch/data-access. We have also updated speciated organic compound data (Section 3.3.4) on the same web page.

During the year, we gave meteorological and chemical datasets we collected to regulators, environmental consultants, and energy companies for use in their own analyses.

17.6. Outcomes from Annual Air Quality Project Objectives

We established project objectives for the current reporting period in Section 17 of our previous annual report, which is available here: https://www.usu.edu/binghamresearch/files/reports/UBAQR_2022_AnnualReport.pdf. In Table 17-2, we report on any discrepancies between planned work and actual outcomes for each of the project objectives outlined in the previous annual report.

Table 17-2. Outcomes of annual project objectives for the current reporting period.

OBJECTIVE	OUTCOMES
Priority 1: Air Chemistry	
Operate air quality monitoring stations	We completed this objective (see information in Sections 3, 4, and 5). We will continue operation of these stations in the coming year.
Continue Investigation of Carbonyl Fluxes at the Air-snow Interface	We have made progress on this objective, but it is not complete. See information about our progress and plans in Section 6.
Investigate Wintertime Increases in Ozone-forming Emissions	We did not complete this objective because the employee assigned to it retired.
Investigate Ozone Formation in Summertime Wildfire Smoke	We set up a summertime measurement system at the Roosevelt monitoring station as planned for this project, but we didn't have enough wildfire smoke this summer to collect any measurements. Following our original plan, we will set up the measurement system in Roosevelt again in summer 2024 and proceed with the project if the site experiences significant wildfire smoke.
Priority 2: Air Quality Modeling	
Compare chemical mechanisms in photochemical models	We completed this objective. A summary of the final report is available in Section 7.
Use F0AM box model to investigate winter ozone chemistry	We completed this objective and are preparing a manuscript for peer-reviewed publication. See Section 9.
Investigate Chemical Performance of Improved Meteorological Simulations	We investigated a series of model parameterizations in the WRF meteorological model to determine how these parameterizations impact winter inversion meteorology. This work was begun in 2022 and is now complete. We found that the parameterizations our team and other groups have been using are not ideal for winter inversion simulations. See our report in Section 8. While this project resulted in significant advancements, more work is needed for WRF to accurately simulate wintertime inversions because the improved WRF model is still not able to simulate winter ozone levels accurately.

OBJECTIVE	OUTCOMES
Develop Quantitative Ozone Forecasts Using WRF-Chem	We did not complete this objective due to personnel changes.
Use the F0AM box model to investigate incremental reactivities	This work is complete. Section 10 contains a report.
Priority 3: Emissions	
Complete Top-down Emissions Inventory Study	This objective is complete. See Section 12 for a summary of the project's final report.
Compare Organic Compound Composition in Ambient Air Against Emissions Composition Data	This objective is complete. See Section 12 for a summary of the project's final report.
Prepare for an Emission Source Characterization Study, to Begin in Fall 2023	We completed this objective. Section 20.3 contains information about emissions characterization studies planned and underway.
Priority 4: Stakeholder Engagement	
Operate ubair.usu.edu website to display map-based, real-time air quality information to the public	We completed this objective for the reporting period. See information about performance in Section 18.
Operate the Ozone Alert program	We completed this objective for the reporting period. See information about performance in Section 16.
Uinta Basin Ozone Working Group	We completed this objective for the reporting period. See the group's website at https://basinozonegroup.usu.edu.

18. Stakeholder Engagement

The mission of our research is to generate knowledge and provide information that helps stakeholders (industry, regulators, and others) to make better decisions. Thus, we strive to engage stakeholders in our research process and help them understand and utilize the information we produce. In this section, we report on our efforts to accomplish this goal during the reporting period.

18.1. Stakeholder Activities

18.1.1. Ozone Alert Program

Section 16 provides information about our ozone alert program, which alerts industry and others when high ozone is expected so they can reduce emissions when it matters most.

18.1.2. Uinta Basin Ozone Working Group

In 2018 we worked with individuals from government, industry, and environmental advocacy organizations to organize the Uinta Basin Ozone Working Group, and this group has continued into the present. The purpose of this group is to determine and promote actions that will reduce wintertime ozone in the Uinta Basin. The group's website is here: https://basinozonegroup.usu.edu. Marc Mansfield serves as the group's facilitator and leads its steering committee. Seth Lyman constructed and manages the group's website and is responsible for group communications. Our team regularly gives presentations to the group about the science of wintertime ozone and actively participates in all working group meetings. The group's website provides agendas for the meetings and links to presentations given.

18.1.3. Other Stakeholder Activities

Below we list additional actions undertaken to learn from and provide information to government entities, industry, and the public during the reporting period. This list does not include formal presentations given or reports produced since those are already listed in Section 17.1.

18.1.3.1. Websites

- ubair.usu.edu, our real-time air quality data website, has hundreds of unique users in thousands of sessions every year.
- Our main website, https://www.usu.edu/binghamresearch and the ozone working group website, https://www.usu.edu/basinozonegroup, had hundreds of unique visitors over the reporting period.

18.1.3.2. Information and data sharing

- We gave dozens of presentations to many different stakeholder groups during the reporting period. See Section 17.1.3 for a list of all presentations given.
- We provided our annual report, specific project reports, report summaries, and datasets to members of our stakeholder committee and others in government and industry upon request.
- We have made updated datasets available at https://www.usu.edu/binghamresearch/data-access.
- We have made all of our project reports and peer-reviewed papers publicly available at https://www.usu.edu/binghamresearch/papers-and-reports.

18.1.4. Use of Our Air Quality Research by Stakeholders

The following is a list of uses of our research by others, excluding reports and formal presentations (which are reported on in Section 17.1), that we were able to document for the current reporting period. A list of all stakeholder uses of our research that we have been able to document is available at https://usu.box.com/s/1k70hyz1dgca2kr9zuynz0locogd9uti.

- Best Practice Award from the Association of Air Pollution Control Agencies (AAPCA). October 2023. The Wyoming Department of Environmental Quality received an award in recognition of the Wyoming Pond Emissions Calculator (WYPEC). Marc Mansfield and others at the Bingham Research Center developed WYPEC for Wyoming in collaboration with GSI Environmental.
- The Utah Division of Air Quality added data from our engines measurement study to the EPA SPECIATE emissions composition database.
- The Utah Division of Air Quality is using our engines measurement study to develop a new method to estimate emissions from engines used in the oil and gas industry.
- The U.S. Environmental Protection Agency used our work in development of the 2015 Ozone NAAQS Good Neighbor Plan.
- Our most recent organic compound concentration data, which are the only ongoing dataset of organics in ambient air in the Uinta Basin, have been included in EPA's AQS database, which allows anyone from around the world to access and utilize it. It is available here: https://www3.epa.gov/ttn/amtic/toxdat.html#data.
- The Western Environmental Law Center relied on our research for comments made regarding an oil and gas lease parcel sale.

18.2. Stakeholder Input

18.2.1. General Air Quality Stakeholder Survey

We conducted an online survey to learn how stakeholders feel about the Bingham Research Center and how they use our research products. We advertised the survey at our exhibitor's booth and oral presentation at the August 2023 Uintah Basin Energy Summit. We received 17 verified responses.

Survey respondents were asked how much they agreed or disagreed with the following three statements. 0 indicated complete disagreement, and 100 indicated complete agreement. We categorized respondents as representatives of either government or industry.

- USU's Uinta Basin air quality research helps the local public deal with air quality issues.
    - Government: 88
    - Industry 89
- USU's Uinta Basin air quality research helps industry respond more effectively to air quality issues.
    - Government: 90
    - Industry: 80
- USU's Uinta Basin air quality research helps government agencies make better decisions.
    - Government: 89
    - Industry: 89

Survey respondents were asked, "How do you use research products and other output from the USU Bingham Research Center?" Responses included:

- Excellent resources on website and expert scientific personnel.
- It's a great help in forecasting Uinta Basin ozone events. It also helps to explain ozone exceedances.
- It is good to be able to use the data provided to form opinions regarding environmental air quality statements.
- I regularly check the air quality website during the winter.
- Community development policy
- For reports and references
- This research is important because it can help to shape regulation and implementation. It also provides data to help reduce emissions and help improve air quality here.
- The collected data are very helpful in NEPA study and process.
- Just informational
- We keep in communication with them.
- We help with field trips for oil and gas research.

Survey respondents were asked, "What specific actions might the USU Bingham Center undertake to better disseminate its research products and/or help interested parties put them to use?" Responses included:

- Greater presence in metropolitan area for exposure to importance of work done on behalf of Utah.
- Have key members of a department or group explain what you do and share your email.
- Publishing data on accessible websites is the most effective way to reach the users of this data.
- I appreciate the regular updates already undertaken.
- Seems to be sufficient, participating in conferences like this one is a good thing
- I think they are doing a great job of getting info to the public. Using the Collaborative group meeting, the Energy Summit and other public settings.
- These types of conferences to explain what they are finding.
- Promote their brand at conferences more.
- Work with stakeholders in evaluation of areas to monitor.

Survey respondents were asked, "What areas of research should the USU Bingham Center pursue to understand and resolve the wintertime ozone issue in the Uinta Basin?" Responses included:

- Continued studies to understand sources and best way to mitigate impacts.
- I'll have to think about that. What you've been doing is very helpful.
- I believe finding the sources of ozone are critical to be identified, and more importantly, how do we help the public react to weather patterns to attempt to mitigate poor air quality?
- I'm going to defer here to the subject matter expert.
- Traffic effects as well as oil and gas.
- Snow depth and cover versus air quality.
- CO_2 research
- Doing a great job. No need to change anything.

Survey respondents were asked to provide any additional comments or suggestions they might have. Responses included:

- As a former member of the team, I know firsthand the excellent quality of research and outreach to the communities of Utah.
- You do great work. Thank you for your valuable contribution to Uinta Basin air quality research.
- More swag at conferences.
- Thank you!

18.2.2. Emissions Source Survey

Our team has carried out work to better characterize a number of Uinta Basin emission source types, including emissions from well pads (Lyman et al., 2019b; Wilson et al., 2020), liquid storage tanks (Lyman and Tran, 2015; Lyman et al., 2019b; Wilson et al., 2020), produced water ponds (Lyman et al., 2018; Mansfield et al., 2018; Tran et al., 2017), subsurface leaks (Lyman et al., 2020c; Lyman et al., 2017), and pumpjack engines (Lyman et al., 2022c). We have measured emissions of NO_X, methane, non-methane hydrocarbons, alcohols, carbonyls, and other gases from emission sources. Many oil and gas-related emission sources remain poorly characterized, however. According to surveys we conducted, many stakeholders feel that additional emissions measurements are needed (see Section 17.2 in our 2020 Annual Report and Section 15.2 in our 2021 Annual Report).

We conducted a survey of stakeholders in 2023 to determine which emission sources they think are the most important for us to study. Those who took the survey were asked to rank a variety of emission source types as the most important to study, the second most important, or the third most important. We received 33 verified responses. Figure 18-1 and Figure 18-2 show summaries of survey responses. The figures only show results for emission source types that ranked highly in the survey. In the full survey, we asked respondents about all of the following source types:

- Pipeline leaks and pigging
- Compressor engines and other large stationary engines
- Flares and combustors
- Liquid storage tanks
- Large, infrequent emissions (i.e., super-emitters)
- Oil and gas solid waste
- Produced water storage and disposal
- Drilling and completions
- Well maintenance/workover
- Vehicle emissions (including Spatial and temporal distribution)
- Gas processing plants
- Loading liquids into trucks
- Natural gas dehydrators
- Pumpjack engines
- Wellpad fugitives (i.e., leaks) other than from tanks
- Pneumatic valves and pumps
- Separators and heaters

Rankings were different for different groups of respondents. For example, industry respondents rated drilling and completions as the most important source type to study, while respondents associated with government entities rated liquid storage tanks more highly. Overall, respondents indicated that produced water, liquid storage tanks, and pipelines are the most important source types to research.

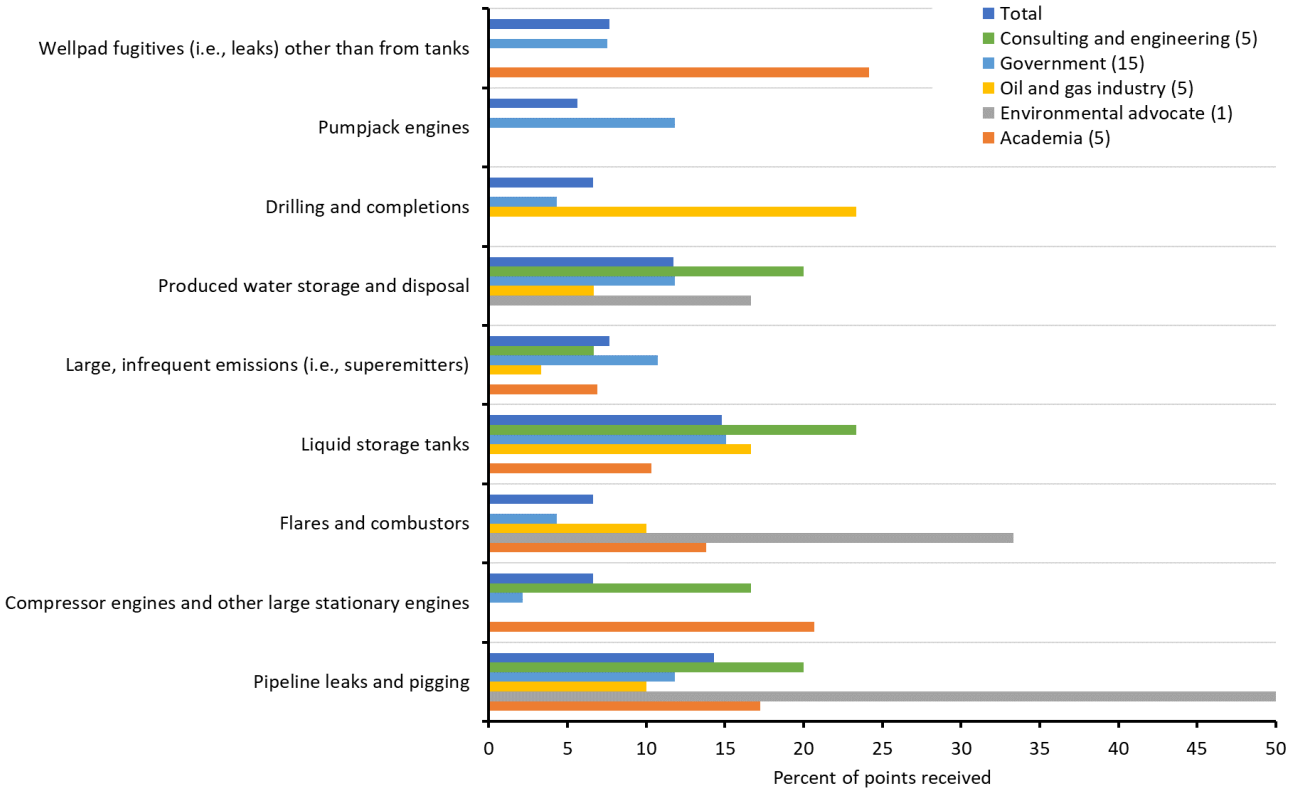

Figure 18-1. Responses to a stakeholder survey about the most important emission sources to research. Bars show the percent of total points for each group of respondents that were given to each source type. A ranking as most important was given three points, the second most important was given two points, the third most important was given one point, and any other ranking was given zero points. Total is the result for all respondents. Respondent groups are shown in the legend with the number of responses received for each group in parentheses. Source types that received less than 5% of total points are not shown.

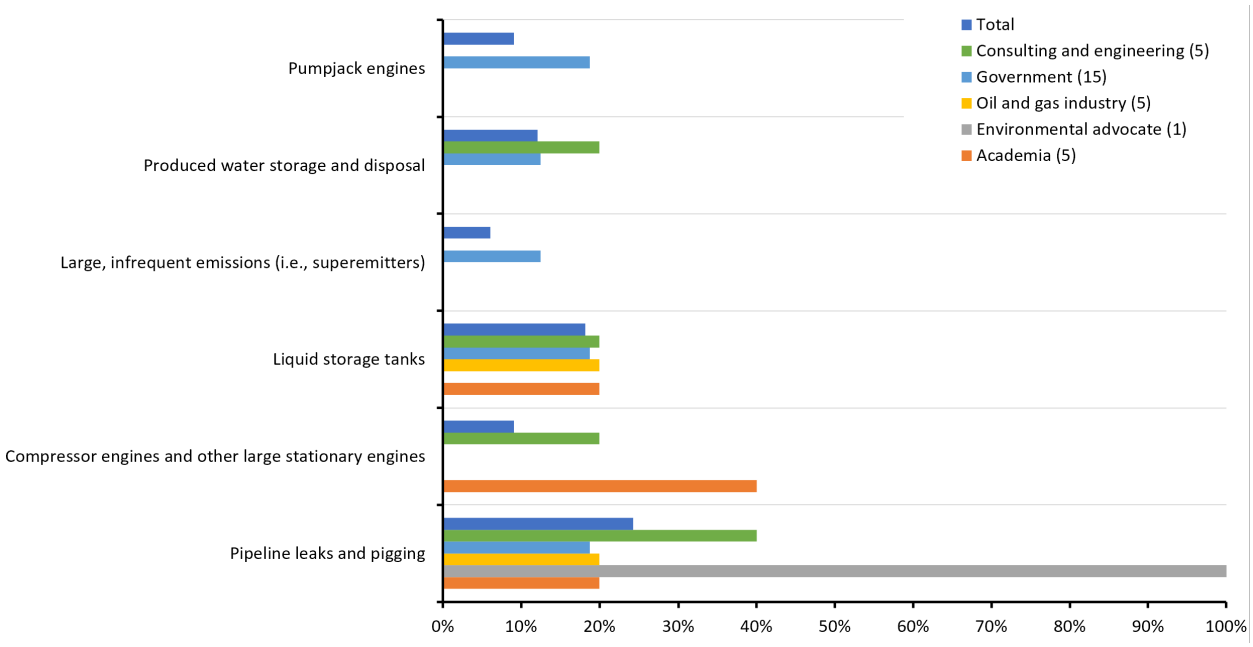

Figure 18-2. Same as previous figure, except bars represent the percent of respondents that ranked a given emission source as most important to research.

18.2.3. Air Quality Stakeholder Guidance Committee

We asked a group of stakeholders to review and provide comments on our research priorities (Section 19) and our research plan for the coming year (Section 20). Stakeholders who agreed to help formed our stakeholder guidance committee. We provided them with a draft plan and our management plan on 16 October and invited them to review these documents and provide comments. We held a virtual meeting to discuss the plan and receive verbal comments on 24 October. Stakeholders included representatives from:

- Ute Indian Tribe
- Utah Petroleum Association
- Several local oil and gas companies
- Environmental consulting companies
- Uintah County
- Duchesne County
- Utah Division of Air Quality
- TriCounty Health
- Bureau of Land Management
- Environmental Protection Agency

Stakeholders provided the following comments. Most comments were verbal, were taken from our team's handwritten notes, and can be considered to be paraphrased:

- USU should work with others on various climate pollution reduction funding opportunities that are currently available from the federal government.
- Emissions from pigging operations are not known with any certainty. Little is known about the frequency and locations of emissions related to pipeline maintenance and repair, including operations to vent pipelines completely and those to insert and receive pigs. Studies of pipelines should also include pigging.
- Emission factors used for pneumatic controllers in the official inventory may need to be updated for oil and gas wells using newly available raw gas measurements.
- Flaring is reported in the emissions inventory, but no Uinta Basin-specific studies of NO_X and organic compound emissions from flaring have been conducted. Work is needed in this area.
- The direct impacts of hazardous organic compounds on local populations should be studied, especially for communities in close proximity to oil and gas operations.
- The CAMx photochemical model now includes a surface reaction tool to simulate conversion of HNO_3 to HONO. The impact of snowpack on HONO in the Uinta Basin could be studied with this tool, or the tool could be used to apply information about carbonyl emissions from snow researched at the Bingham Center.

18.2.4. Next Steps

Stakeholder input has been a great help to us in planning research projects. We will evaluate the stakeholder input presented above, engage in additional discussions with stakeholders, and use this input in developing future projects. To the extent possible, we have already incorporated stakeholder suggestions in our 2024 research plan (Section 20). We may not be able to undertake all work suggested by stakeholders, however. The following are some reasons we are not able to carry out all stakeholder suggestions:

- *Outside of our scope of operations*: Some suggestions by stakeholders, while important ways to understand or improve aspects of Uinta Basin air quality, are outside of the Bingham Research Center's mission. For example, our mission focuses on regional air quality, rather than climate. Stakeholders have sometimes suggested work specific to methane and carbon dioxide, which are important greenhouse gases but are not important for production of wintertime ozone or $PM_{2.5}$. The Center's core funding from Uintah Special Service District 1 and the Utah Legislature can only be used for air quality, not climate, research. We have carried out research specifically targeting emissions and concentrations of methane and carbon dioxide, but only with separate funding.
- *Overlap with responsibilities of government agencies*: Stakeholders have suggested we increase our engagement with the public, including air quality alerts, advertisements, lay-oriented media releases, etc. In general, these are tasks better suited to government agencies and non-profit organizations, and we avoid treading in space these entities traditionally occupy. Our ozone alert program (see Section 16) is a form of air quality alert, but we only started the program at the urging of industry and after extensive consultation with regulatory agencies. Another example of this is monitoring. Routine monitoring for leaks, routine ambient air monitoring, and the like, are tasks already undertaken by regulatory agencies and are generally outside the scope of our work unless they have a specific research purpose.

- *Lack of resources*: Our small team focuses limited resources on research that we and stakeholders view as the most important, which means some tasks that have merit must be neglected. We try to balance the interests and needs of different stakeholder groups, including industry, government, and others. Our role is to generate knowledge that can be widely used rather than replacing functions of specific entities or groups. Also, we don't have expertise in every area of environmental science, so not every good research idea is well suited to our team's skill set.

19. Priorities for Uinta Basin Air Quality Research

The following is a working list of what we feel are the most important winter ozone research topics we can focus on. The purpose of this list is to guide current and future air quality research in the Uinta Basin. Our project objectives for the coming year, which are detailed in Section 20, are intended to address these questions.

Priority 1: Air Chemistry

- How are ozone, NO_X, and organic compound concentrations in the wintertime atmosphere changing spatially and temporally due to changes in (1) industry operations and (2) the regulatory landscape?
- What chemical reactions and processes that impact ozone formation are unique to winter conditions?
- How can we understand and characterize non-local and non-anthropogenic influences on Uinta Basin air quality, including during summer?

Priority 2: Air Quality Modeling

- What model parameterizations and techniques will allow us to best reproduce actual meteorological conditions during winter inversion episodes?
- What model parameterizations and techniques will allow us to best reproduce actual chemical conditions during winter inversion episodes, including winter ozone production?
- What can photochemical models tell us about how changes in emissions of NO_X and organic compounds impact wintertime ozone production?

Priority 3: Emissions

- What specific oil and gas production processes and/or equipment types are responsible for discrepancies between regulatory emissions inventories and actual emissions from the oil and gas industry?
- How do emissions vary across time and space?
- What is the composition of organic compounds (including alcohols and carbonyls) emitted from specific areas, industry processes, and/or equipment types?
- What strategies for emissions reductions (NO_X versus organics, specific equipment types, etc.) may be effective?

Priority 4: Stakeholder Engagement

- How can we ensure that our work is useful to and utilized by regulators, industry, and others?
- How can we work with industry and others to (1) facilitate emissions reductions and (2) improve our understanding of oil and gas processes that lead to emissions?

20. Uinta Basin Air Quality Research Plan for 2024

This section provides information about our specific research objectives for 2024. Each activity falls under one of the research priorities from Section 19. Information about the Bingham Research Center's general operations and goals is available in our management plan. Our research objectives are listed in Table 1. Details about each objective are available in the following sections.

Table 20-1. Summary of research objectives for 2024, organized by research priority headings in Section 19.

Priority 1: Air Chemistry
Operate ambient air monitoring stations
Continue Investigating Carbonyl Fluxes at the Air-snow Interface
Investigate Ozone Formation in Summertime Wildfire Smoke
Priority 2: Air Quality Modeling
Improve WRF Simulations of Uinta Basin Winter Inversions
Develop a System for Quantitative Winter Ozone Forecasts
Box Model Investigation of the Impact of Chemical Mechanisms on Simulations of Winter Ozone
Priority 3: Emissions
Establish a Method for Monthly Basin-wide Pollutant Emissions Estimates
Development of Methods to Determine Oil Storage Tank Emission Factors in the Uinta Basin
Drone-based Measurement of Emissions from Oil and Gas Sources
Priority 4: Stakeholder Engagement
Real-time Data Website
Ozone Alert Program
Uinta Basin Ozone Working Group

20.1. 2024 Research Plan for Priority 1: Air Chemistry

20.1.1. Operate Ambient Air Monitoring Stations

We will operate meteorology and air quality monitoring equipment at the following stations during winter 2023-24 (1 December through 15 March; Figure 20-1):

- Horsepool
- Roosevelt
- Castle Peak
- Seven Sisters

These stations are not official regulatory monitors but are instead operated for research purposes. They have two main purposes. The first is to measure chemical conditions around the Uinta Basin that are not captured at regulatory stations. Most regulatory NO_X instruments suffer from a high bias during winter inversion episodes and thus do not provide accurate NO_X measurements during these periods, whereas we measure NO_X via an unbiased technique at Horsepool, Roosevelt, and Castle Peak. Our measurements of speciated organic compounds at Horsepool and Roosevelt are the only long-term organics measurements in the Uinta Basin (hydrocarbons, alcohols, and carbonyls). We also measure

NO_Y, CO, particulate matter smaller than 2.5 μm ($PM_{2.5}$), snow depth, solar radiation, and albedo at various wavelengths.

Our monitoring stations' second purpose is to provide information about the spatial distribution of ozone in the Uinta Basin region. Eight regulatory monitoring stations operate in the Uinta Basin, but they are not evenly distributed around the Basin. We operate ozone monitoring stations to provide a more spatially representative dataset to compare against results from our photochemical modeling work (Figure 20-1). Data from these stations can be downloaded from our website (https://www.usu.edu/binghamresearch/data-access).

Most of our stations have been operating since 2010. The entire dataset, including data from regulatory stations and stations we operate, constitutes an essential long-term record of meteorology and air quality in the Uinta Basin.

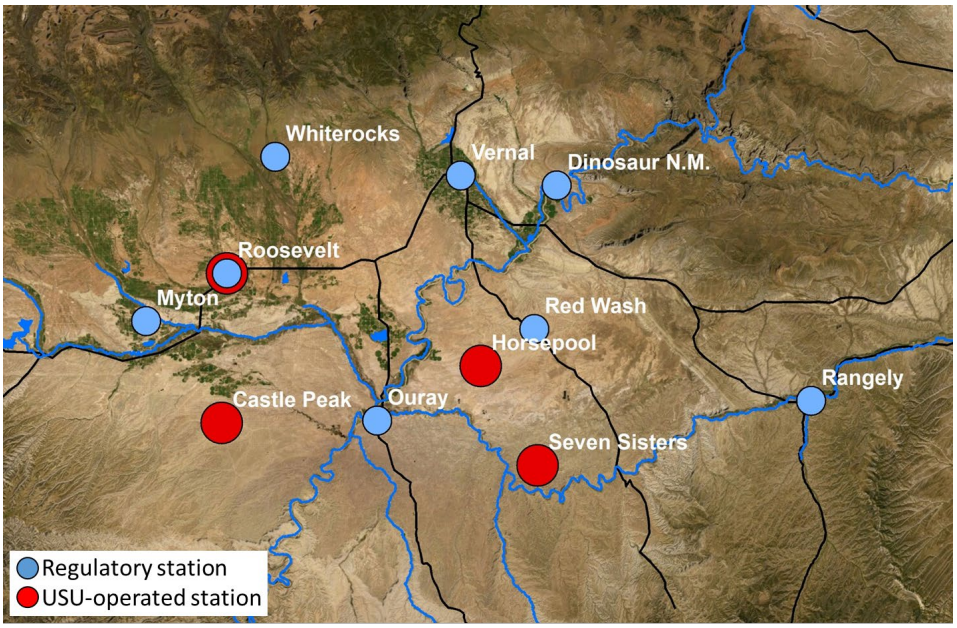

Figure 20-1. Air quality monitoring stations that will operate in the Uinta Basin during the coming winter. The Roosevelt location includes regulatory monitoring equipment operated by the Utah Division of Air Quality and research equipment operated by USU.

20.1.1.1. Responsibilities

- *Responsible persons:* Seth Lyman will lead this effort. Seth Lyman, Trevor O'Neil, and students will operate, maintain, and repair the monitoring stations and analyze collected laboratory samples. Seth Lyman and Trevor O'Neil will quality-assure and archive the resultant data.
- *How we will measure performance:* Data quality, data uptime, datasets available to the public, use of data in reports and publications.

20.1.1.2. Funding

All costs for this project will be paid with funds from Uintah Special Service District 1 and the Utah Legislature, except that student wages will be paid from the Anadarko Student Fellowship.

20.1.2. Continue Investigating Carbonyl Fluxes at the Air-snow Interface

A large body of work by others shows that carbonyl compounds, including formaldehyde and acetaldehyde, are emitted from snow when snow is irradiated with UV light, including UV from natural sunlight. Carbonyls are important precursors to wintertime ozone production. Most of this work has been conducted in the Arctic. Our hypothesis has been that carbonyl emission rates from snow in polluted environments, such as the Uinta Basin during winter inversions, will be greater than in the Arctic and that emissions could be high enough to significantly impact winter ozone.

We have measured fluxes of organic compounds at the air-snow interface in past years, including flux chamber measurements at the Horsepool field station and laboratory measurements under controlled conditions. Section 12 of our 2020 annual report describes our most recent work. These measurements provide evidence that carbonyl compounds are emitted from the snow under some conditions. We will continue laboratory studies in the coming year. The basic laboratory apparatus is described in the 2020 annual report. That apparatus proved the concept (see results from it in Figure 20-2), but an upgrade was needed to perform a larger range of experiments with better control of conditions.

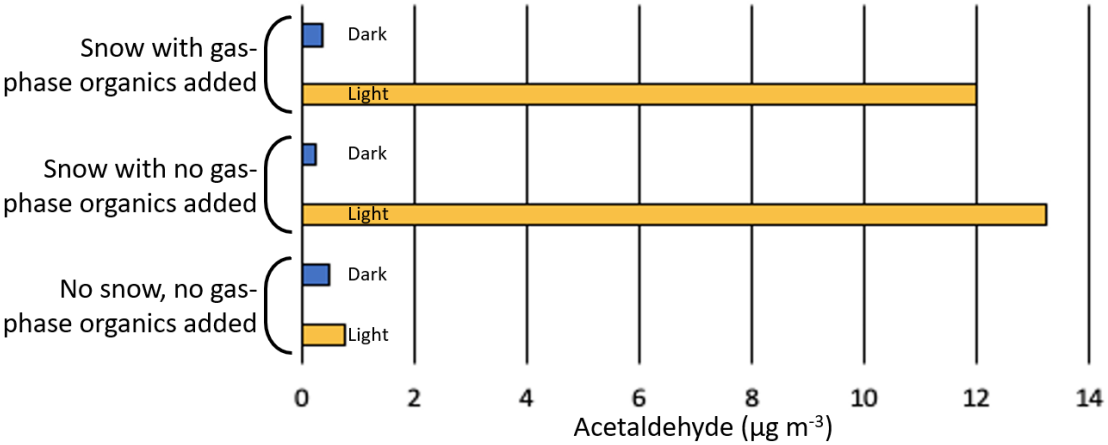

Figure 20-2. Concentrations of acetaldehyde in a proof-of-concept laboratory apparatus. Bags were incubated for 6 hours before analysis. Blue bars show results for bags containing snow that were left in the dark, and yellow bars show results in natural sunlight.

We built an improved apparatus in 2022. It is built within a chest freezer that has been divided into two sections. A temperature control system allows for differential cooling of each section with liquid nitrogen. For each of the two sections, the freezer lid is partially cut away and replaced with UV-transparent acrylic to allow natural sunlight to enter the freezer. Within each section, a PFA Teflon tray is filled with snow and placed within a UV-transparent PTFE Teflon bag. The bag is inflated with outdoor ambient air, and the air is circulated with a PFTE Teflon-lined pump. We allow the snow to incubate

within the bags for several hours and then collect air samples from each bag to determine how air has changed within each one. We measure UV-A and UV-B light within the apparatus and analyze the contents of each bag for concentrations of a suite of 70 different hydrocarbons, alcohols, and carbonyls.

We performed a series of quality assurance tests on the snow irradiation and sampling apparatus in 2023 and continued measurements with the system. Details of the 2023 results will be given in our 2023 Annual Report. We will finish these experiments by early summer 2024. The work planned for 2024 will complete laboratory studies we have planned for this line of research. We will use the results obtained to determine whether carbonyl emissions from the snow are important relative to other carbonyl sources in the Uinta Basin and whether additional research in this area is necessary.

2024 experiments will include:

- Determination of whether carbonyl emissions depend on snow surface area and depth
- Quantification of the relationship between organic compound levels in snow and carbonyl emissions
- Comparisons of snow of different origins and ages
- Quantification of the relationship between carbonyl emissions and available sunlight
- Quantification of the relationship between carbonyl emissions and temperature

We have performed some of these experiments already. We will replicate the experiments in 2024, use the results to estimate total carbonyl emissions from snow across the Uinta Basin, and compare the magnitude of those emissions to total anthropogenic emissions of carbonyls.

20.1.2.1. Responsibilities

- *Responsible persons:* A student researcher will conduct laboratory measurements of air-snow exchange of organic compounds. Seth Lyman and Trevor O'Neil will assist with measurements and work with the student to analyze the collected data.
- *How we will measure performance:* Successful completion of the laboratory tests with data that meet quality objectives, report of results.

20.1.2.2. Funding

All costs for this project will be paid with funds from Uintah Special Service District 1 and the Utah Legislature, except that student wages will be paid from the Anadarko Student Fellowship.

20.1.3. Investigate Ozone Formation in Summertime Wildfire Smoke

In 2022, we were involved in a collaborative study of the impacts of wildfire smoke on summertime ozone and particulate matter in the Salt Lake City area. The study was funded by the Utah Division of Air Quality and several Wasatch Front oil refineries. Smoke plumes from wildfires emit significant amounts of reactive organic compounds that are key precursors to ozone formation, and when these organics combine with high levels of oxides of nitrogen (NO_X) emitted from vehicles and other urban sources,

they can increase the ability of urban atmospheres to produce ozone. The Salt Lake City study used measurements of organic compound concentrations, along with existing measurements of other pollutants, in a box model to learn how wildfires impact ozone production in Salt Lake. A final report for the Salt Lake study is available at https://www.usu.edu/binghamresearch/files/reports/Samoza_finalreport.pdf.

We prepared to conduct a similar study at the Roosevelt air quality monitoring station during summer 2023. We collected measurements during a smoke-free period, but the Uinta Basin had only minimal impact from wildfires in 2023, so we didn't collect measurements during a smokey period. We will conduct the study in summer 2024 if significant wildfire smoke materializes.

In some recent summers (including 2020 and 2021), ozone at Roosevelt rose above the U.S. Environmental Protection Agency standard when wildfire smoke plumes influenced the area, and those summertime exceedances of the standard have been more common at Roosevelt than at other sites. Roosevelt is, of course, a much smaller urban area than Salt Lake City, but NO_X concentrations there tend to be elevated relative to other parts of the Uinta Basin (see Figure 20-3). Also, ambient organic compound concentrations are elevated in Roosevelt due to oil and gas activity in the area (Lyman et al., 2022a).

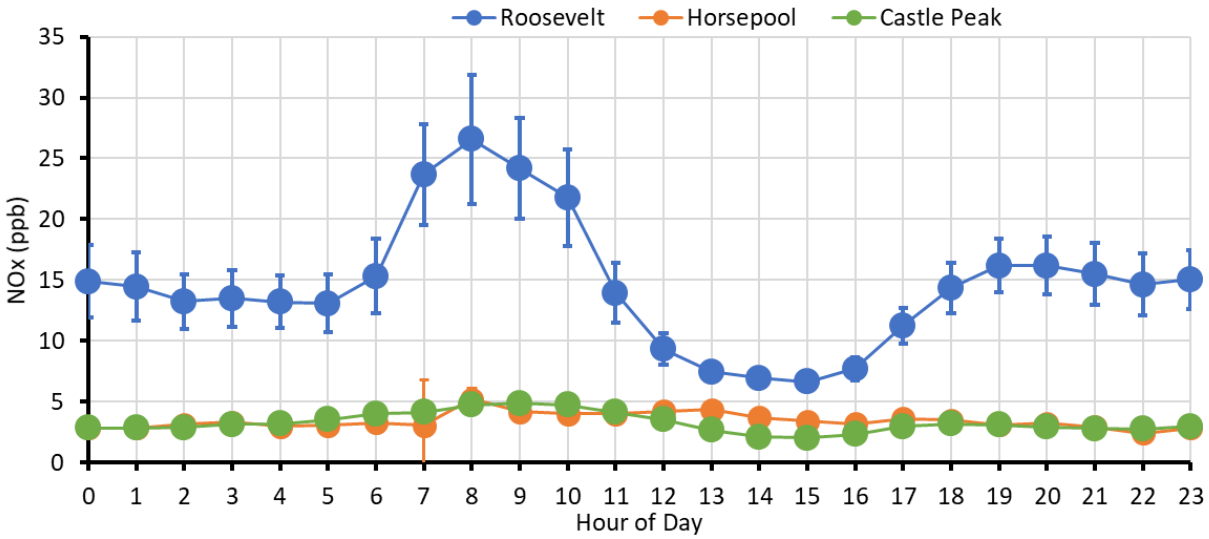

Figure 20-3. Average NO_X at Roosevelt, Horsepool, and Castle Peak during each hour of the day during inversion episodes that occurred during winter 2020-21. Whiskers represent 95% confidence intervals. See Figure 20-1 for the locations of each site.

We will measure ozone, carbonyls (including aldehydes), hydrocarbons, alcohols, methane, total non-methane hydrocarbons (TNMHC), carbon monoxide, particulate matter, NO_X, and total reactive nitrogen (NO_Y) in summer 2024 at the Roosevelt monitoring station if the site experiences significant wildfire smoke. We will also utilize all available data collected by Utah DAQ at the same facility. We will use smoke forecasts provided by the National Weather Service (https://hwp-viz.gsd.esrl.noaa.gov/smoke/index.html) to determine whether smoke impacts are likely at the site. We

will collect a maximum of two weeks of smoke-impacted measurements and two weeks of measurements during periods without smoke impact. If wildfire smoke does not materialize, we will not collect any measurements, and we will resume the project in summer 2025.

We will use the collected data in the F0AM box model to simulate the average conditions of smoke-impacted and smoke-free days. We will use these simulations to determine (1) how smoke impacts the ozone production rate and the ozone production efficiency of NO_X at Roosevelt and (2) whether reductions in non-fire NO_X or organic compound emissions in the Roosevelt area are likely to decrease ozone production on smoke-impacted days. This work will be similar to that conducted by Ninneman and Jaffe (2021). We have already used the F0AM model to simulate winter ozone production in the Horsepool area (Lyman et al., 2022b).

20.1.3.1. Study Goals

The goals of this study are to:

1. Improve understanding of the determinants of summertime ozone pollution in the Uinta Basin.
2. Provide information that will improve the ability of regulatory agencies to determine whether summer ozone exceedances qualify as exceptional events.
3. Determine whether summertime emissions reductions would decrease ozone during wildfire events.

20.1.3.2. Responsibilities

Responsible persons: Trevor O'Neil, Seth Lyman, and student researchers will conduct field measurements. Trevor O'Neil will analyze the collected data and run the F0AM model.

How we will measure performance: Successful completion of field data collection with data that meet quality objectives, successful application of the F0AM model.

20.1.3.3. Funding

All costs for this project will be paid with funds from Uintah Special Service District 1 and the Utah Legislature, except that student wages will be paid from the Anadarko Student Fellowship.

20.2. 2024 Research Plan for Priority 2: Air Quality Modeling

20.2.1. Improve WRF Simulations of Uinta Basin Winter Inversions

The computer model used to simulate meteorological conditions for most regulatory photochemical modeling is the Weather Research and Forecasting (WRF) model. WRF simulates winter inversion events poorly (Neemann et al., 2015; Tran et al., 2018). Attempts to improve WRF performance have had some success but have not been able to simulate conditions that hold pollutants under the inversion layer as tightly as reality, and this results in underprediction of winter ozone and other pollutants (Lyman et al., 2020a; Tran and Tran, 2021; Tran et al., 2018). WRF and similar models were not developed with

complex mountainous terrain and winter inversion conditions in mind, and the extremely strong inversions experienced during some Uinta Basin winters (Mansfield and Hall, 2018) present a unique modeling challenge. We have shown that assimilating balloon-borne vertical measurements into WRF can improve its ability to simulate inversions (Figure 20-4), but the improvements are inconsistent.

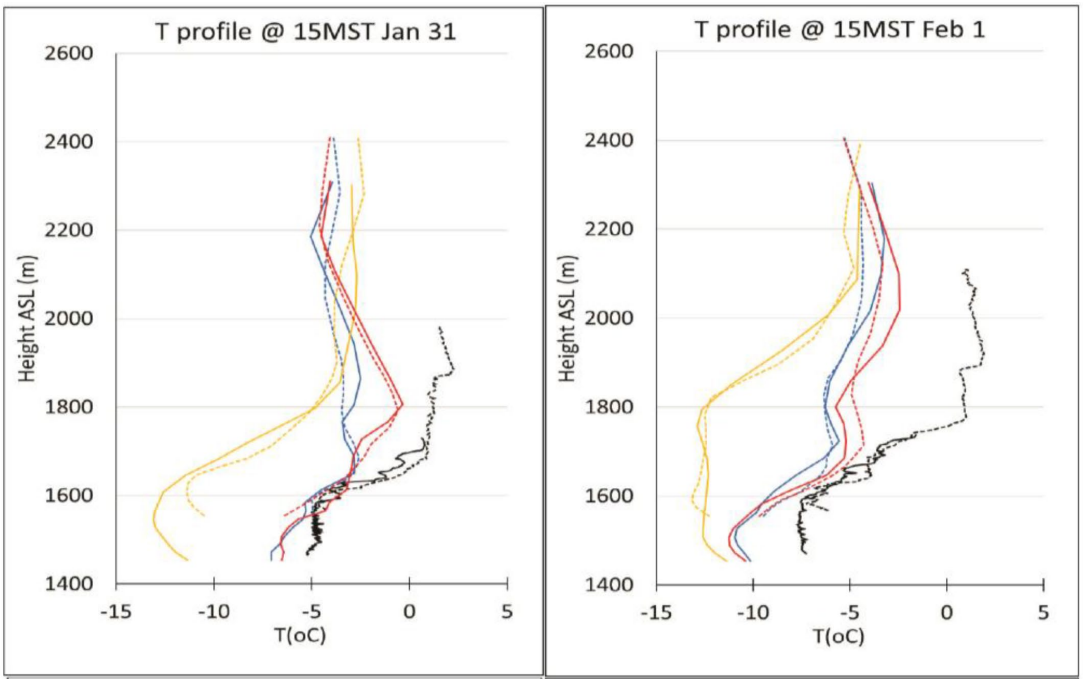

Figure 20-4. Simulated and observed vertical temperature profiles at Horsepool (dashed lines) and Fantasy Canyon (solid lines), from Lyman et al. (2019a). The Y-axis indicates height above sea level (ASL). Observed data were collected by NOAA Tethersondes (black). Simulated data were derived from ONU (orange – assimilation of surface-level meteorological data only), G4 (blue – assimilation of vertical data at Ouray and surface-level data), and G4_plus (red – same as G4, but with vertical data at Horsepool added for nudging). T is temperature.

Given the importance of a correct atmosphere to simulation of the dispersion of pollutants, it is paramount to address why the inversion is poorly captured by the WRF model. We will work to improve WRF simulations by:

- Evaluating "vanilla" WRF simulations on previous winter inversions
    - Archive of hourly forecasts from HRRR model, including snow depth and vertical temperature profiles to estimate inversion strength in the model
    - This allows an immediate "baseline" from which to improve while we develop research models
- Diagnosing specific ways this model misrepresents reality
    - For instance, how accurate are the current snowfall forecasts?
    - Are the inversions captured by the simulations?
- Developing new methods to improve WRF simulations of the inversion onset/dissipation

    - To address uncertainty, we will test the sensitivity of success to how the model is configured
    - We will assess whether uncertainty can be reduced by taking more high quality measurements
- Add the chemical aspect (WRF-CHEM) and evaluate pollutants in simulations.
    - We suspect it is the meteorology – specifically, the inversion – that is most at fault for poor simulations rather than emissions inventory or chemical-dispersion simulations.

The high-resolution rapid refresh (HRRR) model covers the continental United States and is a forecast based on the WRF model. This represents our best-guess and forms a baseline from which we will assess improvements. We will access Winter 2022/2023 HRRR simulation archives and evaluate past predictions of weather and chemical variables using observation towers located around the Basin as truth. Ultimately, it is difficult to issue a single score or number when evaluating the simulation of a complex event, so visualizations of the Basin's atmospheric behavior will be generated and analyzed by eye rather than solely with performance metrics.

Methods to improve simulations will need to address the poorly represented mixing of air below and above the inversion layer, snow-depth predictions, chemical dispersion by wind within the inversion, and whether the estimated small-scale wind flows around canyons and mesas in the Basin influence simulations more than previously thought.

20.2.1.1. Responsibilities

- *Responsible person:* John Lawson
- *How we will measure performance:* This work will take longer than the 2024 calendar year. We will produce a progress report for the 2024 Annual Report to provide an update on the status of these action points.

20.2.1.2. Funding

All costs for this project will be paid with funds from Uintah Special Service District 1 and the Utah Legislature, except that student wages will be paid from the Anadarko Student Fellowship.

20.2.2. Develop a System for Quantitative Winter Ozone Forecasts

Winter inversions are difficult to predict due to their inherent uncertainty, such as their sensitivity to snow depth, wind speeds, and temperature profiles. Small errors in the initial state of the atmosphere will become large errors in the coming forecast. Also, issuing solely “yes” or “no” forecasts for ozone events masks the true uncertainty of the prediction and can be misleadingly confident. In our team’s past attempts to forecast winter ozone episodes, our prediction methods compared well against historical datasets but performed poorly when we used them for real-time prediction (Lyman et al., 2020a; Mansfield, 2018). Figure 20-5 shows a random-forest numerical forecast for winter 2020. It shows that while actual ozone stayed below the EPA standard of 70 ppb, forecast ozone varied strongly in response to forecast snow depth, exceeding the EPA standard in some cases. Because of these

failures, we have thus far relied on qualitative forecasts rather than numerical prediction methods for our ozone alert program.

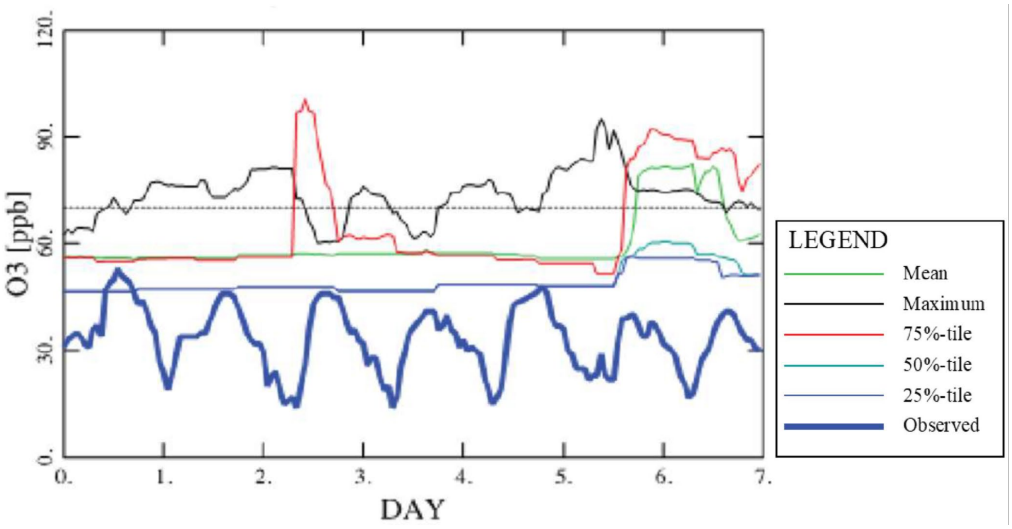

Figure 20-5. Ozone forecast for the Ouray monitoring station for the week starting 10 March 2020 (Lyman et al., 2020a). Observed ozone, as well as predictions using a random forest method, are shown. Predictions using forecast mean, maximum, 75th percentile, 50th percentile, and 25th percentile snow depth data are shown.

As an alternative to past efforts, we propose development of a probabilistic winter ozone forecasting system that gives the risk of an ozone event rather than a *yes* or *no*. This percentage risk can be directly used by decision-makers as a critical point at which it costs less to shut down operations than the loss incurred by continuing to operate. A key element is the communication of these risk predictions; meetings with decision-makers will be critical to optimize the predictions we would issue. Action points include:

- Running multiple simulations in the WRF-CHEM model that represent different scenarios of how the atmosphere is behaving – how different the simulations are represents how (un)sure we are that an inversion will occur;
- Compensating for models' shortcomings in forecast determination. For example, the WRF model currently simulates inversion conditions that are weaker than reality. We will investigate how inversion conditions in the model relate to real conditions and adjust forecasts to compensate for the model's weaknesses;
- Using artificial intelligence (machine learning) to improve the system further by learning where the forecasts could be improved and how;
- Using AI chatbots such as OpenAI's GPT-4 to generate a paragraph of text discussing the weather for the next few hours based on weather data and maps and using automated computer code. The text can be generated at a level appropriate for the receiver (e.g., public, emergency managers, scientists).

Once the prediction system is running as an experiment, we can evaluate how reliable the risk percentages are. For instance, we expect a forecast of 20% to be correct 1 in 5 times. We can also

evaluate how certain the prediction system is: confidence (high probability) is rewarded when the event occurs. For text-based and number-based predictions alike, we require meetings with those stakeholders who make decisions based on the risk forecast guidance. We will hold these meetings as part of the ozone working group. This will be a continuing feedback loop where the forecasts can be tuned to be most useful to the user.

20.2.2.1. Responsibilities

- *Responsible persons:* John Lawson
- *How we will measure performance:* This work will take longer than the 2024 calendar year. We will produce a progress report for the 2024 Annual Report to provide an update on the status of these action points.

20.2.2.2. Funding

All costs for this project will be paid with funds from Uintah Special Service District 1 and the Utah Legislature, except that student wages will be paid from the Anadarko Student Fellowship.

20.2.3. Box Model Investigation of the Impact of Chemical Mechanisms on Simulations of Winter Ozone

A chemical mechanism is a list of all chemicals and reactions used in a chemical model. Thousands of chemical species and well over ten thousand chemical reactions are relevant to winter ozone photochemistry. Explicit simulation of all these reactions and species requires more computational resources than is possible for 3D photochemical models. 3D models instead use simplified chemical mechanisms that group similar compounds and reactions together. Several different simplified mechanisms exist, and all were developed for summer ozone, not winter ozone.

We have conducted several studies to investigate the impact of different chemical mechanisms on the performance of 3D photochemical models (Lyman et al., 2020a; Tran et al., 2015; Tran et al., 2023) and have shown that choice of mechanism can have a large impact on the amount of simulated winter ozone (Figure 20-6) and ozone precursors (Figure 20-7). Unfortunately, the most comprehensive of these studies, Tran et al. (2023), used meteorological inputs to the model that allowed for unrealistically high mixing of pollution out of the inversion layer. This led to ozone production that was much lower in the model than in reality, which leaves lingering ambiguity as to the importance of the chemical mechanism in winter ozone simulations.

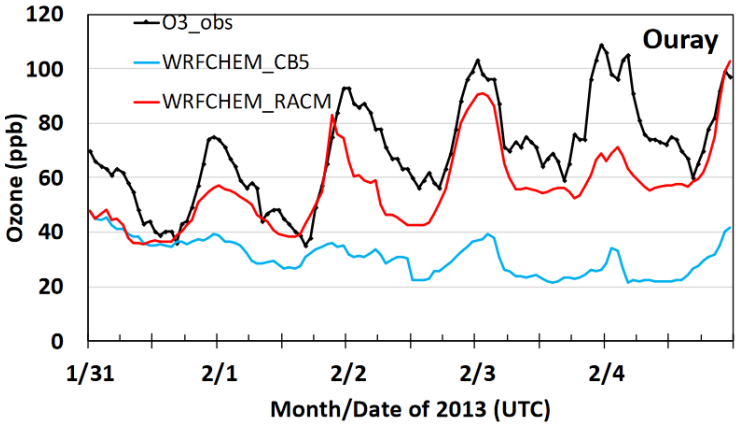

Figure 20-6. Ozone concentrations simulated using the WRF-CHEM 3D photochemical model at Ouray with the CB05 mechanism (WRFCHEM_CB5; blue), WRF-CHEM with the RACM mechanism (WRFCHEM_RACM; red), and observed ozone concentrations (black). From Lyman et al. (2020a).

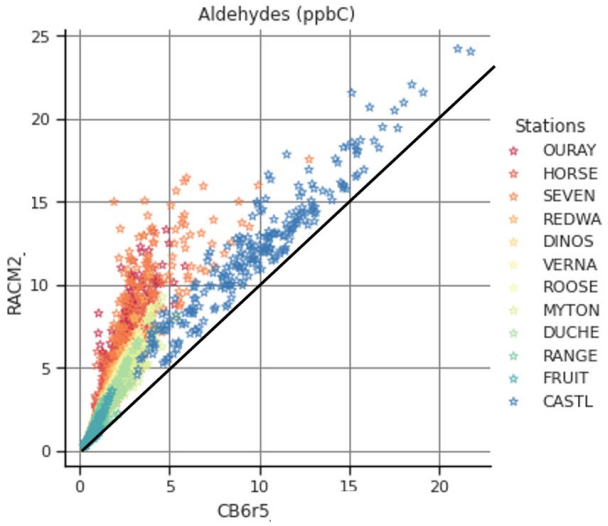

Figure 20-7. Aldehydes in ambient air (units of parts per billion of carbon, or ppbC) at the stations listed, simulated by the CAMx 3D photochemical model with the RACM2 versus the CB6r4 chemical mechanism. From Tran et al. (2023)

We will investigate winter ozone chemistry and chemical mechanisms with the F0AM box model (Wolfe et al., 2016), which we have used in previous studies (Lyman et al., 2022a; Lyman et al., 2022b). 3D photochemical models divide the atmosphere into thousands of cubes that cover the spatial extent of the modeled area. Differential equations for the chemical and physical processes of the atmosphere are solved for each cube, and transport is simulated across adjacent cubes. A box model is essentially the same, except that it contains only a single cube of indeterminate size. Because chemical reactions are computed for just one cube, box models can use explicit chemistry with thousands of chemical species and reactions. Transport and emissions processes are treated coarsely in box models, and meteorological conditions are usually forced to measured values.

We will run the F0AM box model for a 2019 winter ozone episode we have modeled previously. We will compare the Master Chemical Mechanism (Saunders et al., 2003), a detailed mechanism with more than 1,000 species and 12,000 reactions, against simplified mechanisms used in 3D photochemical models, including CB6 (Yarwood et al., 2010), RACM2 (Tran et al., 2023), and SAPRC (Carter, 2010; Tran et al., 2015). Meteorological inputs will be forced to match measured values and will be the same for all model runs. We will follow standard species mapping guidance for converting measured chemical concentrations into model species for each mechanism and force NO_X and organic compounds to match measured values (for the organic species we measured during the modeled episode). We will use outputs from the models to explore the following questions:

1. How do concentrations of ozone and other photochemical precursors and products compare for the different mechanisms?
2. How do ozone and carbonyls respond to changes in NO_X and organic compound concentrations?
3. What are the mechanistic reasons behind any observed differences?

Ultimately, reliable 3D photochemical models, not just box models, are needed by researchers, regulators, and industry. We will use the findings of this study to determine which simplified mechanism performs best for winter ozone. If needed, we will modify one of the simplified mechanisms to improve its performance. Modifications may include addition of reactions or species. In a subsequent phase of this work, we will then apply the optimal mechanism in a 3D photochemical model with reliable meteorological inputs and compare its performance against mechanisms used in previous studies.

20.2.3.1. Responsibilities

- *Responsible persons:* Seth Lyman and graduate student Loknath Dhar will carry out this work.
- *How we will measure performance:* Completion of the project, publication of results.

20.2.3.2. Funding

Seth Lyman's time for this project, as well as any incidental costs, will be paid with funds from Uintah Special Service District 1 and the Utah Legislature. Loknath Dhar will be paid from the Anadarko Student Fellowship.

20.3. 2024 Research Plan for Priority 3: Emissions

20.3.1. Establish a Method for Monthly Basin-wide Pollutant Emissions Estimates

In 2023, we completed a study to determine how Uinta Basin-wide pollutant emissions have changed over time (download a draft final report). Figure 20-8 shows an interannual time series of Basin-wide emissions derived from the study. It shows, as other studies have shown (Lin et al., 2021; Mansfield and Lyman, 2021), that ozone-forming emissions declined through 2020. As oil and gas production in the Uinta Basin has increased since 2021, however, emissions have again increased.

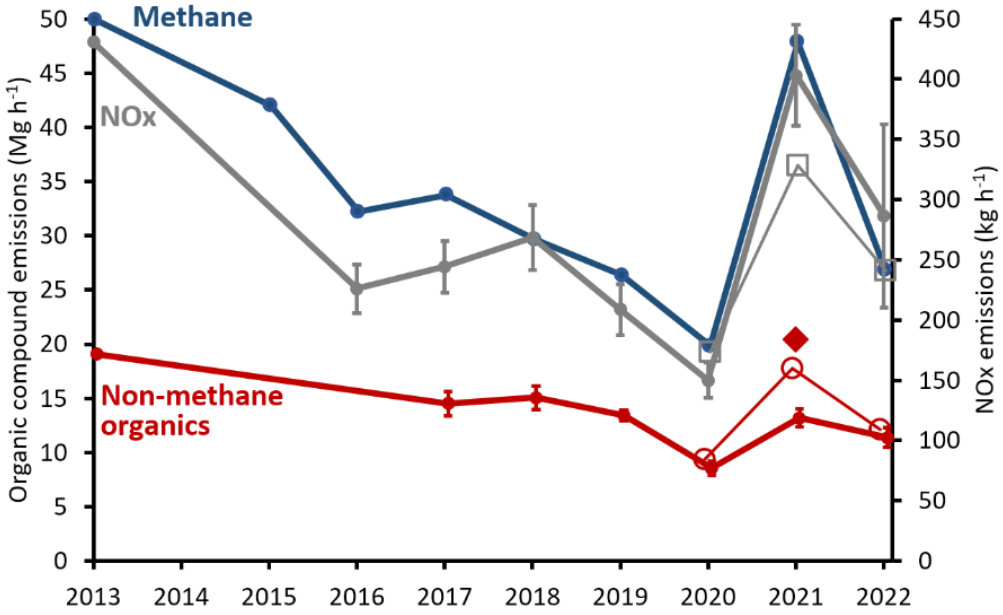

Figure 20-8. Uinta Basin-wide annual emissions estimates for methane, NO_X, and total non-methane organic compounds. 2013 estimates are from Karion et al. (2013) and Ahmadov et al. (2015). Closed circles show estimates derived from Horsepool measurements. Open symbols show estimates derived from Castle Peak measurements. The diamond shows the estimate derived from measurements at portable stations. Whiskers show 95% confidence intervals.

We believe that continuing Basin-wide emissions estimates will be valuable for research and policy. Tracking changes in emissions over time allows us to understand whether changes in industry practices and regulations are effective, and it allows us to investigate the root causes of the changes.

The methods used in the recently completed study rely on measurements at surface sites, and these measurements may be impacted by local sources that contaminate the Basin-wide signal. Figure 20-8 shows very high methane and NO_X emissions in 2021. We found no evidence for a local cause of the 2021 spike, but we were also unable to completely rule it out.

New satellite-based methods of determining area-wide pollutant emissions have been used successfully in the Permian Basin, and we believe they could be applied here. Satellite measurements average pollutant concentrations over a broad area, eliminating the possibility of errors created by one or a few large sources. Also, satellite-based estimates can be conducted monthly or even weekly, giving rapid information to stakeholders about emissions. It may also be possible to determine emissions from different areas of the Basin using satellite methods rather than just the Basin as a whole.

Varon et al. (2023) determined weekly methane emissions estimates for the Permian Basin using methane data from the TROPOMI satellite and an inverse chemical transport modeling technique. Their estimates compared reasonably with other estimates and with indicators of oil and gas activity. What is more, they prepared a separate publication with method details (Varon et al., 2022) and prepared a cloud-based system by which others can apply their method at any location and time period.

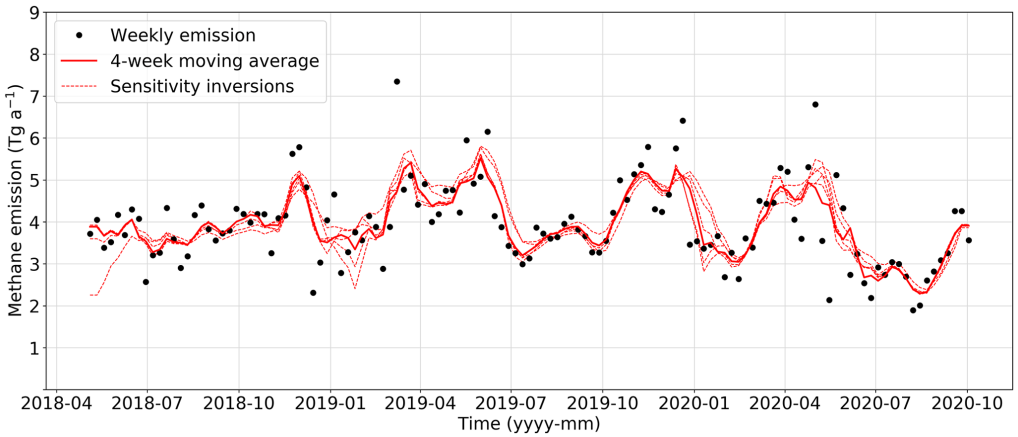

Figure 20-9. Weekly methane emissions from the Permian Basin from 1 May 2018 to 5 October 2020 (Varon et al., 2023). Emissions are inferred by inversion of weekly TROPOMI satellite observations using a suboptimal Kalman filter. The dashed lines are 4-week moving averages of the weekly emission estimates from four sensitivity inversions.

For this work, we will apply the methods developed by Varon et al. to the Uinta Basin. We will determine whether the method works during winter inversion conditions, the best frequency with which to make estimates, and whether sub-Basin scale estimates are possible. We will compare the emissions estimates from this method to those determined in our recently completed study and compare emissions trends against various indicators of oil and gas activity and meteorology. We will determine whether the Varon et al. method is viable and, if so, establish a system to regularly calculate emissions estimates for the Basin and to distribute those estimates to stakeholders. We will also compare the Basin-wide emissions estimate to satellite and aircraft data available for specific days from Carbon Mapper, which provides publicly-available, location-specific emissions data for large methane sources. Carbon Mapper has some data available for the Uinta Basin that may give insight about the percentage of methane emissions due to large versus small sources.

20.3.1.1. Responsibilities

- *Responsible Person:* Seth Lyman will carry out this work, possibly with help from student researchers.
- *How we will measure performance:* We will determine the value of this method by comparing the results to other emissions estimates and indicators of oil and gas emissions. We will produce a final report of this work. If this work is successful, we will establish a system to continue ongoing estimates of basin-wide emissions that will be publicly released on a regular basis.

20.3.1.2. Funding

Most costs for this project will be paid with funds from Uintah Special Service District 1 and the Utah Legislature. Student wages will be paid from the Anadarko Student Fellowship.

20.3.2. Development of Methods to Determine Oil Storage Tank Emission Factors in the Uinta Basin

We have been working with the Utah Petroleum Association and several oil and gas companies over the past year to plan a project to investigate methods for determining emission factors for oil storage tanks in the Uinta Basin. For the study, we will collect replicate pressurized oil samples from four different oil wells and send the samples to three different laboratories for analysis. The laboratories will analyze the pressurized liquid and will conduct flash liberation analyses, wherein pressurized oil samples are depressurized, and the evolved gas and residual oil are analyzed. These laboratory results will then be used with computational models to determine the ratio of evolved gas to residual oil and the composition of evolved gas in field conditions. We will analyze the variability among and within laboratories and variability caused by different model platforms and methods. We will determine whether some laboratories and methods produce more reliable results than others and compare the results of this study to existing datasets.

The desired outcomes of this work are:

1. A robust agreed methodology by which emission factors for Uinta Basin waxy crude can be determined;
2. Improvements to understanding of the uncertainty in emission factors derived from field samples collected in the Uinta Basin (e.g., 1.0 lb/bbl ± 0.5 lb/bbl, with ± uncertainty calculated from sampling, measurement, and analysis uncertainty evaluations);
3. Comparison of emission factor uncertainty to variability in existing high-quality emission factor data for the Uinta Basin; and
4. A publication describing the study and its outcomes.

Utah Division of Air Quality recently led a tank emission factor study for the Uinta Basin (Wilson et al., 2020). The Division of Air Quality study's primary purpose was to determine emission factors, whereas the primary purpose of the work proposed here is to determine how methods for determining emission factors compare, why they differ, and what methods are the most defensible.

Field sampling will occur in fall 2023. Analysis and modeling will occur in the first half of 2024.

Additional information can be found in the study proposal.

20.3.2.1. Responsibilities

- *Responsible Person:* Seth Lyman
- *How we will measure performance:* Successful sampling, analysis, and modeling. Completion of the final report.

20.3.2.2. Funding

USU personnel time on this project will be paid with funds from Uintah Special Service District 1 and the Utah Legislature. ChampionX has agreed to carry out the field sampling for the project without charge. Participating companies will reimburse USU for laboratory analysis costs and will pay for modeling costs.

20.3.3. Drone-based Measurement of Emissions from Oil and Gas Sources

20.3.3.1. Background

Our team has carried out work to better characterize a number of Uinta Basin emission source types, including emissions from well pads (Lyman et al., 2019b; Wilson et al., 2020), liquid storage tanks (Lyman and Tran, 2015; Lyman et al., 2019b; Wilson et al., 2020), produced water ponds (Lyman et al., 2018; Mansfield et al., 2018; Tran et al., 2017), subsurface leaks (Lyman et al., 2020c; Lyman et al., 2017), and pumpjack engines (Lyman et al., 2022c). We have measured emissions of NO_x, methane, non-methane hydrocarbons, alcohols, carbonyls, and other gases from emission sources. Many oil and gas-related emission sources remain poorly characterized, however. According to surveys we conducted, many stakeholders feel that additional emissions measurements are needed (see Section 17.2 in our 2020 Annual Report and Section 15.2 in our 2021 Annual Report).

We conducted a survey of stakeholders 2023 to determine which emission sources they think are the most important for us to study. Those who took the survey were asked to rank a variety of emission source types as the most important to study, the second most important, or the third most important. We received 33 verified responses. Figure 18-1 shows a summary of survey responses. Rankings were different for different groups of respondents. For example, industry respondents rated drilling and completions at the most important source to study, while respondents associated with government entities rated liquid storage tanks more highly. Many respondents indicated the need to research emissions from produced water, liquid storage tanks, and pipelines as very important. These same three source types were also most likely to be respondents' first choice (data not shown).

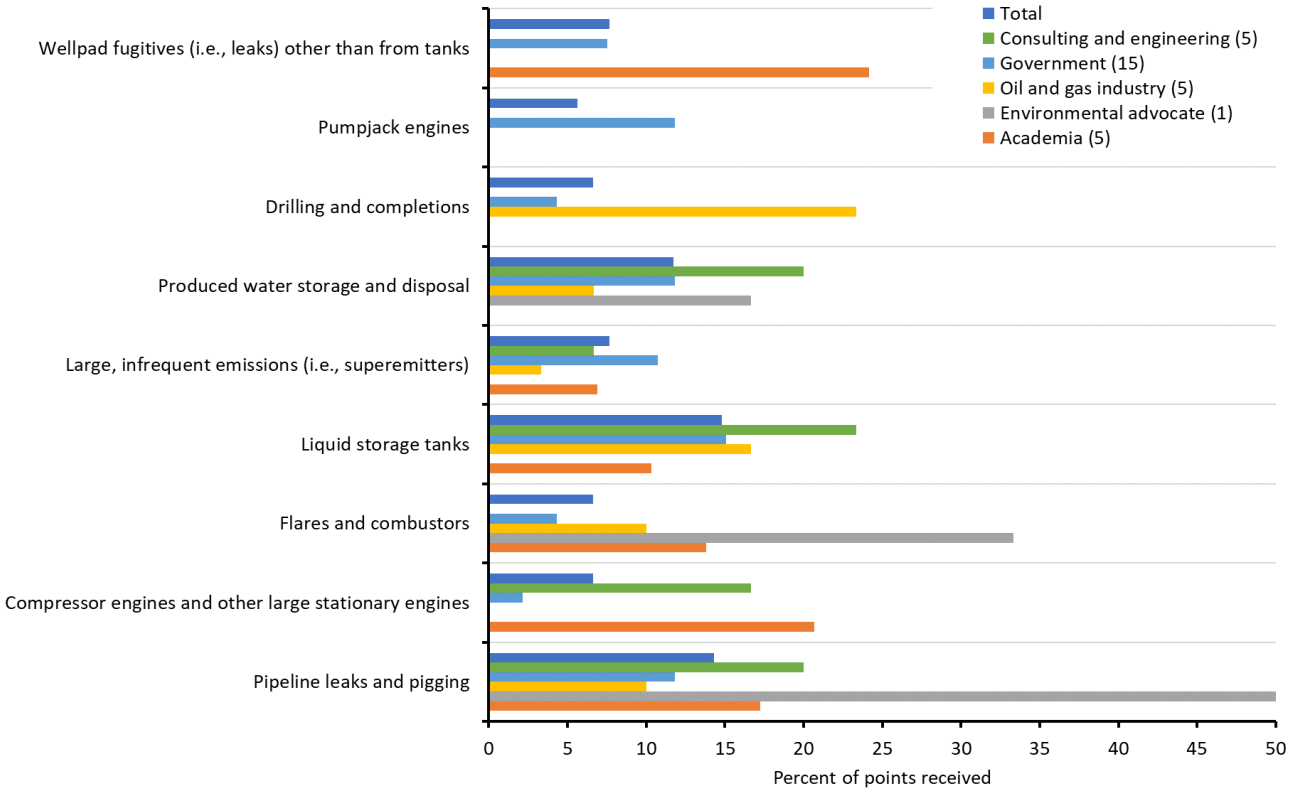

Figure 20-10. Responses to a stakeholder survey about the most important emission sources to research. Bars show the percent of total points for each group of respondents that were given to each source type. A ranking as most important was given three points, the second most important was given two points, the third most important was given one point, and any other ranking was given zero points. Total is the result for all respondents. Respondent groups are shown in the legend with the number of responses received for each group in parentheses. Source types that received less than 5% of total points are not shown.

20.3.3.2. The Case for Drone-based Emission Measurements

The methods we have used to measure emissions in the past (referenced in the first paragraph) are component-specific, labor-intensive, and require site access. They are accurate and specific, but the time and coordination required to carry them out limits the number of samples that can be collected. Also, the methods we have used in the past can't be used efficiently for characterization of pipeline emissions. New drone-based methods have shown great promise for measuring emissions from a variety of sources. Drones equipped with new lightweight sensors for methane, ethane, and meteorological conditions can rapidly determine emission rates by mapping the net transport of methane and ethane away from a source relative to background values (Figure 20-11).

We already have a drone capable of collecting these measurements (a DJI Matrice 210). We will outfit the drone with chemical and meteorological sensors following Gålfalk et al. (2021) and will use their method for calculating emission rates (also see mass balance methods in Hollenbeck et al. (2021)). Drone-based emissions measurement systems have mostly been used for methane and ethane, but we also need to measure emissions of speciated non-methane organics, NO_X, and sometimes CO and CO_2.

We can measure NO_X, CO, and CO_2 on a drone with lightweight electrochemical sensors, but speciated non-methane organics must be collected in large sample containers that are analyzed in our laboratory. We will collect these samples from a sampling tube with an inlet at the drone's height. We will first characterize the emission source with on-board sensors. Then, we will use the drone's real-time data stream to determine the downstream location(s) where methane and ethane emissions are elevated, and we will lift a sample inlet tube to that location. We will flush the inlet tube with air and then collect samples from the tube while the drone collects data at the same location(s). We will then analyze the samples in our laboratory. We will follow the method of Gålfalk et al. to calculate emissions of pollutants measured by the drone in real-time, and we will calculate emissions of individual organics from the ratio of those organics to methane and ethane.

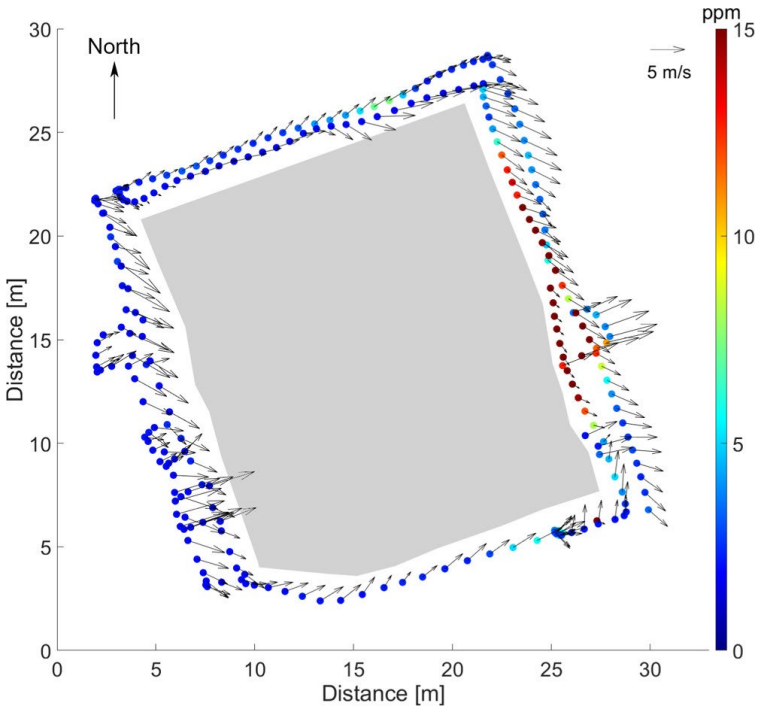

Figure 20-11. Example of methane concentrations and wind vectors for a flight around the edges of a source (several altitudes combined). Taken from Gålfalk et al. (2021). The lengths of the arrows correlate with wind speeds.

This drone-based method won't allow us to definitively distinguish emissions from individual components at a facility, but it will allow us to determine emission rates quickly and without direct equipment access. For the three source types indicated by stakeholders to be most important (pipelines, liquid storage tanks, and produced water), drone-based measurements will be much more efficient than the hands-on techniques we have used in the past.

20.3.3.3. Research Plan

The first step in this work is to purchase the sensors needed, connect them to the drone, and build and test the electrical and communication systems for the drone and the sensors. As we build the drone

system, we will also build a calibration system so we can verify that emissions determined with the drone are accurate. The calibration system will consist of certified source gases (we already have source gases for methane, a suite of non-methane organics, NO_X, and CO), a mass flow controller to regulate the emission rate, and tubing from which the gases will be released. UB Tech, the technical college next to the USU Vernal campus, has non-functional oil and gas equipment on its grounds for training purposes. We will obtain permission from UB Tech to release calibration gas from different points on these pieces of equipment to test and troubleshoot the drone system.

As we begin testing the drone, we will build a Python program that receives the drone data stream, including location information, meteorological parameters, and chemical data and calculates emission rates using the mass balance method detailed by Gålfalk et al. The program will also take in speciated non-methane organics data that are not part of the drone data stream. It will also provide a 3-D visualization of the collected data.

After the drone system, calibration system, and emission calculation program are complete, we will begin collecting measurements of emissions from actual oil and gas sources. After we are confident in the timeline for completion, we will work with energy companies to arrange for site visits to collect measurements. We expect to be ready to begin field measurements in fall 2024.

20.3.3.4. Responsibilities

- *Responsible Persons:* Colleen Jones and Trevor O'Neil
- *How we will measure performance:* We will consider our 2024 work to be successful if (1) the drone-based measurement system is constructed and tested, (2) the emissions calculation program is completed and tested, and (3) we have successfully used the drone system to characterize emissions from a few sources.

20.3.3.5. Funding

Most costs for this project will be paid with funds from Uintah Special Service District 1 and the Utah Legislature. Student wages will be paid from the Anadarko Student Fellowship.

20.4. 2024 Research Plan for Priority 4: Stakeholder Engagement

Funding for stakeholder engagement tasks will come from Uintah Special Service District 1 and the Utah Legislature.

20.4.1. Real-time Data Website

We will continue to operate our real-time data website at ubair.usu.edu. The site provides data about air quality and meteorological conditions around the Uinta Basin and is used by industry, government, and the public to assess current air quality conditions.

20.4.1.1. Responsibilities

- *Responsible persons:* Seth Lyman and Trevor O'Neil
- *How we will measure performance:* Number of unique users each year

20.4.2. Ozone Alert Program

We will continue to operate our ozone alert program (http://binghamresearch.usu.edu/OzoneAlert. The purpose of the program is to alert oil and gas operators and others when high ozone is forecast so they can take action to reduce ozone-forming emissions.

20.4.2.1. Responsibilities

- *Responsible persons:* Seth Lyman and John Lawson
- *How we will measure performance:* Number of unique users (including industry users), performance of alerts compared to actual observed ozone.

20.4.3. Uinta Basin Ozone Working Group

The Uinta Basin Ozone Working Group is a collaborative forum to facilitate attainment of the ozone standard in the Uinta Basin (https://www.usu.edu/basinozonegroup). The group includes representation from government, industry, researchers, and environmental advocates. We will continue to facilitate the ozone working group in 2024.

20.4.3.1. Responsibilities

- *Responsible persons:* Marc Mansfield or another Bingham Center staff member will participate as the leader of the group's steering committee and as the meeting facilitator, and Seth Lyman will maintain the group's website and be responsible for group communications. Our entire team will participate in group meetings and provide information for the group as needed.
- *How we will measure performance:* Meeting attendance.

21. Acknowledgments

One of the main purposes of this document is to report on activities we have carried out with financial support from the Utah Legislature and Uintah Special Service District 1. We are grateful to these two entities for their ongoing support of our Uinta Basin air quality work. Other funding sources are acknowledged in the appropriate sections of the document. We administer an endowment from Anadarko Petroleum Corporation that provides opportunities for students to participate in air quality research. Student recipients of those funds participated in the work presented here. Site access, electricity, and/or equipment at some of our monitoring stations is provided by the Utah Division of Air Quality, Ovintiv, Middle Fork Energy, and the Bureau of Land Management. Many energy companies have provided data and access to oil and gas facilities for our work.

22. References

Ahmadov, R., McKeen, S., Trainer, M., Banta, R., Brewer, A., Brown, S., Edwards, P.M., de Gouw, J.A., Frost, G.J., Gilman, J., Helmig, D., Johnson, B., Karion, A., Koss, A., Langford, A., Lerner, B., Olson, J., Oltmans, S., Peischl, J., Petron, G., Pichugina, Y., Roberts, J.M., Ryerson, T., Schnell, R., Senff, C., Sweeney, C., Thompson, C., Veres, P.R., Warneke, C., Wild, R., Williams, E.J., Yuan, B., Zamora, R., 2015. Understanding high wintertime ozone pollution events in an oil- and natural gas-producing region of the western US. Atmos. Chem. Phys. 15, 411-429.

Anneken, D., Striebich, R., DeWitt, M.J., Klingshirn, C., Corporan, E., 2015. Development of methodologies for identification and quantification of hazardous air pollutants from turbine engine emissions. J. Air Waste Manag. Assoc. 65, 336-346.

Bishop, G.A., Haugen, M.J., McDonald, B.C., Boies, A.M., 2022. Utah wintertime measurements of heavy-duty vehicle nitrogen oxide emission factors. Environ. Sci. Technol. 56, 1885-1893.

Bouillon, M., Safieddine, S., Hadji-Lazaro, J., Whitburn, S., Clarisse, L., Doutriaux-Boucher, M., Coppens, D., August, T., Jacquette, E., Clerbaux, C., 2020. Ten-year assessment of IASI radiance and temperature. Remote Sensing 12, 2393.

Bouillon, M., Safieddine, S., Whitburn, S., Clarisse, L., Aires, F., Pellet, V., Lezeaux, O., Scott, N.A., Doutriaux-Boucher, M., Clerbaux, C., 2022. Time evolution of temperature profiles retrieved from 13 years of infrared atmospheric sounding interferometer (IASI) data using an artificial neural network. Atmos. Meas. Tech. 15, 1779-1793.

Brown, J.L., 2017. Implementable Changes to a Large-Bore Single Cylinder Natural Gas Engine for Improved Emissions Performance. Texas A&M University, Corpus Christi, Texas, https://hdl.handle.net/1969.1/161579.

Carter, W.P., 2009. Updated maximum incremental reactivity scale and hydrocarbon bin reactivities for regulatory applications, https://ww3.arb.ca.gov/regact/2009/mir2009/mir10.pdf.

Carter, W.P., 2010. Development of the SAPRC-07 chemical mechanism. Atmos. Environ. 44, 5324-5335.

Carter, W.P., Seinfeld, J.H., 2012. Winter ozone formation and VOC incremental reactivities in the Upper Green River Basin of Wyoming. Atmos. Environ. 50, 255-266.

Chou, C.C.K., Tsai, C.Y., Shiu, C.J., Liu, S.C., Zhu, T., 2009. Measurement of NOy during Campaign of Air Quality Research in Beijing 2006 (CAREBeijing-2006): Implications for the ozone production efficiency of NOx. J. Geophys. Res. Atmos. 114, D00G01.

Dardiotis, C., Martini, G., Marotta, A., Manfredi, U., 2013. Low-temperature cold-start gaseous emissions of late technology passenger cars. Applied energy 111, 468-478.

Edwards, P.M., Brown, S.S., Roberts, J.M., Ahmadov, R., Banta, R.M., deGouw, J.A., Dube, W.P., Field, R.A., Flynn, J.H., Gilman, J.B., Graus, M., Helmig, D., Koss, A., Langford, A.O., Lefer, B.L., Lerner, B.M., Li, R., Li, S.-M., McKeen, S.A., Murphy, S.M., Parrish, D.D., Senff, C.J., Soltis, J., Stutz, J., Sweeney, C., Thompson, C.R., Trainer, M.K., Tsai, C., Veres, P.R., Washenfelder, R.A., Warneke, C., Wild, R.J., Young, C.J., Yuan, B., Zamora, R., 2014. High winter ozone pollution from carbonyl photolysis in an oil and gas basin. Nature 514, 351-354.

EPA, 2022. What is the definition of VOC. United States Environmental Protection Agency, https://www.epa.gov/air-emissions-inventories/what-definition-voc.

EPA, U., 1999. Compendium Method TO-11A. U.S. Environmental Protection Agency, Research Triangle Park, North Carolina, https://www3.epa.gov/ttnamti1/files/ambient/airtox/to-11ar.pdf.

EPA, U.S., 1998. Technical Assistance Document for Sampling and Analysis of Ozone Precursors. United States Environmental Protection Agency, Research Triangle Park, North Carolina, http://www.epa.gov/ttn/amtic/files/ambient/pams/newtad.pdf.

Gålfalk, M., Nilsson Påledal, S.r., Bastviken, D., 2021. Sensitive drone mapping of methane emissions without the need for supplementary ground-based measurements. ACS Earth and Space Chemistry 5, 2668-2676.

Gorchov Negron, A.M., McDonald, B.C., McKeen, S.A., Peischl, J., Ahmadov, R., de Gouw, J.A., Frost, G.J., Hastings, M.G., Pollack, I.B., Ryerson, T.B., Thompson, C., Warneke, C., Trainer, M., 2018. Development of a fuel-based oil and gas inventory of nitrogen oxides emissions. Environ. Sci. Technol. 52, 10175-10185.

Grange, S.K., Farren, N.J., Vaughan, A.R., Rose, R.A., Carslaw, D.C., 2019. Strong temperature dependence for light-duty diesel vehicle NO x emissions. Environ. Sci. Technol. 53, 6587-6596.

Grannas, A., Jones, A.E., Dibb, J., Ammann, M., Anastasio, C., Beine, H., Bergin, M., Bottenheim, J., Boxe, C., Carver, G., 2007. An overview of snow photochemistry: evidence, mechanisms and impacts. Atmos. Chem. Phys. 7, 4329-4373.

Griffin, A.A., 2015. Combustion Characteristics of a Two-Stroke Large Bore Natural Gas Spark-Ignited Engine. Texas A&M University, Corpus Christi, Texas, https://hdl.handle.net/1969.1/155685.

Griffin, A.A., Jacobs, T.J., 2015. Combustion Characteristics of a 2-Stroke Large Bore Natural Gas Spark-Ignited Engine, Internal Combustion Engine Division Fall Technical Conference. American Society of Mechanical Engineers, Houston, Texas, p. V001T001A002.

Hall, D.L., Anderson, D.C., Martin, C.R., Ren, X., Salawitch, R.J., He, H., Canty, T.P., Hains, J.C., Dickerson, R.R., 2020. Using near-road observations of CO, NOy, and CO2 to investigate emissions from vehicles: Evidence for an impact of ambient temperature and specific humidity. Atmos. Environ. 232, 117558.

Hollenbeck, D., Zulevic, D., Chen, Y., 2021. Advanced leak detection and quantification of methane emissions using sUAS. Drones 5, 117.

Horel, J., Splitt, M., Dunn, L., Pechmann, J., White, B., Ciliberti, C., Lazarus, S., Slemmer, J., Zaff, D., Burks, J., 2002. Mesowest: Cooperative mesonets in the western United States. Bulletin of the American Meteorological Society 83, 211-226.

Jacob, D.J., Horowitz, L.W., Munger, J.W., Heikes, B.G., Dickerson, R.R., Artz, R.S., Keene, W.C., 1995. Seasonal transition from NOx-to hydrocarbon-limited conditions for ozone production over the eastern United States in September. J. Geophys. Res. Atmos. 100, 9315-9324.

Jin, X., Fiore, A.M., Murray, L.T., Valin, L.C., Lamsal, L.N., Duncan, B., Folkert Boersma, K., De Smedt, I., Abad, G.G., Chance, K., 2017. Evaluating a space-based indicator of surface ozone-NOx-VOC sensitivity over midlatitude source regions and application to decadal trends. J. Geophys. Res. Atmos. 122, 10,439-410,461.

Jung, J., Lee, J., Kim, B., Oh, S., 2017. Seasonal variations in the NO2 artifact from chemiluminescence measurements with a molybdenum converter at a suburban site in Korea (downwind of the Asian continental outflow) during 2015–2016. Atmos. Environ. 165, 290-300.

Karion, A., Sweeney, C., Petron, G., Frost, G., Hardesty, R.M., Kofler, J., Miller, B.R., Newberger, T., Wolter, S., Banta, R., Brewer, A., Dlugokencky, E., Lang, P., Montzka, S.A., Schnell, R., Tans, P., Trainer, M., Zamora, R., Conley, S., 2013. Methane emissions estimate from airborne measurements over a western United States natural gas field. Geophys. Res. Lett. 40, 4393-4397.

Kendall, M.G., 1948. Rank correlation methods. Griffin.

Kerry, K., Hawick, K.A., 1998. Kriging interpolation on high-performance computers, High-Performance Computing and Networking: International Conference and Exhibition Amsterdam, The Netherlands, April 21–23, 1998 Proceedings 6. Springer, pp. 429-438.

Kleinman, L.I., 1991. Seasonal dependence of boundary layer peroxide concentration: The low and high NO x regimes. J. Geophys. Res. Atmos. 96, 20721-20733.

Koss, A., Gouw, J.d., Warneke, C., Gilman, J., Lerner, B., Graus, M., Yuan, B., Edwards, P., Brown, S., Wild, R., Roberts, J.M., Bates, T., Quinn, P.K., 2015. Photochemical aging of volatile organic compounds associated with oil and natural gas extraction in the Uintah Basin, UT, during a wintertime ozone formation event. Atmos. Chem. Phys. 15, 5727-5741.

Li, X., Dallmann, T.R., May, A.A., Presto, A.A., 2020. Seasonal and long-term trend of on-road gasoline and diesel vehicle emission factors measured in traffic tunnels. Applied Sciences 10, 2458.

Liang, J., Horowitz, L.W., Jacob, D.J., Wang, Y., Fiore, A.M., Logan, J.A., Gardner, G.M., Munger, J.W., 1998. Seasonal budgets of reactive nitrogen species and ozone over the United States, and export fluxes to the global atmosphere. J. Geophys. Res. Atmos. 103, 13435-13450.

Lin, J.C., Bares, R., Fasoli, B., Garcia, M., Crosman, E., Lyman, S., 2021. Declining methane emissions and steady, high leakage rates observed over multiple years in a western US oil/gas production basin. Sci. Rep. 11, 1-12.

Lyman, S., Mansfield, M.L., Tran, H., Tran, T., Holmes, M., 2019a. 2019 Annual Report: Uinta Basin Air Quality Research. Utah State University, Vernal, Utah, https://usu.box.com/s/co626elackqkw9ead14wkma14jjv9eng.

Lyman, S., Mansfield, M.L., Tran, H., Tran, T., Holmes, M., O'Neil, T., 2020a. 2020 Annual Report: Uinta Basin Air Quality Research. Utah State University, Vernal, Utah, https://www.usu.edu/binghamresearch/files/reports/UBAQR-2020-AnnualReport.pdf.

Lyman, S., Tran, T., 2015. Measurement of Carbonyl Emissions from Oil and Gas Sources in the Uintah Basin. Utah State University, Vernal, Utah, http://binghamresearch.usu.edu/files/CarbonylEmiss_FnlRprt_31jul2015.pdf.

Lyman, S.N., David, L.M., Mansfield, M.L., O'Neil, T., 2022a. 2022 Annual Report: Uinta Basin Air Quality Research. Bingham Research Center, Utah State University, Vernal, Utah, https://www.usu.edu/binghamresearch/files/reports/UBAQR_2022_AnnualReport.pdf.

Lyman, S.N., Elgiar, T., Gustin, M.S., Dunham-Cheatham, S.M., David, L.M., Zhang, L., 2022b. Evidence against Rapid Mercury Oxidation in Photochemical Smog. Environ. Sci. Technol. 56, 11225-11235.

Lyman, S.N., Gratz, L.E., Dunham-Cheatham, S.M., Gustin, M.S., Luippold, A., 2020b. Improvements to the accuracy of atmospheric oxidized mercury measurements. Environ. Sci. Technol. 54, 13379-13388.

Lyman, S.N., Holmes, M., Tran, H., Tran, T., O'Neil, T., 2021. High ethylene and propylene in an area dominated by oil production. Atmos. *12*, 1.

Lyman, S.N., Mansfield, M.L., Tran, H.N., Evans, J.D., Jones, C., O'Neil, T., Bowers, R., Smith, A., Keslar, C., 2018. Emissions of organic compounds from produced water ponds I: Characteristics and speciation. Sci. Tot. Environ. 619, 896-905.

Lyman, S.N., Tran, H.N., Mansfield, M.L., Bowers, R., Smith, A., 2020c. Strong temporal variability in methane fluxes from natural gas well pad soils. Atmospheric Pollution Research 11, 1386-1395.

Lyman, S.N., Tran, H.N.Q., O'Neil, T.L., Mansfield, M.L., 2022c. Low NOX and high organic compound emissions from oilfield pumpjack engines. Elem. Sci. Anth. 10, 00064.

Lyman, S.N., Tran, T., Mansfield, M.L., Ravikumar, A.P., 2019b. Aerial and ground-based optical gas imaging survey of Uinta Basin oil and gas wells. Elem. Sci. Anth. 7, 43.

Lyman, S.N., Watkins, C., Jones, C.P., Mansfield, M.L., McKinley, M., Kenney, D., Evans, J., 2017. Hydrocarbon and Carbon Dioxide Fluxes from Natural Gas Well Pad Soils and Surrounding Soils in Eastern Utah. Environ. Sci. Technol. 51, 11625-11633.

Mann, H.B., 1945. Nonparametric tests against trend. Econometrica: Journal of the econometric society, 245-259.

Mansfield, M.L., 2018. Statistical analysis of winter ozone exceedances in the Uintah Basin, Utah, USA. J. Air Waste Manag. Assoc. 68, 403-414.

Mansfield, M.L., Hall, C.F., 2018. A survey of valleys and basins of the western United States for the capacity to produce winter ozone. J. Air Waste Manag. Assoc., 1-11.

Mansfield, M.L., Lyman, S.N., 2021. Winter Ozone Pollution in Utah's Uinta Basin is Attenuating. Atmosphere 12, 4.

Mansfield, M.L., Tran, H.N.Q., Lyman, S.N., Smith, A., Bowers, R., Keslar, C., 2018. Emissions of organic compounds from produced water ponds III: mass-transfer coefficients, composition-emission correlations, and contributions to regional emissions. Sci. Tot. Environ. 627, 860-868.

Martin, R.V., Fiore, A.M., Van Donkelaar, A., 2004. Space-based diagnosis of surface ozone sensitivity to anthropogenic emissions. Geophys. Res. Lett. 31.

Matichuk, R., Tonnesen, G., Luecken, D., Gilliam, R., Napelenok, S.L., Baker, K.R., Schwede, D., Murphy, B., Helmig, D., Lyman, S.N., 2017. Evaluation of the Community Multiscale Air Quality Model for Simulating Winter Ozone Formation in the Uinta Basin. J. Geophys. Res. Atmos. 122, 13545–13572.

Neemann, E.M., Crosman, E.T., Horel, J.D., Avey, L., 2015. Simulations of a cold-air pool associated with elevated wintertime ozone in the Uintah Basin, Utah. Atmos. Chem. Phys. 15, 135-151.

Ninneman, M., Jaffe, D.A., 2021. The impact of wildfire smoke on ozone production in an urban area: Insights from field observations and photochemical box modeling. Atmos. Environ. 267, 118764.

Oltmans, S., Schnell, R., Johnson, B., Pétron, G., Mefford, T., Neely III, R., 2014. Anatomy of wintertime ozone associated with oil and natural gas extraction activity in Wyoming and Utah. Elem. Sci. Anth. 2, 000024.

Parrish, D.D., Faloona, I.C., Derwent, R.G., 2022. Observational-based assessment of contributions to maximum ozone concentrations in the western United States. J. Air Waste Manag. Assoc. 72, 434-454.

Reiter, M.S., Kockelman, K.M., 2016. The problem of cold starts: A closer look at mobile source emissions levels. Transportation Research Part D: Transport and Environment 43, 123-132.

Restek, 2018. Improve Analysis of Aldehydes and Ketones in Air Samples with Faster, More Accurate Methodology. Restek, Bellefonte, Pennsylvania, https://www.restek.com/en/technical-literature-library/articles/improve-analysis-of-aldehydes-and-ketones-in-air-samples-with-faster-more-accurate-methodology/.

Rickard, A., Salisbury, G., Monks, P., Lewis, A., Baugitte, S., Bandy, B., Clemitshaw, K., Penkett, S., 2002. Comparison of measured ozone production efficiencies in the marine boundary layer at two European coastal sites under different pollution regimes. Journal of atmospheric chemistry 43, 107-134.

Saha, P.K., Khlystov, A., Snyder, M.G., Grieshop, A.P., 2018. Characterization of air pollutant concentrations, fleet emission factors, and dispersion near a North Carolina interstate freeway across two seasons. Atmos. Environ. 177, 143-153.

Saunders, S.M., Jenkin, M.E., Derwent, R., Pilling, M., 2003. Protocol for the development of the Master Chemical Mechanism, MCM v3 (Part A): tropospheric degradation of non-aromatic volatile organic compounds. Atmos. Chem. Phys. 3, 161-180.

Shimadzu, 2011. Nexera Application Data Sheet No.13: Ultrafast Analysis of Aldehydes and Ketones. Shimadzu, Tokyo, Japan, https://www.shimadzu.com/an/literature/hplc/jpl212018.html.

Silcox, G.D., Kelly, K.E., Crosman, E.T., Whiteman, C.D., Allen, B.L., 2012. Wintertime PM 2.5 concentrations during persistent, multi-day cold-air pools in a mountain valley. Atmos. Environ. 46, 17-24.

Sillman, S., 1995. The use of NO y, H2O2, and HNO3 as indicators for ozone-NO x-hydrocarbon sensitivity in urban locations. J. Geophys. Res. Atmos. 100, 14175-14188.

Sillman, S., 1999. The relation between ozone, NOx and hydrocarbons in urban and polluted rural environments. Atmos. Environ. 33, 1821-1845.

Sillman, S., He, D., 2002. Some theoretical results concerning O3-NOx-VOC chemistry and NOx-VOC indicators. J. Geophys. Res. Atmos. 107, ACH 26-21-ACH 26-15.

Sillman, S., He, D., Cardelino, C., Imhoff, R.E., 1997. The use of photochemical indicators to evaluate ozone-NOx-hydrocarbon sensitivity: Case studies from Atlanta, New York, and Los Angeles. J. Air Waste Manag. Assoc. 47, 1030-1040.

Sillman, S., He, D., Pippin, M.R., Daum, P.H., Imre, D.G., Kleinman, L.I., Lee, J.H., Weinstein-Lloyd, J., 1998. Model correlations for ozone, reactive nitrogen, and peroxides for Nashville in comparison with measurements: Implications for O3-NO x-hydrocarbon chemistry. J. Geophys. Res. Atmos. 103, 22629-22644.

Stoeckenius, T., McNally, D., Eds., 2014. Final Report: 2013 Uinta Basin Winter Ozone Study, https://binghamresearch.usu.edu/files/UBOS_2013_Final_Report_-_PDF.zip.

Suarez-Bertoa, R., Astorga, C., 2018. Impact of cold temperature on Euro 6 passenger car emissions. Environmental pollution 234, 318-329.

Tran, H., Mansfield, M.L., Tran, T., Kumbhani, S., Hansen, J., 2015. Final Report: Adapting the SAPRC Chemistry Mechanism for Low Temperature Conditions. Utah State University, Vernal, Utah, https://usu.box.com/s/3fc9fnq0g7929onu2wj70atcdun6gwcw.

Tran, H., Yarwood, G., Stockwell, W., 2023. Assessing Wintertime Ozone Prediction Sensitivity to Photochemical Mechanism. Ramboll and Utah State University, Salt Lake City, Utah, https://www.usu.edu/binghamresearch/files/reports/Ramboll_USU_S4S_RACM2_FinalReport_24Feb2023.pdf.

Tran, H.N.Q., Lyman, S.N., Mansfield, M.L., O'Neil, T., Bowers, R.L., Smith, A.P., Keslar, C., 2017. Emissions of organic compounds from produced water ponds II: evaluation of flux-chamber measurements with inverse-modeling techniques. J. Air Waste Manag. Assoc. 68, 713-724.

Tran, T., Tran, H., 2021. Uinta Basin Ozone State Implementation Plan Meteorological Modeling: Weather Research And Forecasting (WRF) Model Performance Evaluation. Utah State Univesrity, Vernal, Utah, https://www.usu.edu/binghamresearch/files/reports/WRF_UintaBasin_OSIP_MPE_Report_v2.pdf.

Tran, T., Tran, H., Mansfield, M., Lyman, S., Crosman, E., 2018. Four dimensional data assimilation (FDDA) impacts on WRF performance in simulating inversion layer structure and distributions of CMAQ-simulated winter ozone concentrations in Uintah Basin. Atmos. Environ. 177, 75-92.

Uchiyama, S., Naito, S., Matsumoto, M., Inaba, Y., Kunugita, N., 2009. Improved measurement of ozone and carbonyls using a dual-bed sampling cartridge containing trans-1, 2-bis (2-pyridyl) ethylene and 2, 4-dinitrophenylhydrazine-impregnated silica. Anal. Chem. 81, 6552-6557.

UDAQ, 2023. Statewide Oil and Gas Emissions Inventory, https://deq.utah.gov/air-quality/statewide-oil-gas-emissions-inventory.

Varon, D.J., Jacob, D.J., Hmiel, B., Gautam, R., Lyon, D.R., Omara, M., Sulprizio, M., Shen, L., Pendergrass, D., Nesser, H., 2023. Continuous weekly monitoring of methane emissions from the Permian Basin by inversion of TROPOMI satellite observations. Atmos. Chem. Phys. 23, 7503-7520.

Varon, D.J., Jacob, D.J., Sulprizio, M., Estrada, L.A., Downs, W.B., Shen, L., Hancock, S.E., Nesser, H., Qu, Z., Penn, E., 2022. Integrated Methane Inversion (IMI 1.0): a user-friendly, cloud-based facility for inferring high-resolution methane emissions from TROPOMI satellite observations. Geosci. Mod. Dev. 15, 5787-5805.

Wærsted, E.G., Sundvor, I., Denby, B.R., Mu, Q., 2022. Quantification of temperature dependence of NOx emissions from road traffic in Norway using air quality modelling and monitoring data. Atmospheric Environment: X 13, 100160.

Wang, D., Austin, C., 2006. Determination of complex mixtures of volatile organic compounds in ambient air: canister methodology. Anal. Bioanal. Chem. 386, 1099-1120.

Wang, L., Wang, J., Tan, X., Fang, C., 2019. Analysis of NOx pollution characteristics in the atmospheric environment in Changchun city. Atmos. 11, 30.

Weber, C., Sundvor, I., Figenbaum, E., 2019. Comparison of regulated emission factors of Euro 6 LDV in Nordic temperatures and cold start conditions: Diesel-and gasoline direct-injection. Atmos. Environ. 206, 208-217.

Wilson, L., Tran, T., Lyman, S., Pearson, M., McGrath, T., Cubrich, B., 2020. Uinta Basin Composition Study. Utah Department of Environmental quality, Salt Lake City, Utah, https://documents.deq.utah.gov/air-quality/planning/technical-analysis/DAQ-2020-004826.pdf.

Wolfe, G.M., Marvin, M.R., Roberts, S.J., Travis, K.R., Liao, J., 2016. The framework for 0-D atmospheric modeling (F0AM) v3.1. Geosci. Mod. Dev. 9, 3309-3319.

Yarwood, G., Jung, J., Whitten, G.Z., Heo, G., Mellberg, J., Estes, M., 2010. Updates to the Carbon Bond mechanism for version 6 (CB6), 2010 CMAS Conference, Chapel Hill, North Carolina.